UNIVERSIDADE FEDERAL DE PERNAMBUCO
CENTRO DE TECNOLOGIA E GEOCIÊNCIAS
DEPARTAMENTO DE GEOLOGIA
PROGRAMA DE PÓS-GRADUAÇÃO EM GEOCIÊNCIAS

VIVIAN SILVANI DE ARRUDA PASSOS

CARACTERIZAÇÃO ESTRUTURAL DAS ZONAS DE FALHA DA BORDA LESTE DA BACIA DO ARARIPE, NE BRASIL

Recife
2022

VIVIAN SILVANI DE ARRUDA PASSOS

CARACTERIZAÇÃO ESTRUTURAL DAS ZONAS DE FALHA DA BORDA LESTE DA BACIA DO ARARIPE, NE BRASIL

Dissertação apresentada ao Programa de Pós-graduação em Geociências da Universidade Federal de Pernambuco, como requisito parcial para a obtenção do título de Mestra em Geociências.

Área de concentração: Geologia Sedimentar e Ambiental

Orientador: Prof. Dr. Tiago Siqueira de Miranda.

Coorientador: Prof. Dr. Jefferson Tavares Cruz Oliveira.

Recife

2022

Catalogação na fonte:
Bibliotecária Sandra Maria Neri Santiago, CRB-4 / 1267

P289c Passos, Vivian Silvani de Arruda.
Caracterização estrutural das zonas de falha da borda leste da Bacia do Araripe, NE Brasil / Vivian Silvani de Arruda Passos. – 2022.
135 f.: il.

Orientador: Prof. Dr. Tiago Siqueira de Miranda.
Coorientador: Prof. Dr. Jefferson Tavares Cruz Oliveira.
Dissertação (Mestrado) – Universidade Federal de Pernambuco. CTG. Programa de Pós-Graduação em Geociências. Recife, 2022.
Inclui referências.

1. Geociências. 2. Lineamentos magnéticos e topográficos. 3. Deformação frágil. 4. Bandas de deformação. 5. Arranjo especial. 6. Deconvolução de Euler. I. Miranda, Tiago Siqueira de (Orientador). II. Oliveira, Jefferson Tavares Cruz (Coorientador). III. Título

UFPE

551 CDD (22. ed.) BCTG/2022-316

VIVIAN SILVANI DE ARRUDA PASSOS

CARACTERIZAÇÃO ESTRUTURAL DAS ZONAS DE FALHA DA BORDA LESTE DA BACIA DO ARARIPE, NE BRASIL

Dissertação apresentada ao Programa de Pós-Graduação em Geociências da Universidade Federal de Pernambuco, Centro de Tecnologia e Geociências, como requisito parcial para a obtenção do título de Mestre em Geociências. Área de Concentração: Geologia Sedimentar e Ambiental.

Aprovada em: 29/04/2022.

BANCA EXAMINADORA

____

Prof. Dr. Tiago Siqueira de Miranda (Orientador)
Universidade Federal de Pernambuco

____

Prof. Dr. Virgínio Henrique de Miranda Lopes Neumann (Examinador Interno)
Universidade Federal de Pernambuco

____

Prof. Dr. José Ricardo Gonçalves Magalhães (Examinador Externo)
Universidade Federal do Recôncavo da Bahia

AGRADECIMENTOS

"Em todos os momentos daí graças". Sou grata a Deus por me permitir concluir mais esta etapa, por me fortalecer, guiar e iluminar. O caminho até aqui nem sempre foi fácil, mas foi rodeado de pessoas maravilhosas que tornaram minha jornada mais simples e leve. Dedico esta conquista a minha mãe, Silvana, e a minha irmã, Vitória. Mulheres incríveis, que eu amo e admiro. Todas as minhas conquistas, por menores que sejam, são nossas. Ao meu namorado, Willams, obrigada por ser luz na minha vida sempre que eu preciso. A vocês o meu muito obrigada por tantas coisas, mas, principalmente, por me motivarem a ser um pouco melhor todos os dias.

Agradeço também, a todos os bons amigos que a Universidade Federal de Pernambuco me proporcionou, sobretudo a Alcione, que além de amiga é uma irmã que a vida acadêmica me apresentou. Foram longos anos até aqui, e que bom que pude ter cada um de vocês comigo. O meu muito obrigada pela paciência, carinho e momentos compartilhados.

Aos meus orientadores, Tiago Miranda e Jefferson Oliveira, obrigada pela confiança, paciência e por todo apoio para a construção deste trabalho. Aprendi muito com vocês nessa jornada. A Gabriel Topan e Germano por toda ajuda nas etapas de campo. A todos os autores dos artigos frutos deste trabalho, em especial Rodrigo Corrêa pelas excelentes sugestões. Aos membros da banca examinadora, pelas recomendações e disponibilidade. Muito obrigada por todas as contribuições que enriqueceram este trabalho.

Aos professores e funcionários do Programa de Pós-graduação em Geociências, em especial a Krishnamurti. Ao Laboratório de Modelagem de Bacias (ModLad-UFPE) o qual puder fazer parte durante a construção desta pesquisa. Ao CNPq (Conselho Nacional de Desenvolvimento Científico e Tecnológico) e ao Projeto Zonas de Falha (Petrobrás-ANP-UFPE) pelo financiamento desta pesquisa.

A todos o meu muito obrigada!

RESUMO

Zonas de falha são faixas de deformação rúptil importantes em bacias sedimentares porque exercem forte controle na compartimentação estrutural, migração e trapeamento de fluidos como hidrocarbonetos e água subterrânea. Além disso, zonas de falha são estruturas complexas e podem representar um importante papel na evolução tectônica de bacias sedimentares. Esta pesquisa apresenta a caracterização estrutural da deformação rúptil associada à borda leste da Bacia do Araripe, NE Brasil. Esta região abrange o contato entre rochas miloníticas (Zona de Cisalhamento Patos) do embasamento e a cobertura sedimentar da bacia (Formação Cariri). Neste trabalho, foram aplicados métodos de quantificação estrutural (*software* CorrCount) visando preencher uma lacuna na bibliografia, pois este setor da bacia não dispõe de estudos sobre zonas de falha. Permitindo assim, compreender as implicações tectônicas para este setor. A partir de estudos sobre a organização do arranjo espacial de lineamentos estruturais regionais (topográficos e aeromagnéticos) e das bandas de deformação da Formação Cariri. Além disso, com a utilização da técnica da Deconvolução de Euler foi investigado a variação da profundidade das fontes de anomalias magnéticas que estão associadas às zonas de falha da área de estudo (falhas Mauriti, Coité e Umburanas). O arranjo espacial dos lineamentos topográficos, aeromagnéticos e das bandas de deformação apresentam padrões de espaçamentos irregulares. Os lineamentos estruturais regionais são caracterizados por arranjos aleatórios, enquanto as bandas de deformação possuem arranjos agrupados. Os lineamentos estruturais regionais no setor da bacia e as bandas de deformação configuram pares conjugados com orientação NW-SE (R) e N-S (R'), e ENE-WSW (R) e NNE-SSW (R’) de acordo com o modelo de Riedel, para transcorrência destral e sinistral, respectivamente. Os dados de posição e profundidade das anomalias magnéticas (técnica da Deconvolução de Euler) referente às zonas de falha (falhas Mauriti, Coité e Umburanas) mostram valores assimétricos de profundidade das fontes magnéticas (200 a 800 m) que delineiam altos e baixos estruturais (*horsts* e grabens). Os resultados deste trabalho indicaram que as principais zonas de falha da borda leste da Bacia do Araripe apresentam uma concentração de deformação rúptil com clusters de lineamentos topográficos e bandas de deformação. Adicionalmente, esta pesquisa propõe que a reativação rúptil da trama dúctil da zona de cisalhamento Patos controlou a evolução tectônica da borda leste da Bacia do Araripe.

Palavras-chave: lineamentos magnéticos e topográficos; deformação frágil; bandas de deformação; arranjo especial; deconvolução de Euler.

ABSTRACT

Fault zones are important brittle deformation in sedimentary basins due to their strong control over structural compartmentation, migration, and trapping of fluids such as hydrocarbons and groundwater. Furthermore, fault zones are generally complex structures and may play an important role in the tectonic evolution of sedimentary basins. This research presents the structural characterization of the brittle deformation associated with the eastern border of the Araripe Basin, northeast of Brazil. This region encompasses the contact between mylonitic rocks (Patos Shear Zone) of the basement and the sedimentary cover of the basin (Cariri Formation). In this work, structural quantification methods (CorrCount software) were applied to fill a gap in the literature, since this sector of the basin does not have studies on fault zones. Thus, allowing us to understand the tectonic implications for this sector. Studies were carried out on the organization of the spatial arrangement of regional structural lineaments (topographic and aeromagnetic) and deformation bands of the Cariri Formation. Furthermore, using the Euler Deconvolution technique, we investigated the variation in the depth of the sources of magnetic anomalies that are associated with the fault zones of the study area (Mauriti, Coité, and Umburanas faults). The spatial arrangement of topographic and aeromagnetic lineaments and deformation bands show irregular spacing patterns. The regional structural lineaments are characterized by random arrangements, while the deformation bands have clustered arrangements. The regional structural lineaments in the basin sector and the deformation bands configure conjugated pairs with NW-SE (R) and N-S (R') orientation, and ENE-WSW (R) and NNE-SSW (R') according to the Riedel's model, for dextral and sinistral strike-slip regime, respectively. The position and depth data of the magnetic anomalies (Euler Deconvolution technique) referring to the fault zones (Mauriti, Coité, and Umburanas faults) show asymmetrical values depth of the magnetic source (200 to 800 m) that delineate structural highs and lows (horsts and graben). The results of this work indicated that the main fault zones of the eastern border of the Araripe Basin show a concentration of brittle deformation with clusters of topographic lineaments and deformation bands. Additionally, this research proposes that the brittle reactivation of the ductile Patos shear zone controlled the tectonic evolution of the eastern border of the Araripe Basin.

Keywords: magnetic and topographic lineaments; brittle deformation; deformation bands; spatial arrangement; Euler deconvolution.

SUMÁRIO

1 INTRODUÇÃO

A Bacia do Araripe é classificada como uma bacia intraplaca localizada no nordeste brasileiro. Esta bacia possui aproximadamente 9.000 km² de área e abrange a Chapada do Araripe (900 metros de altitude) até a Depressão do Vale do Cariri (500 metros de altitude), onde predominam, respectivamente, a unidades das sequências pré-rifte, rifte e pós-rifte, representadas pelas formações Cariri, Brejo Santo, Missão Velha e Abaiara (Assine, 1992, 2007; Neumann, 1999; Figura 1).

Nesta pesquisa foram aplicados métodos de quantificação estrutural multiescalar de estruturas rúpteis visando preencher uma lacuna na bibliografia sobre a evolução tectônica deste setor da bacia. Foram realizados estudos sobre a caracterização do arranjo espacial de lineamentos estruturais a partir de dados topográficos e aeromagnéticos. Este setor da bacia acomoda importantes lineamentos estruturais que são representados pelas falhas Mauriti, Coité e Umburanas. Adicionalmente foi investigada a organização espacial de bandas de deformação da Formação Cariri na região da borda leste da Bacia do Araripe. Além disso, esta pesquisa também teve foco na análise da profundidade das fontes de anomalias magnéticas que, possivelmente, representam o sistema de falhas que está associado à zona de cisalhamento Patos (ZCPa) e que possui um importante papel na evolução tectônica da Bacia do Araripe.

Figura 1- Mapa topográfico com a localização das bacias intraplaca do Nordeste do Brasil. O quadrado vermelho marca a área de estudo. Zonas de cisalhamento: ZCPa, Patos; ZCPE, Pernambuco Leste; ZCPW, Pernambuco Oeste. Bacias interiores: BA, Bacia do Araripe; BJ, Bacia do Jatobá; BF, Bacia de Fátima; BSJB, Bacia de São José do Belmonte; BC, Bacia do Cedro; BRP, Bacia do Rio do Peixe; BM, Bacia de Mirandiba; BS, Bacia do Socorro; BB, Bacia da Betânia; BCP, Bacia da Carnaubeira da Penha.

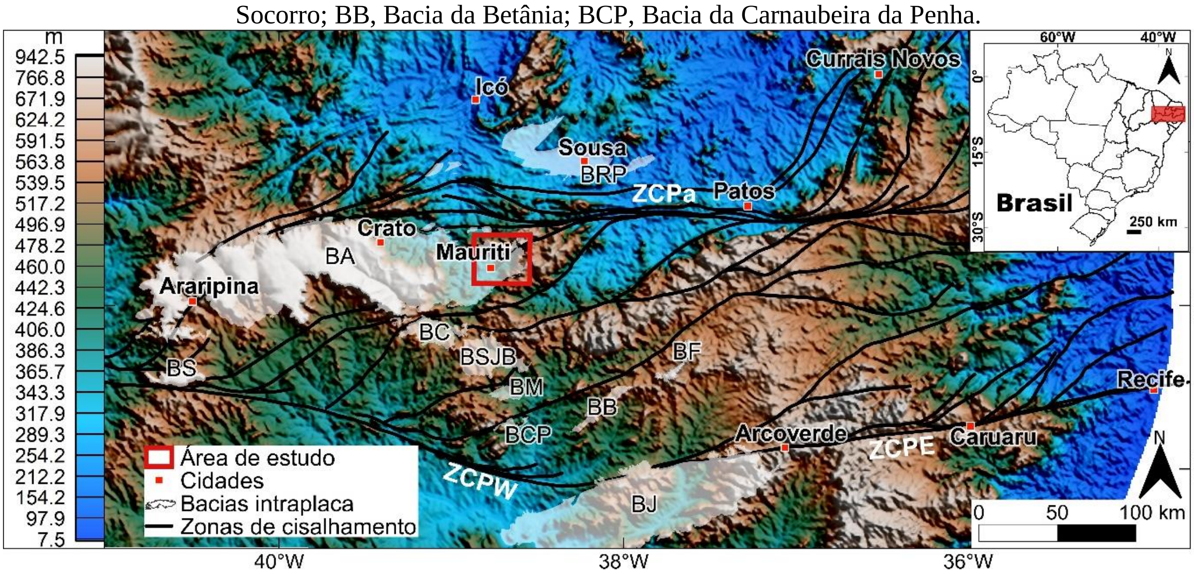

Fonte: A autora (2022).

1.1 JUSTIFICATIVAS

A Bacia do Araripe é uma importante bacia intraplaca do nordeste brasileiro, que possui unidades litoestratigráficas similares a sistemas petrolíferos reais. Por exemplo, na borda leste desta bacia, afloram rochas Paleozoicas, Jurássicas e Cretáceas que representam as tectonosequências pré-rifte e rifte (Assine, 1992, 2007; Neumann, 1999; Cerri et al., 2022). Este setor da bacia, também comporta importantes zonas de falhas (falhas Mauriti, Coité e Umburanas). Estruturas rúpteis (falhas, fraturas, bandas de deformação) podem ser simplificadas como descontinuidades mecânicas de fraqueza que estão sujeitas a reativações durante novas acumulações de esforços. Este acúmulo de esforços resulta em mudanças nas propriedades das rochas, influenciando diretamente em sistemas de reservatórios, tornando estas estruturas responsáveis pelas variações na porosidade e permeabilidade, aumento da coesão, atuando assim, como barreiras ou condutos para fluxo de fluidos (*e.g.*, Fossen et al., 2007; Fletcher et al., 2020). Apesar disso, não são verificados estudos sobre estas zonas de falha e como estas influenciaram no arranjo arquitetural da borda leste da Bacia do Araripe. Nesta contribuição, investigamos o arranjo espacial das estruturas (zonas de falha e bandas de deformação) e reunimos informações sobre as profundidades das fontes de anomalias magnéticas para estas zonas de falha. A partir da análise dos padrões estruturais em diferentes escalas, nossos resultados também permitem correlacionar estas zonas de falha as reativações da ZCPa. Possibilitando a correlação com os modelos geodinâmicos.

Investigações acerca do arranjo espacial das estruturas e da profundidade das fontes de anomalias magnética, fornecem resultados complementares que possibilitaram reunir importantes informações estruturais sobre o setor da borda leste da Bacia do Araripe. A análise do arranjo demonstra a posição e a organização das estruturas (falhas, bandas de deformação) no espaço, possibilitam compreender, por exemplo, o comportamento do fluxo de fluidos subterrâneos (água e hidrocarbonetos), depósitos minerais hidrotermais, e o armazenamento de CO_2. Enquanto a técnica da Deconvolução de Euler possibilita estimar a profundidade das fontes de anomalias magnéticas. A integração de dados estruturais e magnéticos representa uma importante ferramenta a quantificação da deformação rúptil em áreas estruturalmente complexas. Além disso, a caracterização estrutural multiescalar pode ser utilizada para o mapeamento de estruturas do embasamento pré-cambriano, relação tectonomagmática de bacias sedimentares, a localização de estruturas e os contatos geológicos, entre outras aplicações.

1.2 OBJETIVOS

O principal objetivo desta pesquisa foi realizar a caracterização estrutural multiescalar, a partir da quantificação estrutural de dados topográficos, aeromagnéticos e de afloramentos. Portanto, buscou-se caracterizar os eventos deformacionais rúpteis e suas implicações nas reativações de estruturas que, possivelmente, controlaram a origem tectônica da Bacia do Araripe.

1.2.1 Objetivos específicos

Esta pesquisa possui os seguintes objetivos específicos:

i. Elaborar um estudo de morfotectônica a partir da identificação de lineamentos estruturais em escala regional;
ii. Processar e interpretar os dados aeromagnéticos, com intuito de mapear o arcabouço estrutural da borda leste da Bacia do Araripe;
iii. Realizar *scanlines* perpendiculares aos principais lineamentos estruturais (dados topográficos e aeromagnéticos) e às bandas de deformação da Formação Cariri;
iv. Caracterizar o arranjo espacial de lineamentos estruturais e bandas de deformação com a utilização do *software* CorrCount (Marrett et al., 2018);
v. Analisar a variação da profundidade das fontes de anomalias magnéticas que estão associadas às zonas de falha da borda leste, a partir da Deconvolução de Euler;
vi. Identificar a orientação dos principais esforços tectônicos a partir da correlação de dados topográficos, aeromagnéticos e de campo, permitindo assim, verificar os regimes tectônicos responsáveis pelo desenvolvimento das estruturas rúpteis que ocorrem na área de estudo.

1.3 LOCALIZAÇÃO DA ÁREA

A área de estudo está localizada na borda leste da Bacia do Araripe e possui aproximadamente 1.110 km² (Figuras 1 e 2). Esta área abrange o município de Mauriti, estado do Ceará, distando 503 km de Fortaleza, capital desse estado. Posicionada à 570 km de Recife, Pernambuco. Na área de estudo, mais precisamente o setor centro-sul, é beneficiado com o canal de transposição do Rio São Francisco, fornecendo assim, bons acessos por vias não pavimentadas por toda área de estudo (Figura 2).

Figura 2 - Mapa de localização da área de estudo. Estados brasileiros: BA, Bahia; CE, Ceará; PB, Paraíba; PE, Pernambuco; PI, Piauí; RN, Rio Grande do Norte.

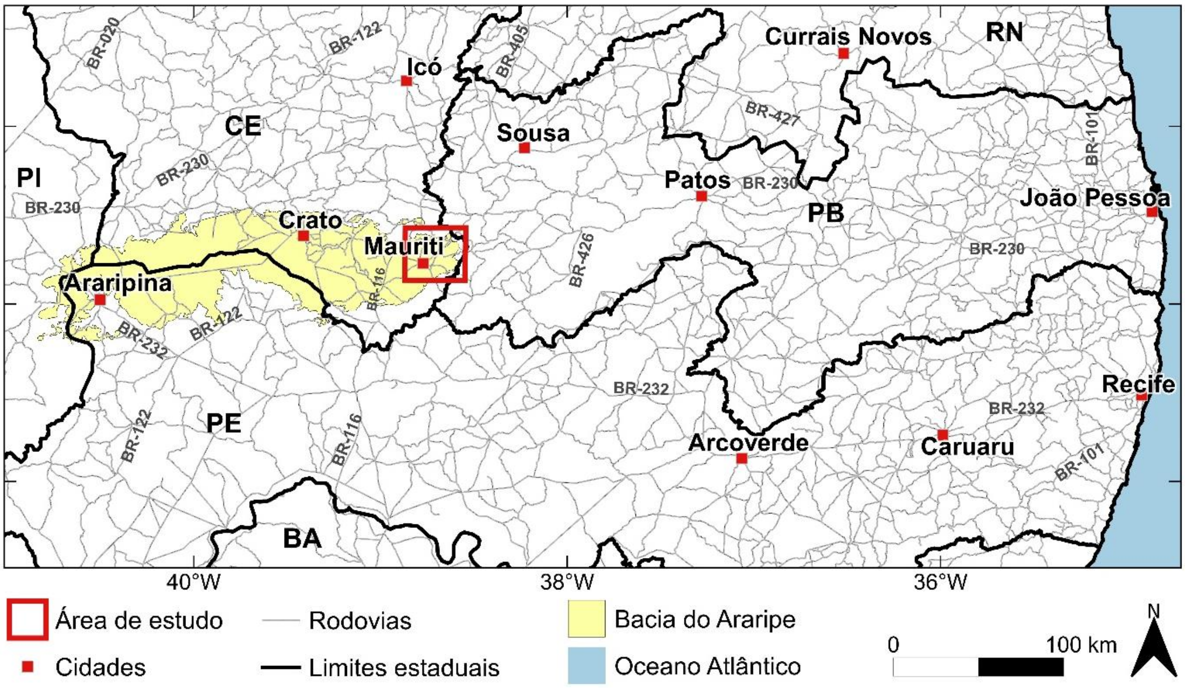

Fonte: A autora (2022).

2 MATERIAIS E MÉTODOS

Foram aplicadas ferramentas (topográficas e magnéticas) que fornecem informações geológicas regionais, de acesso remoto e gratuito. Reunimos para a borda leste da Bacia do Araripe: modelos digitais de elevação; imagens multiespectrais orbitais; e dados aeromagnéticos. Esse conjunto de dados regionais foi integrado aos resultados provenientes dos dados obtidos em campo (Figura 3), descritos nos tópicos a seguir. O método de análise do arranjo estrutural foi empregue para a quantificação estrutural dos dados regionais e das bandas de deformação. Também foi investigada a variação da profundidade das fontes de anomalias magnéticas, por meio da técnica da Deconvolução de Euler para as principais zonas de falha deste setor da bacia.

Figura 3 - Fluxograma simplificado com os métodos aplicados neste trabalho, para os dados regionais e de campo. Os dados topográficos referem-se aos modelos digitais de elevação e imagens multiespectrais orbitais.

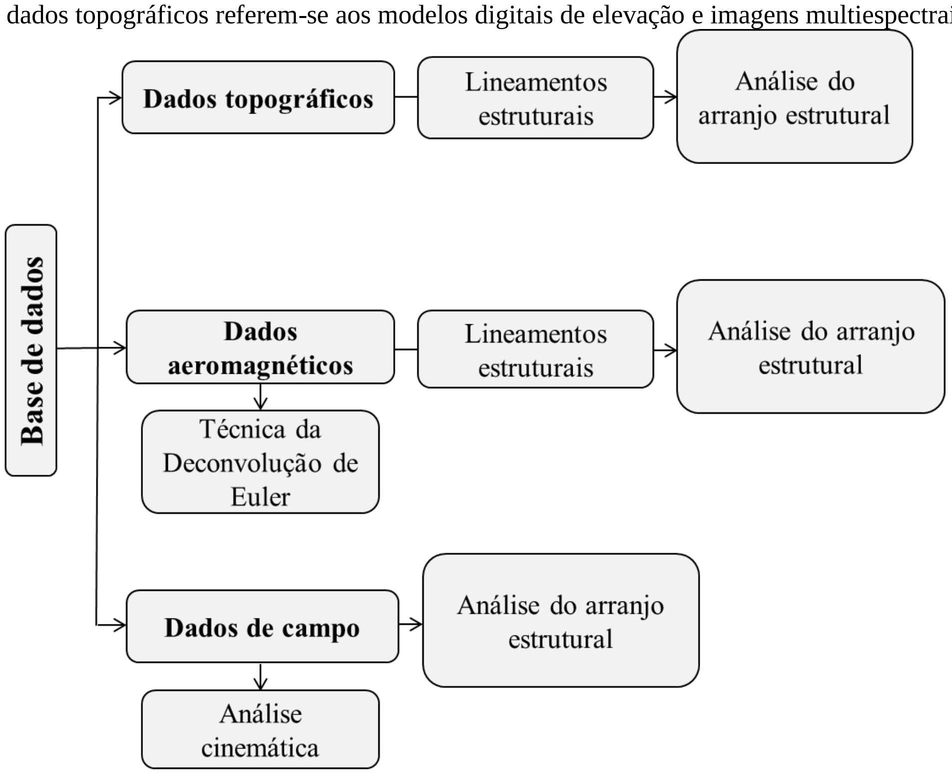

Fonte: A autora (2022).

2.1 MODELO DIGITAL DE ELEVAÇÃO

A técnica de sombreamento interativo, permite o realce de estruturas ortogonais às direções de iluminação, possibilitando uma interpretação confiável dos lineamentos topográficos (Wise et al., 1985; Drury, 2001; Grohmann et al., 2011a; Jacques et al., 2014;

Lima e Sá, 2017). Por meio de imagens da *Shuttle Radar Topography Mission* (SRTM), com resolução espacial de 30 m, obtidas gratuitamente via internet (https://gdex.cr.usgs.gov/gdex/), foram gerados quatro modelos digitais de elevação (MDE) com altitude de insolação de 45º, e azimutes de iluminação nas direções 0°, 45º, 90º e 315º para a região da borda leste da Bacia do Araripe (*e.g.,* Celestino et al., 2020).

Esta interpretação é baseada em uma abordagem visual realizada a partir dos MDE's, na qual foram analisados lineamentos com dimensões representativas (maiores que um quilômetro), podendo ou não vir constatados nos quatro cenários de iluminação. Estes lineamentos foram então validados a partir do mapa topográfico (obtido via imagens multiespectrais orbitais, vide tópico 2.2) (*e.g.,* Lima e Sá, 2017; Meixner et al., 2018). Essa abordagem permite indicar lineamentos significativos, com dimensões que se destacam, os quais, por exemplo, podem estar reproduzindo zonas de falha.

Os lineamentos topográficos da borda leste da Bacia do Araripe foram divididos em dois setores, bacia e embasamento, que foram agrupados por dois parâmetros, lineamentos de vales (cotas baixa, relevo negativo) e lineamentos de cristas (cotas alta, relevo positivo). Usando o *software* QGIS 3.10.3 (https://qgis.org/en/site/forusers/download.html), diagramas de rosetas foram produzidos para cada MDE (0º, 45º, 90º e 315º) com intervalo de classe (*bin size*) de 10° separados de acordo com o setor (bacia ou embasamento) e o parâmetro (crista ou vale), possibilitando analisar os padrões de orientação dos lineamentos interpretados (*e.g.,* Celestino et al., 2018; 2020).

2.2 IMAGENS MULTIESPECTRAIS ORBITAIS

As imagens multiespectrais orbitais gratuitas, foram adquiridas via aplicativo *Google Earth PRO* v. 7.3.2.5491, são imagens da empresa *DigitalGlobe* com alta resolução espacial (0,31 a 0,6 m a depender do satélite que adquiriu a imagem), contendo composições coloridas de bandas de sensores como Geoeye-1 e WorldView-2 a 4. Essas imagens foram utilizadas para a interpretação de redes de drenagem, lineamentos, estradas e morfologia (*e.g.,* Grohmann et al., 2011a; Nicolas e Clayton, 2015; Lima e Sá, 2017; Meixner et al., 2018; Araújo Neto et al., 2018), auxiliando nas interpretações regionais e de campo.

Os dados multiespectrais são significativos na validação da existência dos lineamentos topográficos provenientes da análise dos MDE's, possibilitando excluir artefatos, independente da iluminação utilizada (*e.g.,* Lima e Sá, 2017). Portanto, estas imagens permitem a inclusão de algum lineamento topográfico que não tenha sido verificado nas interpretações dos MDE's.

2.3 DADOS AEROMAGNÉTICOS

Os dados aeromagnéticos foram adquiridos no Banco de Dados do Serviço Geológico Brasileiro (CPRM) (http://geosgb.cprm.gov.br/). Estes dados magnéticos foram obtidos a partir de linhas de voo de direção N-S e as de controle E-W, com espaçamento de 500 m e 10 km, respectivamente. Pertencentes ao projetos aerogeofísicos Pernambuco Piauí (1067), Pernambuco Piauí (1091), Pernambuco Paraíba (1091), Paraíba Rio Grande do Norte (1092) e Centro sudoeste do Ceará (1101). O processamento dos dados foi desenvolvido a partir do *software* Oasis Montaj 9.1, com o objetivo de remover ruídos sem que isso afete a interpretação do dado. O processamento foi dividido em quatro etapas: i) Analisar o nível de ruído (por exemplo, identificação e remoção de *spike*); ii) Remoção do *International Geomagnetic Reference Field* (IGRF); iii) Uso dos filtros de Cosseno Direcional e Butterworth para remover artefatos resultantes do nivelamento (Pilkington e Roest, 1997); iv) Interpolação pela técnica de gridagem bi-direcional com tamanho de célula de 125 m (Reeves, 2005).

Em seguida, foi gerado o mapa de campo anômalo (CMA) com filtragem de continuação para cima na altitude de 500 m. Aplicou-se a técnica de redução ao polo que tem como objetivo centralizar os picos das anomalias (assinatura de amplitude positiva) sobre sua fonte causadora (Baranov, 1957). Posteriormente, o filtro gaussiano regional/residual foi utilizado para interpretar fontes rasas e profundas (Li e Oldenburg, 1998). A aplicação desse filtro (regional/residual) é desenvolvida através do ponto de corte k_o efetuado a partir da análise do espectro de potência (Figura 4). O número de onda (k_o) utilizado foi de 0,11 ciclos/km, correspondente ao limite entre as fontes magnéticas mais profundas (profundidade entre 2 a 3 km), referentes as estruturas do embasamento cristalino, enquanto as fontes mais rasas (profundidade entre 500 m e 2 km), podem estar refletindo a trama rúptil da bacia e do embasamento. O filtro gaussiano foi aplicado aos dados de anomalia magnética e anomalia magnética reduzida ao polo.

Como critérios de interpretação dos lineamentos magnéticos, utilizamos as bordas e centros das anomalias, para analisar o mapa aeromagnético residual e o mapa aeromagnético reduzido ao polo residual, respectivamente. Posteriormente, foram gerados diagramas de rosetas, com intervalo de classe (*bin size*) de 10°, utilizando o *software* Qgis 3.10.3. Esses gráficos ajudam a revelar os padrões de orientação dos lineamentos magnéticos para borda leste da Bacia do Araripe, nos setores da bacia e do embasamento cristalino.

Figura 4 - Espectro de potência radial médio para os dados aeromagnéticos, mostrando os intervalos dos números de onda (comprimentos de onda) utilizados para determinar a distância de aplicação do filtro gaussiano de separação regional-residual. As linhas vermelhas e azuis marcam as aproximações dos números de onda menores (fontes profundas) e maiores (fontes rasas), respectivamente.

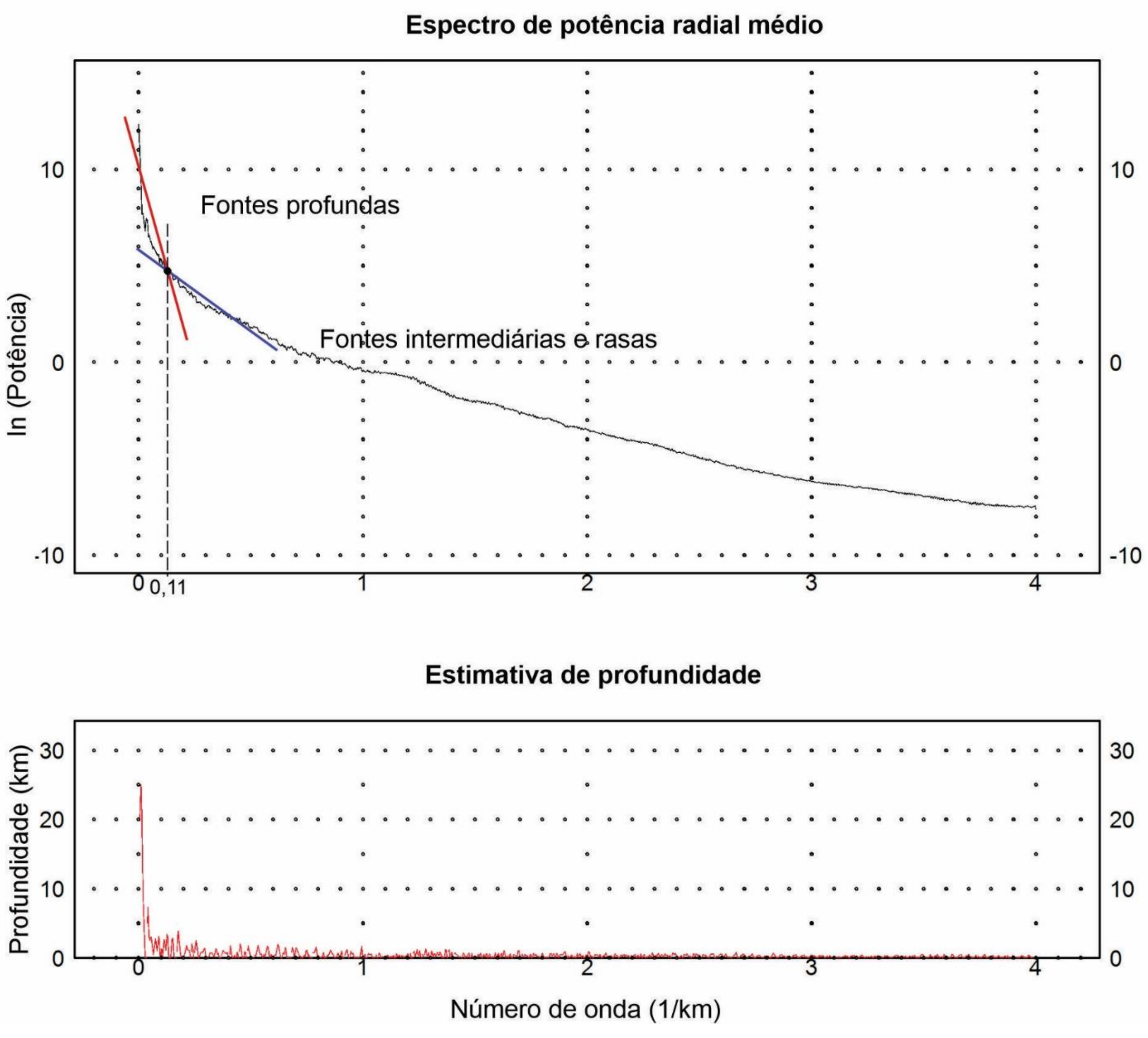

Fonte: A autora (2022).

2.4 DADOS DE CAMPO

Nesta etapa do trabalho foi realizado o reconhecimento dos tipos litológicos, sua distribuição espacial, e a coleta de dados estruturais na escala de mapeamento geológico-estrutural de 1:50.000, ao longo de sete perfis previamente definidos (perpendiculares as estruturas regionais principais, com orientação NW-SE). O setor da borda leste apresenta alguns afloramentos representativos, com destaque para aqueles próximos as regiões de zonas de falha. Este trabalho investigou os afloramentos referentes ao embasamento (granitóides neoproterozoicos) e a sequência sedimentar (Formação Cariri), representados por granitos miloníticos com presença de falhas e pseudotaquilitos, e por arenitos altamente silicificados e ricos em bandas de deformação, respectivamente.

Para os afloramentos da Formação Cariri, realizamos a quantificação estrutural ao longo de linhas de varredura (*scanlines*). Este método representa uma contagem perpendicular a orientação principal das estruturas presentes (bandas de deformação), observando a distância entre estas, sua abertura, orientação, relações de interseção e preenchimento (Ortega et al., 2006; Santos et al., 2015; Miranda et al., 2018). Os dados estruturais foram obtidos por meio de bússolas geológicas do tipo *Clar* e *Brunton*, e de aplicativos para dispositivos móveis, com o *Fieldmove Clino* e *StereoNet*.

2.5 ANÁLISE DO ARRANJO ESTRUTURAL

A análise do arranjo espacial das estruturas rúpteis foi realizada em duas escalas distintas (macro e mesoescala). Em escala regional a análise foi realizada em sete *scanlines* (com orientação NW-SE e extensão de 27 a 45 km), caracterizadas em dois grupos de lineamentos: i) topográficos (MDE e multiespectrais) e ii) anomalia aeromagnética (residual e reduzida ao polo residual). Para a análise em mesoescala, foram realizadas quatro *scanlines* (com 6 a 58 m de extensão), posicionadas perpendiculares a orientação preferencial das bandas de deformação da Formação Cariri. Em ambas escalas (macro e mesoescala) foram coletados dados de espaçamento entre as estruturas ao longo de cada *scanline*. Onde o espaçamento é definido como a distância entre os lineamentos vizinhos (Hooker et al., 2018).

O *software* CorrCount foi utilizado para analisar o conjunto de dados de espaçamento (lineamentos estruturais regionais e bandas de deformação) a partir dos gráficos de intensidade de estruturas normalizados e o método de contagem de correlação normalizada (NCC) para a identificação de *cluster*s e de seus limites (distribuição de seus tamanhos e padrões) (Marrett et al., 2018). O NCC fornece uma análise quantitativa do grau em que um conjunto de estruturas está agrupada. Este método analisa a organização espacial das estruturas e classifica se o arranjo é uniforme (periódico ou anti-*clusters*), ou se as estruturas estão organizadas como *clusters* que surgem devido ao arranjo aleatório e *clusters* não-aleatório (Marrett et al., 2018; Laubach et al., 2018b; Li et al., 2018). A técnica NCC utiliza escalas de comprimento para caracterizar o arranjo espacial e pode aumentar ou diminuir, às vezes seguindo uma lei de potência (Marrett et al., 2018). Wang et al. (2019) destacam que os dados do NCC são mais precisos na identificação e quantificação de padrões de espaçamento. Para ter significância estatística, os picos e vales devem exceder os limites de confiança; caso contrário, os dados indicam um arranjo aleatório (Marrett et al., 2018). Marrett et al. (2018) estabelecem os parâmetros interpretativos para o comportamento dos *clusters* equivalentes às características das curvas NCC, sendo possível verificar combinações de parâmetros ao longo da mesma linha de varredura. Por tanto, esta técnica descreve as posições do arranjo de estruturas no espaço, indicando a ocorrência de *clusters*, indispensável para oferecer, por exemplo, suporte a modelos de redes de fraturas discretas e simulações numéricas (Miranda et al., 2018).

O CorrCount fornece soluções analíticas e de Monte Carlo com o objetivo de quantificar os erros e incertezas (Santos et al., 2015). Para os espaçamentos de entrada aleatórios, foi admitido intervalos de confiança de 95% e 68%. Se a intensidade das estruturas ficar fora dos limites de confiança (superior ou inferior), o espaçamento de estrutura correspondente é estatisticamente significativo e distinto do arranjo aleatório (Marrett et al., 2018; Laubach et al., 2018b; Miranda et al., 2018).

A técnica NCC também permite quantificar o coeficiente de variação (CV), uma vez que $CV = \sigma / \mu$, onde σ é o desvio padrão do espaçamento e μ é a sua média aritmética. O CV aumenta proporcionalmente ao aumento da irregularidade no espaçamento (Hooker, et al., 2018). Dessa forma, como exemplificado na figura 5, teremos que o $CV > 1$, indica estruturas mais agrupadas, mostrando *clusters*; CV próximo ou igual a 1 indica estruturas arranjadas aleatoriamente; $CV < 1$, refere-se a lineamentos menos agrupados, indicando anti-*clusters*; e um CV igual a 0 revela espaçamento de estruturas perfeitamente periódicos. Ambas as técnicas permitem quantificar a presença de arranjos espaciais aleatórios, agrupados ou regulares nas *scanlines*.

Figura 5 - Modelo esquemático ilustrando a heterogeneidade do espaçamento para as estruturas rúpteis de acordo com o coeficiente de variação (CV). CV > 1, estruturas agrupadas; CV = 1, estruturas arranjadas aleatoriamente; CV < 1, estruturas regularmente espaçadas. As linhas pretas indicam a ocorrência da estrutura. As áreas brancas mostram o espaçamento entre essas estruturas.

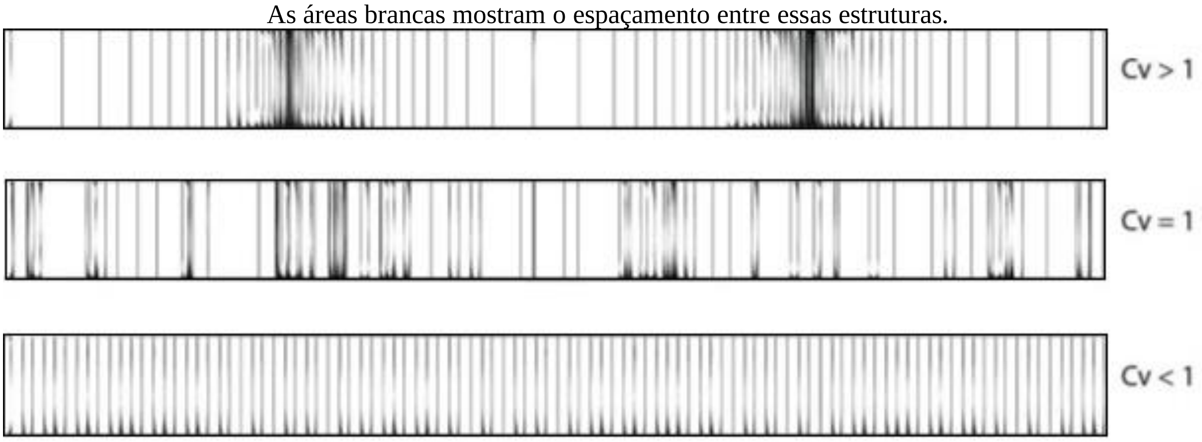

Fonte: Miranda et al. (2018).

2.6 DECONVOLUÇÃO DE EULER

A técnica da Deconvolução de Euler é utilizada para estimar a posição horizontal e as profundidades de fontes magnéticas ou gravimétricas (Reid et al., 1990; Durrheim et al., 1998). Esta técnica é baseada na equação de homogeneidade de Euler dada por (Blakely, 1996):

$$(r - r_0)\nabla T = -n\,T \quad (1)$$

Onde ∇T é o gradiente do campo magnético anômalo medido no ponto $r = r - r_0$, n é um parâmetro conhecido como índice estrutural, sendo uma medida da taxa de decaimento da anomalia magnética com a distância entre a fonte e o ponto de medição e também um indicador da provável geometria da fonte (Thompson, 1982). Desta forma, para a relação com a natureza da fonte, temos que para fontes magnéticas, n = 0 refere-se a contatos, n = 0,5 está associado falhas, n = 1 está relacionado a soleiras ou diques, n = 2 indica cilindro ou *pipe* e n = 3 está associado a uma esfera ou dipolo (Reid et al.,1990). O índice estrutural (n), sistema de coordenadas cartesianas com os eixos x, y e z apontando nas direções norte, leste e para baixo, respectivamente, pode ser escrita como a equação (1) (Thompson, 1982):

$$(x - x_0)\frac{dT}{dx} + (y - y_0) + \frac{dT}{dy} + (z - z_0) + \frac{dT}{dz} = -\eta\,(T - B) \quad (2)$$

As estruturas geológicas são geralmente melhor representadas pelos índices estruturais mais altos, contudo, índices mais baixos, fornecem maior precisão quanto a estimativa de profundidade até o topo da estrutura (Thompson, 1982). Reid et al. (1990) complementa que dados reais podem conter anomalias com várias fontes, nos diferentes índices estruturais (por exemplo índices de 0-3). Para mapear as fontes magnéticas e estimar a sua profundidade a técnica da Deconvolução de Euler foi aplicada ao mapa aeromagnético anômalo e ao mapa aeromagnético reduzido ao polo (descritos no tópico 2.3), que forneceu resultados satisfatórios para os índices estruturais de 0, 0,5, e 1. Com tamanho de valor 10 para as janelas, de acordo com o comprimento de onda do sinal de campo potencial e das profundidades do alvo. Admitimos para estas soluções, erros menores que 15%. A detecção de borda, utilizada para delimitar os lineamentos magnéticos, foi auxiliada pelas interpretações provenientes dos dados de mapeamento geológico, topográfico e aeromagnético.

3 CONTEXTO GEOLÓGICO REGIONAL

A Bacia do Araripe repousa sobre as rochas do Domínio Central da Província tectônica Borborema. Esta província é formada por unidades litoestratigráficas de idade Arqueana a Cambriana que abrange quase todo nordeste brasileiro, com aproximadamente 450.000 km² (Almeida et al., 1981; Vauchez et al., 1995; Van Schmus et al., 2008, 2011). A estruturação da Província Borborema é caracterizada principalmente por zonas de cisalhamento de escala continental que configuram esta província em distintos domínios (subprovíncias) estruturais (Brito Neves et al., 2001; Van Schmus et al., 2008, 2011; Almeida et al., 2015). Assim sendo, a Província Borborema pode ser dividida nas subprovíncias Norte, Central e Sul (Figura 6), que se encontram separadas pelas zonas de cisalhamento Patos, e Pernambuco Leste e Oeste (Vauchez et al., 1995; Neves e Mariano, 1999; Neves et al., 2005). Esta província pode ainda, ser segmentada nos subdomínios tectônicos Sergipano, Pernambuco-Alagoas e Riacho do Pontal, que constituem a Subprovíncia Sul; no Domínio da Zona Transversal, que constitui a Subprovíncia Central; e, nos domínios Rio Grande do Norte, Ceará Central, e o Médio Coreaú, pertencentes a Subprovíncia Norte (Van Schmus et al., 2008, 2011). A Subprovíncia Central é marcada, principalmente, por zonas de cisalhamento transcorrentes com orientação preferencial NE-SW a E-W (Van Schmus et al., 2011) que estão diretamente relacionadas com bacias sedimentares intraplaca, como por exemplo, a Bacia do Araripe (Figura 7).

A origem tectônica da Bacia do Araripe está condicionada aos eventos de fragmentação do Supercontinente Gondwana e abertura do Oceano Atlântico (Matos, 1992, 2000). A estruturação do embasamento Pré-Cambriano é o responsável pela geometria e evolução desta bacia, rearranjando seus depocentros (Assine, 2007; Scherer, 2014). Segundo Ponte e Ponte Filho (1996) três etapas de subsidência ocorreram durante os eventos responsáveis pela formação das bacias intraplaca do tipo rifte: i) fase de pré-rifte, suave subsidência regional; ii) fase de rifte, rápida subsidência local, gerando sistema de graben e/ou meio-graben; e iii) fase pós-rifte, retorno das condições de suave subsidência regional.

Matos (1992, 1999) e Matos et al. (2019, 2021) propuseram que durante o Cretáceo, a ZCPa passou por uma distensão de direção NW-SE, transformando as falhas transpressionais, em falhas normais, dando origem às bacias interiores do Nordeste, retratando um sistema de riftes abortados (Figura 8). Estes autores explanam que a extremidade oeste da ZCPa termina em uma série de falhas curvadas exibindo uma geometria sigmoidal.

Figura 6 - Compartimentação tectônica da Província Borborema. Principais domínios: DMC, Médio Coreaú; DCC, Ceará Central; DRGN, Rio Grande do Norte; DZT, Zona Transversal; DS, Sergipano; DRP, Riacho do Pontal; DPEAL, Pernambuco-Alagoas. CSF, Cráton São Francisco. Zonas de cisalhamento transcorrentes: ZCCG, Campina Grande; ZCPa, Patos; ZCPE e ZCPW, Pernambuco Leste e Pernambuco Oeste, respectivamente; ZCSP, Senador Pompeu; e ZCS, Sobral.

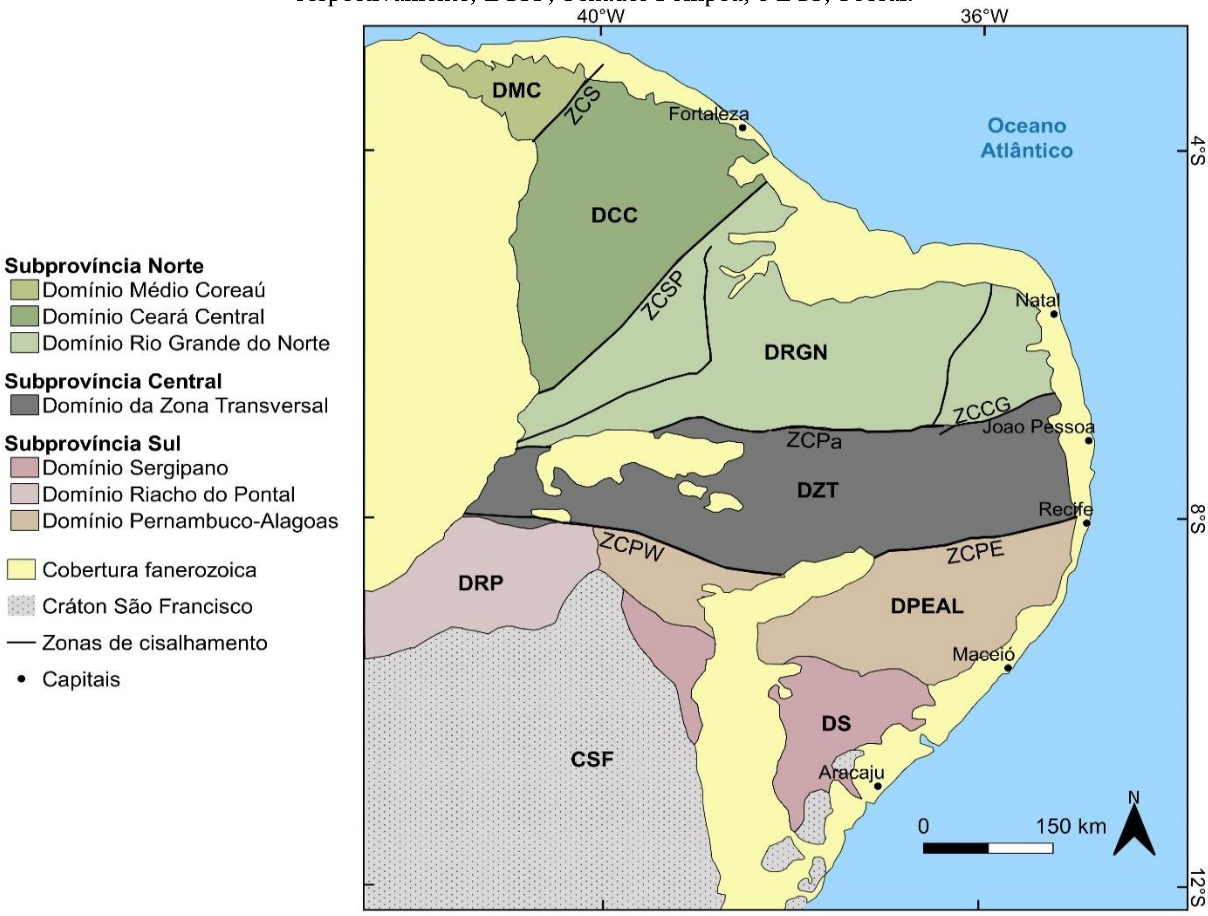

Fonte: Modificado de Van Schums et al. (2008).

Figura 7 - Mapa geológico simplificado da Bacia do Araripe, Nordeste do Brasil. ZCPa, Zona de cisalhamento Patos.

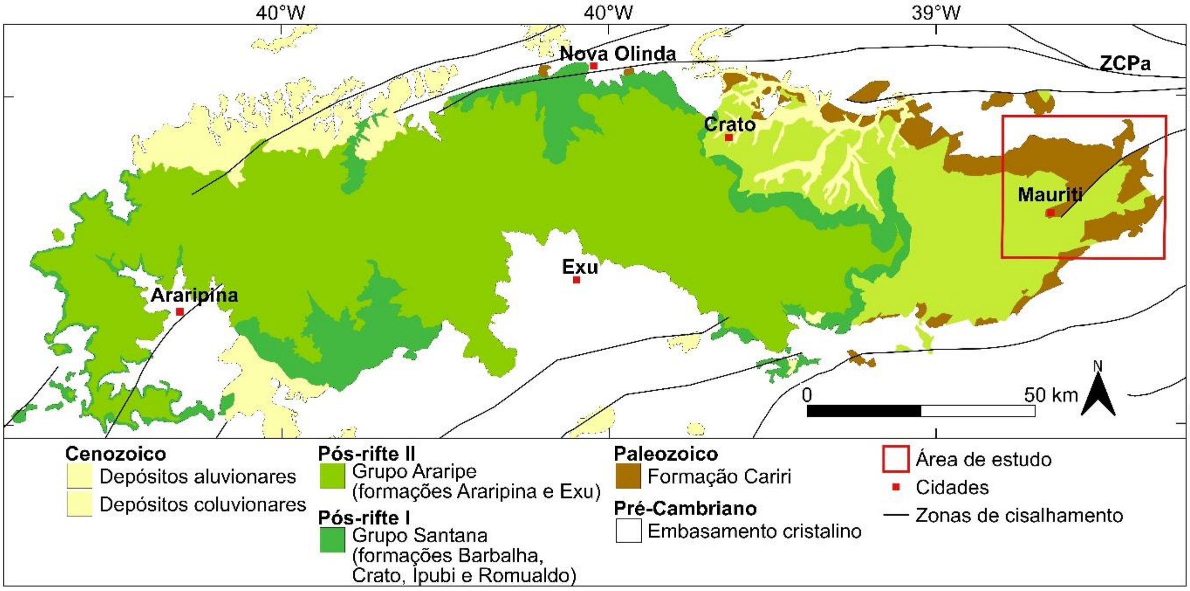

Fonte: Modificado de Angelim et al. (2004).

A evolução tectônica da Bacia do Araripe ainda é motivo de debate, por exemplo o modelo proposto por Miranda et al. (2012, 2014), observando os aspectos geométricos e cinemáticos de anomalias gravimétricas, sugerem que a Bacia do Araripe teria duas fases de evolução tectônica: i) fase I, rifte oblíquo do tipo pull-apart durante Paleozoico; e ii) fase II, rifte distencional durante o Cretáceo. Estes autores sugerem que a ZCPa, que se comporta como falha de borda para a Bacia do Araripe, seria a principal responsável pela formação dessa bacia e de seus depocentros romboédricos. No entanto, durante a fase pós-rifte (Cretáceo Superior ao Cenozoico), a Bacia do Araripe pode ter experimentado uma inversão tectônica, conforme proposto por Marques et al. (2014). Estes autores sugerem que as falhas reversas presentes na bacia foram geradas devido à reativação frágil de zonas de cisalhamento, causada pelo campo de esforço tectônico relacionado à tectônica Andina e da Dorsal Meso-Oceânica. Porém, Peulvast e Betard (2015) sugeriram uma inversão topográfica da Bacia do Araripe durante o pós-rifte relacionada ao soerguimento da Província Borborema, consequentemente, ocasionando processos de erosão diferencial. Desta maneira a topografia atual da bacia estaria relacionada a um soerguimento regional, e não a um processo de inversão tectônica como proposto por Marques et al., (2014). Além disso, Garcia et al. (2019) a partir do método magnetotelúrico, propuseram a presença de uma astenosfera rasa sob a Bacia do Araripe, o que levou ao soerguimento local desta bacia. O modelo mais recente, sugerido por Celestino et al. (2020), obtido a partir da integração de dados topográficos, gravimétricos e dados estruturais de campo, reconhece pelo menos duas fases deformacionais para a evolução tectônica da Bacia do Araripe Dn + 1 (Paleozoico) e Dn + 2 (Cretáceo). Segundo estes autores as zonas de cisalhamento preexistentes no embasamento cristalino (~ 600 Ma) foram reativadas como estruturas frágeis (falhas, fraturas e bandas de deformação) durante o Cretáceo.

A Bacia do Araripe comporta uma série de grabens e *horsts* (Rand e Manso, 1984; Ponte e Ponte Filho, 1996), exibindo estruturas com direções preferencialmente para NE-SW, relacionadas com o rifteamento Cretáceo, orientações E-W, possivelmente, referentes a antigas estruturas influenciados pelas zonas de cisalhamentos Patos e Pernambuco e, orientações NW-SW que estariam representando falhas normais e/ou transcorrentes (Miranda et al., 2020). Esta bacia pode ser dividida, conforme a sua estruturação interna, em duas sub-bacias, separadas pelo Alto estrutural de Dom Leme (Rand e Manso,1984; Ponte e Ponte Filho, 1996; Figura 9): i) Sub-bacia de Feitoria, localizada a oeste do Alto de Dom Leme e, ii) Sub-bacia do Cariri, localizada a leste do Alto de Dom Leme. Castro e Castelo Branco (1999), a partir da modelagem gravimétrica 3D, confirmaram a existência das duas sub-bacias, definindo uma profundidade de até 1.600 m para o topo do embasamento.

O embasamento cristalino da Bacia do Araripe é caracterizado pelas rochas magmáticas e metamórficas Pré-Cambrianas, pertencentes aos terrenos Piancó-Alto Brígida e Granjeiro (Santos et al., 1999; Delgado et al., 2003; Oliveira, 2008; Neves e Alcantara, 2010; Van Schmus et al., 2011). Sendo sua borda leste representada pelas rochas metavulcanicassedimentares do Grupo Cachoeirinha, com idade de deposição entre o Criogeniano e Ediacarano, intrudido pelos granitoides neoproterozoicos, classificados para este setor, como calcioalcalinos (Tipo Conceição) e K-Calcioalcalino (Tipo Itaporanga) (Sial, 1986; Ferreira et al., 2004; Medeiros, 2004; Sial e Ferreira, 2016). O Grupo Cachoeirinha, composto por metapelitos e metarenitos, pode ser dividido na Formação Santana dos Garrotes, onde estas rochas apresentam níveis de metavulcânicas ácidas, formações ferríferas, metacarbonatos e raros metaconglomerados, e na Formação Serra do Olho D'Água, porção superior deste grupo, constituída, em sua porção superior, por metaconglomerados polimíticos e polimodais (Medeiros, 2004). Já os granitóides calcialcalinos e os K-Calcialcalinos, são biotita granodioritos a tonalitos, e granitos e quartzo monzonitos porfiriticos, neste setor leste, marcam o segundo pulso do magmatismo granítico na Província Borborema, entre 590-560 Ma (Sial, 1986; Ferreira et al., 2004).

Figura 8 - Evolução tectônica para as bacias do Vale do Cariri ilustrando a reativação de pequenos seguimentos da porção oeste da Zona de Cisalhamento Patos e formação das bacias interiores (Cretáceo). As setas vermelhas indicam a orientação do movimento dos blocos. A) Modelo da extensão NW-SE ao longo da zona de cisalhamento pré-existente. B) Distribuição e configuração tectônica das bacias interiores do tipo rifte. Bacias interiores: BA, Bacia do Araripe; BI, Bacia de Iguatú; BRP, Rio do Peixe. ZCPa, Zona de Cisalhamento Patos.

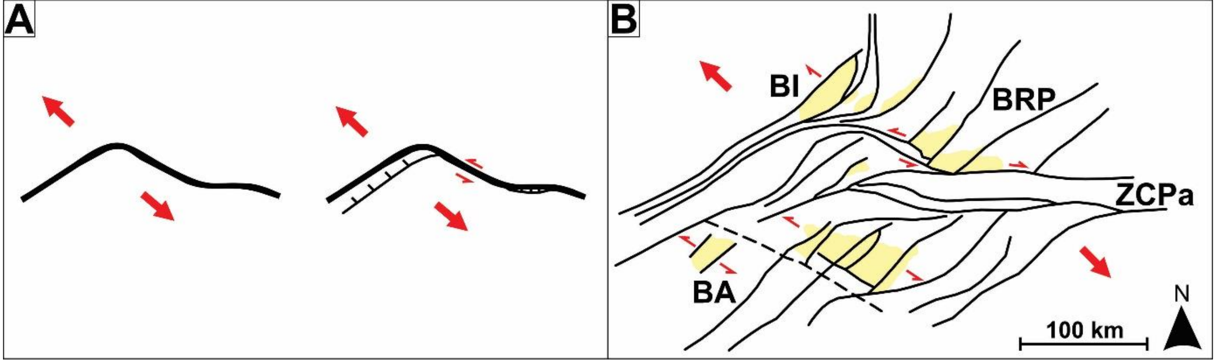

Fonte: Modificado de Matos (1992).

Figura 9 - Estruturação interna da Bacia do Araripe. Ilustrando a posição das sub-bacias: Feitoria e Cariri. ZCPa, Zona de Cisalhamento Patos.

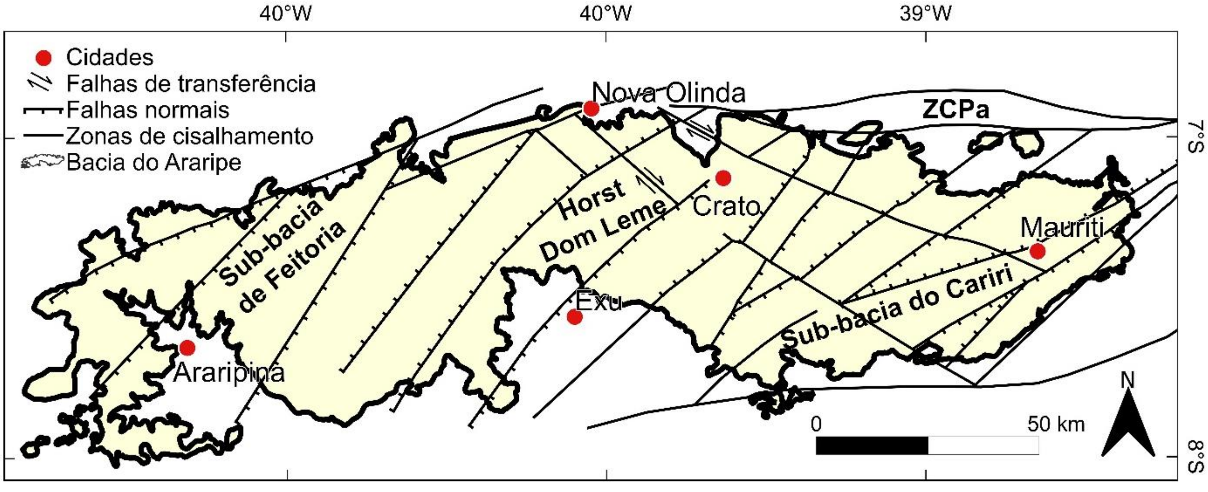

Fonte: Modificado de Ponte e Ponte Filho (1996).

3.1 ESTRATIGRAFIA

A cobertura sedimentar da Bacia do Araripe (Figura 7) é representada por discordâncias regionais e hiatos deposicionais (Assine, 1992, 1997; Ponte e Ponte Filho, 1996; Scherer et al., 2014), várias cartas estratigráficas foram propostas e modificadas ao longo da evolução dos conhecimentos sobre a bacia como por exemplo as propostas de Ponte e Appi (1990), Assine (2007), Assine et al. (2014). Quatro supersequências são descritas para a Bacia do Araripe (Neumann, 1999; Assine, 2007; Assine et al., 2014): i) sequência Paleozoica, fase sinéclise intracratônica, representada pela Formação Cariri; ii) sequência pré-rifte, constituída pelas formações Brejo Santo e Missão Velha, pertencentes ao Grupo do Vale do Cariri (Neojurássico); iii) sequência rifte, representada pela Formação Abaiara, pertencente ao Grupo do Vale do Cariri (Eocretáceo); e iv) sequência pós-rifte, representada pelas formações do Grupo Araripe, subdividida em pós-rifte I, representada pelas formações Barbalha e Santana (Eocretáceo) e, pós-rifte II constituída pelas formações Araripina e Exú (Eocretáceo-Neocretáceo). Assine et al. (2014) incorporam para toda a sequência pós-rifte I, a elevação hierárquica do Grupo Santana (Neumann, 1999), composto, da base para o topo, pelas formações Barbalha, Crato, Ipubi e Romualdo.

A região da borda leste da Bacia do Araripe acomoda as rochas das formações Cariri, Brejo Santo, Missão Velha e Abaiara (Figura 10), descritas brevemente, nos tópicos a seguir. Porém, esta pesquisa teve interesse na investigação da deformação presente nas rochas pertencentes ao embasamento cristalino e a Formação Cariri, sequência basal da cobertura sedimentar.

Figura 10 - Mapa geológico da borda leste da Bacia do Araripe, Nordeste do Brasil.

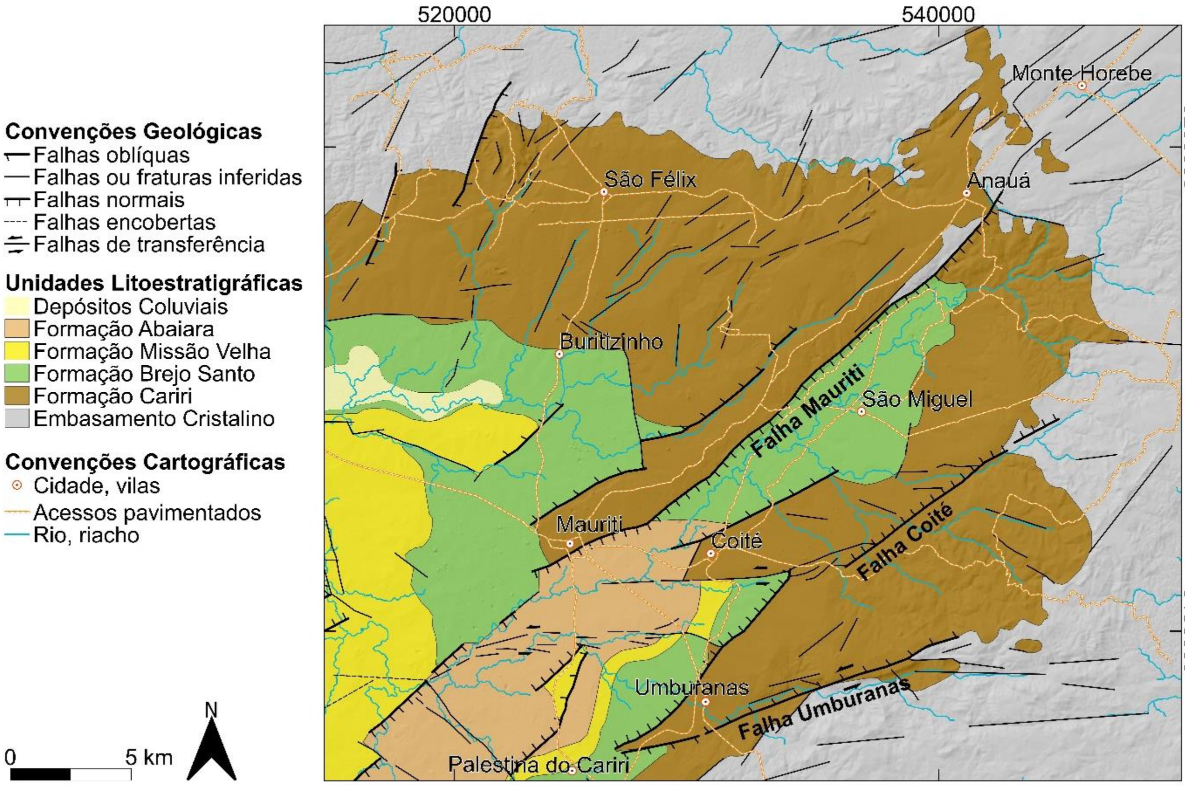

Fonte: Modificado de Cardoso (2010).

3.1.1 Formação Cariri

A Formação Cariri nomeada por Beurlen (1962), compreende uma unidade afossilífera, de idade Paleozoica, com deposição iniciada após o Cambriano (~509-486 Ma), provavelmente estendendo-se até o Ordoviciano (Assine, 1992, 2007; Cerri et al., 2022). Esta formação é correlata ao Grupo Serra Grande da Bacia do Parnaíba e com a Formação Tacaratu da Bacia do Jatobá (Assine, 1992, 2007).

A Formação Cariri é interpretada por Assine (1992, 2007), como fácies de sistemas fluviais entrelaçados, composta por arenitos imaturos, de granulação média a muito grossa, com grãos angulares a subangulares. Ainda segundo este autor, esta formação apresenta níveis de ortoconglomerados, que incluem fragmentos líticos do embasamento e clastos de feldspatos róseos bem preservados. Estes níveis conglomeráticos são observados, principalmente, na base da Formação Cariri, enquanto que, para o topo desta formação, podem ser notados arenitos com intercalações de níveis siltosos de tons claros a arroxeados (Assine, 2007; Silvestre et al., 2017). A Formação Cariri exibe estratificações cruzadas acanaladas e tabulares com *sets* decimétricos a métricos. (Cardoso, 2010; Silvestre et al., 2017).

3.1.2 Formação Brejo Santo

A Formação Brejo Santo de idade Neojurássica, foi originalmente denominada por Gaspary e Anjos (1964). Esta formação é caracterizada pela presença de ostracodes típicos do Andar Dom João, representando o início do rifte na Bacia do Araripe (Assine, 1992, 2007). A presença de formas exclusivamente não-marinhas indica uma sedimentação lacustre, com águas calmas e rasas, e com condições, predominantemente, oxidantes tornando o ambiente propício à formação de *red beds* (Assine, 2007).

A Formação Brejo Santo é constituída por folhelhos e lamitos, vermelhos ou arroxeados, podendo ainda, apresentar níveis esverdeados ou esbranquiçados (Assine, 2007; Cardoso, 2010). Embora sejam raros afloramentos bem preservados desta formação, devido a sua composição, os folhelhos da Formação Brejo Santo podem ainda apresentar concreções e níveis arenosos calcíferos (*e.g.,* Silvestre et al., 2017).

3.1.3 Formação Missão Velha

A Formação Missão Velha (Beurlen, 1962), também de idade Neojurássica, se sobrepõe concordantemente a Formação Brejo Santo, esta formação é marcada por abundantes troncos e fragmentos de madeira silicificada (Assine, 2007). Sua associação faciológica é classificada como sistema fluvial entrelaçado, caracterizados por canais rasos e de alta energia (Assine, 2007; Fambrini et al., 2011) e como sistemas fluviais meandrantes, por apresentar depósitos de planície de inundação (Fambrini et al., 2011).

Esta formação é composta por arenitos quartzosos, por vezes feldspáticos e/ou cauliníticos, localmente conglomeráticos, que podem apresentar níveis de siltitos arroxeados (Assine, 2007). Podem exibir estruturas sedimentares como estratificação cruzada planar e/ou acanalada (Assine, 2007; Cardoso, 2010)

3.1.4 Formação Abaiara

A Formação Abaiara de idade Neocomiana, registra o estágio rifte na Bacia do Araripe. Esta formação possui significativa variação faciológica lateral e vertical, composta desde folhelhos até conglomerados (Assine, 1992, 2007). Estas associações faciológicas e o seu conteúdo fossilífero (madeira fossilizada silicificada, escamas de peixe e ostracodes) indicam que a sedimentação ocorreu em tratos deposicionais continentais substituídos, gradualmente, por planícies fluviais de canais entrelaçados (Assine, 2007).

Os arenitos estão associados, predominantemente, a gradações normais, com estratificações cruzadas tabular, acanalada e convoluta, enquanto os pelitos são constituídos por *red beds* estratigraficamente semelhantes aos da Formação Brejo Santo (Fambrini et al., 2019).

4 RESULTADOS

Os resultados desta dissertação encontram-se na forma de artigos científicos. O primeiro artigo está intitulado: *QUANTIFICATION OF THE SPATIAL ARRANGEMENT OF STRUCTURAL LINEAMENTS AND DEFORMATION BANDS: IMPLICATIONS FOR THE TECTONIC EVOLUTION OF THE EASTERN BORDER OF THE ARARIPE BASIN, NE BRAZIL*. Este artigo trata da quantificação estrutural de lineamentos regionais e bandas de deformação da Formação Cariri, borda leste da Bacia do Araripe. Publicado no Journal of South America Earth Science.

O segundo artigo é intitulado*: FAULT GEOMETRY CHARACTERIZATION ASSESSED BY EULER DECONVOLUTION SOLUTION: INSIGHTS FROM THE ARARIPE BASIN EASTERN BORDER, NE BRAZIL*. Este artigo investiga a geometria das principais zonas de falhas da borda leste da Bacia do Araripe. Artigo submetido ao Journal of South America Earth Science.

4.1 QUANTIFICATION OF THE SPATIAL ARRANGEMENT OF STRUCTURAL LINEAMENTS AND DEFORMATION BANDS: IMPLICATIONS FOR THE TECTONIC EVOLUTION OF THE EASTERN BORDER OF THE ARARIPE BASIN, NE BRAZIL

Quantification of the spatial arrangement of structural lineaments and deformation bands: implications for the tectonic evolution of the eastern border of the Araripe Basin, NE Brazil

Vivian Silvani de Arruda Passos[1], Tiago Siqueira de Miranda[2], Jefferson Tavares Cruz Oliveira[2], Maria Alcione Lima Celestino[1], Rodrigo Corrêa[3,4], João Gabriel Topan[1]; Thiago da Cruz Falcão[5]

[1]Geosciences Graduate Program, Federal University of Pernambuco, Recife, PE, 50740-530, Brazil (vivian.silvani@gmail.com, alcionelimma22@gmail.com, joao.gabrieltopan@ufpe.br)

[2]Department of Geology, Federal University of Pernambuco, Recife, PE, 50740-530, Brazil (tiago.smiranda@ufpe.br, jefferson.tavares@ufpe.br)

[3]Department of Geological Sciences, University of Texas at Austin, Austin, TX 78712, USA (rodrigo.correa@utexas.edu)

[4]Petrobras S.A., Avenida Henrique Valadares, 28, Rio de Janeiro, RJ, 20231-030, Brazil (rodrigo.correa@petrobras.com.br)

[5]Petrobras Research Center (CENPES), Rio de Janeiro, 21941-915, Brazil (tfalcao@petrobras.com.br)

Abstract

Spatial arrangement regards the spatial position of brittle structures. Even though they are important for several industrial applications, quantification of their spatial arrangement remains a challenge. In this contribution, we quantify and compare the spatial arrangement of regional lineaments and deformation bands in the Eastern Araripe Basin, NE Brazil using the normalized correlation count method on topographic, aeromagnetic, and outcrop data. We have noticed irregular and random arrangements of topographic and aeromagnetic clusters of lineaments, while deformation bands are grouped. The use of topographic and aeromagnetic data represents a reliable way to investigate regions with limitations (topographic, climatic, or social) that make field data hard or impossible to acquire. Furthermore, we proposed a preliminary tectonic evolution model for the eastern border of the Araripe Basin.

Keywords: Magnetic and topographic lineaments; brittle deformation; deformation bands; aeromagnetic; normalized intensity; normalized correlation count

1. Introduction

One way to characterize regional fault zones is to combine the use of large scale topographic and aeromagnetic data with local outcrop survey structural data (e.g., Boyce and Morris, 2002; Kinabo et al., 2008; Airo and Wennerström, 2010; Araújo Neto et al., 2018; Celestino et al., 2018, 2020). Regional scale topographic and aeromagnetic data provide information about surface morphology and magnetic trends (Kinabo et al., 2008; Barbosa et al., 2021) in the crystalline basement and sedimentary basins (Boyce and Morris, 2002; Kinabo et al., 2008; Airo and Wennerström, 2010). Aeromagnetic data can also identify subsurface structures based on variations in the geomagnetic field, which results from differences in the magnetic content of the associated rocks (e.g., Castro et al., 2014). Integration of topographic and aeromagnetic data is considered effective in revealing areas of potential mineralization involved in hydrothermal processes (Sanusi and Amigun, 2020; Abdelkareem et al., 2018) and complement geological mapping in areas where it is not feasible. Furthermore, remote sensing techniques and geophysics are useful tools that are gaining attention because they are efficient for understanding geological processes, saving financial resources, and optimizing data acquisition time (e.g., Meixner et al., 2018; Sanusi and Amigun, 2020; Soliman and Han, 2019). Products derived from topographic data are particularly effective for structural analysis, which is applicable in different areas (Soliman and Han, 2019). Likewise, geophysical data provides information to improve the understanding of regional structural networks, filling this important category of geological observation (Sanusi and Amigun, 2020). However, identifying brittle fault zones in images remain a challenge because fault traces are typically difficult to recognize due to their discontinuous aspect and complex arrangement (e.g., Meixner et al., 2018).

The position of structures in space defines the heterogeneity and anisotropy in a volume of rocks, which is important to identify how the deformation can affect, for example, the fluid flow in a naturally fractured reservoir (Kinabo et al., 2008; Laubach et al., 2018a; Li et al., 2018; Wang et al., 2019). Understanding the spatial arrangement of brittle structures is crucial to improve modeling of CO2 storage, subsurface fluid flow, including groundwater and hydrocarbon production, and hydrothermal economic mineral deposits (Harris et al., 2003; Zhang et al., 2015; Laubach et al., 2018a; O'Hara et al., 2017; Fletcher et al., 2020; Torabi et al., 2020). The concept of the spatial arrangement of brittle structures refers to faults, deformation bands or fracture positions in space. The understanding of the spatial organization of structures can reveal their pattern, even for potentially predictable arrangements or arrangements that have no organization, implying a statistically indistinguishable arrangement random positioning (Marrett et al., 2018). In the last two decades, several statistical methods have been used to understand brittle fault zone arrangements (Harris et al., 2003; Riley et al., 2010; Lin and Yamashita, 2013; Choi et al., 2016; O’Hara et al., 2017; Balsamo et al., 2019; Martinelli et al., 2020; Hansberry et al., 2021). However, each method has limitations, either related to the data quality itself or because it does not allow for an understanding of the entire tectonic evolution of the fault over time (Torabi et al., 2020). Techniques able to identify complex hierarchical arrangements, such as the normalized correlation count (Marrett et al., 2018) can characterize and quantify the spatial arrangement of brittle structures and describe the size of fracture clusters, which has potential applications to improve discrete fracture network models and numerical simulations (Miranda et al., 2018).

In this study, we collected field structural data and regional scanlines on the eastern border of the Araripe Basin, northeastern Brazil (Fig. 1) to analyze how well indirect methods like topography and aeromagnetic data can identify the position and spatial arrangement of brittle structures. This sector of the basin accommodates several structural lineaments, including the Mauriti, Coité, and Umburanas faults, which strike NE-SW. Our results show that the topography has been imprinted to some degree by the brittle deformation, preserving position and orientation of structures and that aeromagnetometry was only able to preserve orientation accurately. The spatial arrangement of topographic, aeromagnetic lineaments, and deformation bands obtained from outcrops are different, suggesting that the observation scale and resolution can affect the resulting spatial analysis. Furthermore, we propose a model that explains how the sets of lineaments and deformation bands are integrated within the regional tectonic framework.

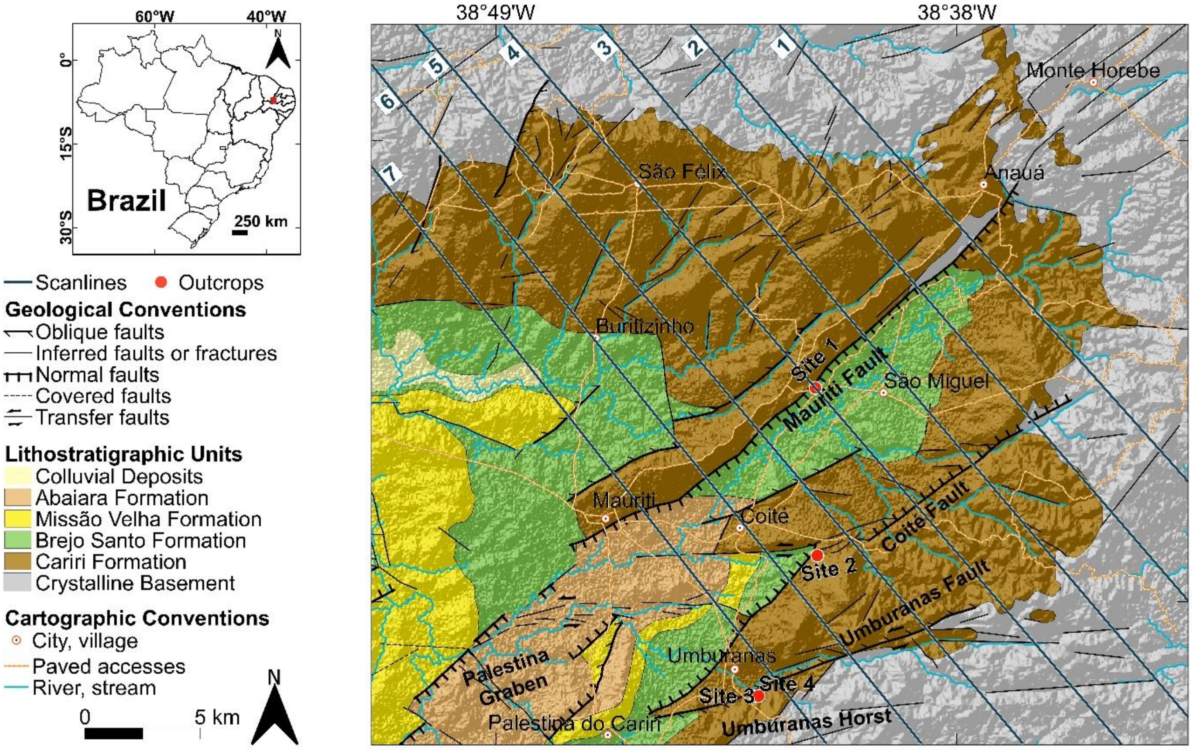

Figure 1. Geological map of the eastern border of the Araripe Basin, northeastern Brazil, showing the regional scanlines and outcrops sites 1, 2, 3, and 4. Modified from Cardoso, 2010.

2. Geological Settings

The Araripe Basin represents one of the most important intraplate basins of northeastern Brazil (Assine, 1992, 2007; Celestino et al., 2020). This basin is located in the Central Domain of the Borborema Province, between the Patos Shear Zone (PASZ) to the north and the West Pernambuco shear zone (WPSZ) to the south (Fig. 2). The Precambrian rocks of the Granjeiro and Piancó-Alto Brígida terranes (Santos et al., 1999; Oliveira, 2008; Neves and Alcantara, 2010; Van Schmus et al., 2011) represent the pre-Cambrian basement of the Araripe Basin.

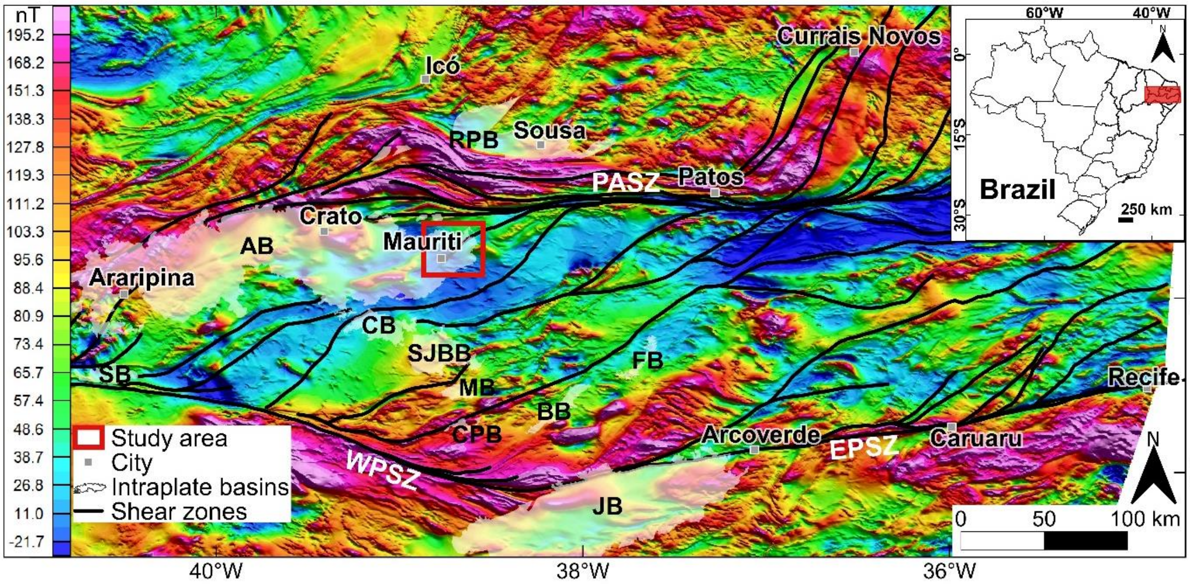

Figure 2. Aeromagnetic anomaly map reduced to the pole with the location of the intraplate basins of Northeast Brazil. The red square marks the study area. Shear zones: PASZ, Patos; EPSZ, East Pernambuco; WPSZ, West Pernambuco shear zone. Intraplate basins: AB, Araripe Basin; JB, Jatobá Basin; FB, Fátima Basin; SJBB, São José do Belmonte Basin; CB, Cedro Basin; RPB, Rio do Peixe Basin; MB, Mirandiba Basin; SB, Socorro Basin; BB, Betânia Basin; CPB, Carnaubeira da Penha Basin.

The tectonic origin of the Araripe Basin is conditioned by the fragmentation events of the Gondwana Supercontinent and the opening of the Atlantic Ocean (Matos, 1999, 2000). The structural inheritance of the basement structures plays an important role in the evolution and geometry of the intraplate basins of northeastern Brazil, by mostly triggering reconfiguration of their depocenters (Assine, 2007; Scherer, et al., 2014). Matos (1992, 1999) and Matos et al. (2020, 2021) proposed that during the Cretaceous, the PASZ underwent NW-SE distension, transforming transpressional faults into normal faults and giving rise to the basins of the northeast in a rift system, later aborted. These authors explained that the west end of the PASZ splays in a series of curved faults exhibiting sigmoidal geometry.

The Araripe Basin has been the focus of several studies that propose different models for its tectonic evolution. For example, the model proposed by Miranda et al. (2012, 2014), observing the geometric and kinematic aspects of gravimetric anomalies, suggests that this basin had two tectonic phases: phase I, a pull-apart rift during the Paleozoic; and phase II, an oblique rift during the Cretaceous. These authors suggested that the PASZ played an important role in the evolution of the basin, by shaping its fault borders and the rhombohedral depocenters. The most recent model suggested by Celestino et al. (2020), obtained from the integration of topographic, aerogeophysical, and field data, recognizes at least three deformational phases for the tectonic evolution of the Araripe Basin: Dn (Neoproterozoic), Dn+1 (Paleozoic), and Dn+2 (Cretaceous). Additionally, it has been proposed that the Araripe Basin could have experienced a Late Cretaceous to Cenozoic tectonic inversion during the post-rift phase (Marques et al. 2014). These authors suggested that the reverse faults present in the basin were generated due to brittle reactivation of shear zones, caused by the far-field stress related to the Andes and Mid-Ocean Ridge pushes. However, Peulvast and Betard (2015) suggested a topographic inversion of the Araripe Basin during the post-rift related to the uplift of the Borborema Province, consequently causing differential erosion processes. Alternatively, Garcia et al. (2019) proposed a shallow asthenosphere under the Araripe Basin, which led to the local uplift of this basin. Thus, the tectonic evolution of the Araripe Basin is still a matter of debate.

The stratigraphy of the Araripe Basin has been traditionally divided into pre-, syn-, and post-rift 1 and 2 sequences (Neumann, 1999; Assine, 2007; Assine et al., 2014) (Fig. 1). In this study, the pre-rift sequence is defined as the Paleozoic Cariri Formation (Cambrian-Ordovician) (Cerri et al., 2022) and the Middle to Late Jurassic Brejo Santo and Missão Velha

Formations. The rift sequence comprises the Early Cretaceous Abaiara Formation. Lastly, the post-rift sequence (Aptian-Cenomanian) is defined as the Barbalha, Crato, Ipubi, and Romualdo formations, which represents the post-rift 1, and the Exú Formation, representing the post-rift 2. However, no outcrops to the post-rift tectonic sequence appear in the study area. In this work, we characterized the structures in the Cariri Formation, which represents the most important lithostratigraphic unit of the eastern border of the Araripe Basin (Fig. 1). This formation is represented by immature sandstones, medium to very coarse-grained, with angular to subangular grains, composed of levels of orthoconglomerates, which include lithic basement fragments and well-preserved pink feldspar clasts (Assine, 2007; Cerri et al., 2022). These conglomeratic levels are mainly observed at the base of the Cariri Formation, while towards the top of this formation, sandstones with intercalations of silty levels of clear to purplish tones can be noted (Assine, 2007; Silvestre et al., 2017). The Cariri Formation shows tabular cross-stratification with decimetric to metric sets (Silvestre et al., 2017), interpreted by Assine (1992, 2007) as an intertwined fluvial depositional system facies.

The studied area is on the eastern border of the Araripe Basin, where the Mauriti, Umburanas, and Coité faults are located (Fig. 1). The Mauriti Fault was previously classified by Cardoso (2010) as a normal fault, which borders the northwest part of the Palestina Graben (filled mainly by the Abaiara Formation, in the region under study occurs partially occupying the southwestern portion (Fig. 1). This author also points out secondary faults in the southeast border of this graben, close to the Umburanas Horst (located partially in the southeast portion (Fig. 1). These structures were classified as normal and oblique faults and named Coité and Umburanas faults (Cardoso, 2010).

3. Datasets and Methods

3.1. Digital elevation model

Our topography database is the Shuttle Radar Topography Mission (SRTM) satellite images, with a spatial resolution of 30 m obtained via the site https://gdex.cr.usgs.gov/gdex/.

We created digital elevation models (DEM) with an insolation altitude of 45º and lighting azimuths of 0°, 45º, 90º, and 315º for the eastern border of the Araripe Basin (e.g., Wise et al., 1985; Salamuni et al., 2004; Grohmann et al., 2011a, 2011b; Jacques et al., 2014; Cianfarra and Salvini, 2015; Lima and Sá, 2017; Meixner et al., 2018; Araújo Neto et al., 2018; Celestino et al., 2020). DEM allows highlighting structures that are nearly orthogonal to the lighting directions (0º, 45º, 90º, and 315º), enhancing the identification of topographic lineaments (Wise et al., 1985; Drury, 2001; Grohmann et al., 2011a; Jacques et al., 2014; Lima and Sá, 2017). Our interpretation of lineaments is based on a visual approach using DEM. For that, we examine the lineaments with representative dimensions larger than a kilometer, the topographic lineaments do not necessarily need to be visualized in the four lighting scenarios. However, these lineaments need to be verified on the topographic map (obtained via orbital multispectral images) (e.g., Lima and Sá, 2017; Meixner et al., 2018). This approach allows us to indicate significant lineaments, with dimensions that stand out, which may be reproducing fault zones.

Basin and basement topographic lineaments were divided into two groups: valleys and crests. Using the software QGIS 3.10.3 (https://qgis.org/en/site/forusers/download.html), we produced rose diagrams for each DEM azimuth (0º, 45º, 90º, and 315º) with a bin size of 10º, separated according to the sector (basin or basement) and the parameter (crest or valley), to analyze the orientation patterns of the interpreted lineaments (e.g., Celestino et al., 2018; 2020).

3.2. Orbital multispectral images

We acquired high spatial resolution orbital multispectral images (0.31 to 0.6 m depending on which satellite acquired the image) from the DigitalGlobe company via Google Earth PRO v. 7.3.2.5491, containing colored compositions of sensor bands such as GeoEye-1 and WorldView-2 to 4.

Multispectral images are fundamental, mainly, for the validation of the existence of topographic lineaments making it possible to exclude artifacts from the DEM analysis, regardless of the lighting used (e.g., Lima and Sá, 2017). It also allows for the inclusion of some topographic lineament that has not been verified in the DEM analysis. We used orbital multispectral images, as auxiliary data, to assist in the interpretation of drainage networks, lineaments, and morphology (e.g., Grohmann et al., 2011a; Nicolas and Clayton, 2015; Lima and Sá, 2017; Meixner et al., 2018; Araújo Neto et al., 2018).

3.3 Aeromagnetic data

We also used aeromagnetic data to map lineaments in the study area. We obtained the aeromagnetic data from the database of the Brazilian Geological Survey (http://geosgb.cprm.gov.br/). These magnetic data were acquired from N-S flight lines and control E-W lines, with a spacing of 500 m and 10 km, respectively. Data processing was performed with Oasis Montaj software 9.1 to remove noise without affecting the signal. The processing was divided into four stages: i) analyzing the noise level (for example, spike identification and removal); ii) removal of the International Geomagnetic Reference Field; iii) use of directional cosine and Butterworth filters to remove artifacts from leveling (Pilkington and Roest, 1997); and iv) interpolation by the bidirectional method with a cell size of 125m (Reeves, 2005).

From the map of the anomalous magnetic field that was generated, an upward continuation filtering was applied at an altitude of 500 m. Then, the pole reduction technique was applied, which aims to centralize the peaks of anomalies (positive amplitude signatures) on their sources (Baranov, 1957). Finally, a regional/residual Gaussian filter was used to interpret shallow and deep sources (Li and Oldenburg, 1998). The application of this filter is made through the cutoff point (k_o) made from the analysis of the power spectrum. The wavenumber (k_o) used was 0.11 cycle/km, corresponding to the limit between the deepest sources, referring to basement structures (depth between 2 to 3 km) and the shallower that can be associated, mainly, with the brittle roof of the basin and the basement (depth between 500 m and 2 km). We used the regional-residual filtration for magnetic anomalies and magnetic anomalies reduced to the pole to highlight shallow residual aeromagnetic anomalies with depths from 500 m to 2 km.

The magnetic lineaments were interpreted in the residual aeromagnetic map and the reduced aeromagnetic map to the residual pole, using the borders and centers of the anomalies as interpretation criteria, respectively. QGIS 3.10.3 software was used to generate the rose diagrams of interpreted lineaments with a bin size of 10º. These graphs helped to reveal the orientation patterns of the magnetic lineaments of the eastern border of the Araripe Basin in the basin and crystalline basement sectors.

3.4. Scanline acquisition

The scanline method consists of measuring the position of structures along a line perpendicular to their strike (e.g., Ortega et al. 2006). We acquired scanlines in two different scales: i) regional, using the lineament interpretation from topographic and aeromagnetic regional data, and ii) outcrop scale, using data acquired in selected outcrops close to the faults in the study area. Following the methods developed over the past 25 years (Priest, 1993; Marrett, 1996; Marrett et al., 1999; Gomez and Laubach, 2006; Ortega et al., 2006; Gale et al., 2007; Guerriero et al., 2010; Lu et al., 2017; Miranda et al., 2018), we measured the spacing between the structures along each scanline. Where spacing is defined as the distance between neighboring lineaments (e.g., Hooker et al., 2018).

For the regional scale, we acquired seven scanlines NW-SE (from 27 to 45 km long) perpendicular to the Mauriti Fault (Fig. 1). We used two groups of lineaments separately: i) topographic (DEM and multispectral images), including all topographic lineaments in different directions, filtering those that are repeated so that the repeated count of these lineaments does not occur, and ii) aeromagnetic anomaly (residual and reduced to the pole), considering all aeromagnetic lineaments obtained, except those lineaments of the same direction that are repeated.

For the outcrop analysis, we acquired four scanlines (from 5.7 to 58 m long) at four key outcrops (sites 1, 2, 3, and 4) (Fig. 1) of the Cariri Formation. We aligned the scanline direction perpendicular to the preferential orientation of the deformation bands. Therefore, these scanlines are oriented WNW-ESE (sites 1, 2, and 4) and E-W (Site 3). We selected these outcrops because they are located close to the structural positions of Mauriti (site 1), Coité (site 2), and Umburanas (sites 3 and 4) fault zones (Fig. 1). We quantified the orientation, thickness, and spacing (perpendicular distance) of deformation bands (Ortega et al., 2006; Santos et al., 2015a; Miranda et al., 2018) through a scanline obtained for each outcrop (sites 1 (with 5.7 m extension), 2 (with 58 m extension), 3 (with 9.9 m extension), and 4 (with 9.9 m extension)). We used a measuring tape lying on the ground to get positions. We measured the thickness of deformation bands using a 10x hand lens and a comparator (Ortega et al., 2006). We acquired orientation of structures using geological compasses such as Clar and Brunton, and Fieldmove Clino and StereoNet mobile applications.

3.5. Spatial arrangement analysis

We used the software CorrCount (Marrett et al. 2018) to analyze the spacing dataset (regional lineaments and deformation bands) with the normalized fracture intensity plots and the normalized correlation count (NCC) technique. The NCC technique provides a quantitative way to distinguish between even spacing (periodic or anti-clustered), clusters arising due to random arrangement, and nonrandom clustering (Marrett et al., 2018; Laubach et al., 2018b; Li et al., 2018). The NCC uses length scales to characterize spatial arrangement and may increase or decrease, sometimes following a power law (Marrett et al., 2018). Wang et al. (2019) highlight that NCC data is more accurate in identifying and quantifying spacing patterns. To have statistical significance, the peaks and valleys must exceed the confidence limits; otherwise, the data indicates a random arrangement (Marrett et al., 2018). Marrett et al.

(2018) establish the interpretive parameters for the behavior of the clusters equivalent to the features of the NCC curves, and it is possible to verify combinations of parameters along the same scanline. In this case, the NCC plot shows that the curves are mostly within the 95% confidence limit, it suggests a random arrangement of regional lineaments. Some length scales are more common, and so eventually the NCC curve plots above the 95% or 68% confidence limit. Sometimes the NCC exhibits a wavy pattern suggesting localized regular spacing. For outcrop data, a large part of the NCC curve extrapolates the confidence limits of 68% and 95% with patterns that suggest a regular clustered spacing.

The CorrCount provides analytical and Monte Carlo solutions to quantify statistical uncertainty of random spatial arrangements (Marrett et al. 2018; Santos et al., 2015a, 2015b), using 95% and 68% confidence intervals. If the NCC curve or intensity curve plots outside the upper or lower confidence limits, the corresponding spatial arrangement is statistically significant and distinct from the random arrangement (Marrett et al., 2018; Laubach et al., 2018b; Miranda et al., 2018).

The CorrCount software also calculates the coefficient of variation (CV), since $CV = \sigma / \mu$, where σ is the standard deviation and μ is the arithmetic mean of spacings. CV increases proportionally to the increase in spacing irregularity (Gillespie et al. 1999; Hooker, et al., 2018). Thus, CV=0 reveals perfectly periodic structure spacing; a CV~1 indicates randomly arranged structures; CV > 1, more grouped structures, indicating clustering; and CV < 1, less grouped structures, indicating anti-clustering. Both of these techniques make it possible to quantify the presence of random, clustered or regular spatial arrangements in scanlines.

4. Results

4.1. Regional scale

4.1.1. Topographic lineaments

The topographic lineaments of the eastern border of the Araripe Basin show the following preferential directions: i) in the 0º lighting, the basin sector presents E-W (crest) and ENE-WSW (valley) trends, and the basement sector trends E-W (crests and valleys) (Fig. 3A); ii) in the 45º lighting, the main trend in the basin sector is NW-SE (crests and valleys) and in the basement sector, NW-SE (crests) and E-W (valleys) (Fig. 3B); iii) in the 90º lighting, the basin sector trends N-S (crests and valleys), and the basement trends N-S (crests) and ENE-WSW (valleys) (Fig. 3C); and iv) in the 315º lighting, the basin sector mainly trends NE-SW (crests and valleys), and the basement sector trends NE-SW (crests) and ENE-WSW (valleys) (Fig. 3D). In summary, the basement lineaments primarily trend E-W and NE-SW, and the basin sector primarily trends NE-SW and NW-SE.

In general, we have that in the basin sector the preferential orientations of the crests and valleys coincide. However, in the basement sector, under 45° and 90° lighting, we found discrepancies between the orientations of the crests and valleys. This is observed in lineaments which show NW-SE (crests) and E-W (valleys) orientation for 45° lighting, and preferred orientation N-S (crests) and ENE-WSW (valleys) for 90° lighting.

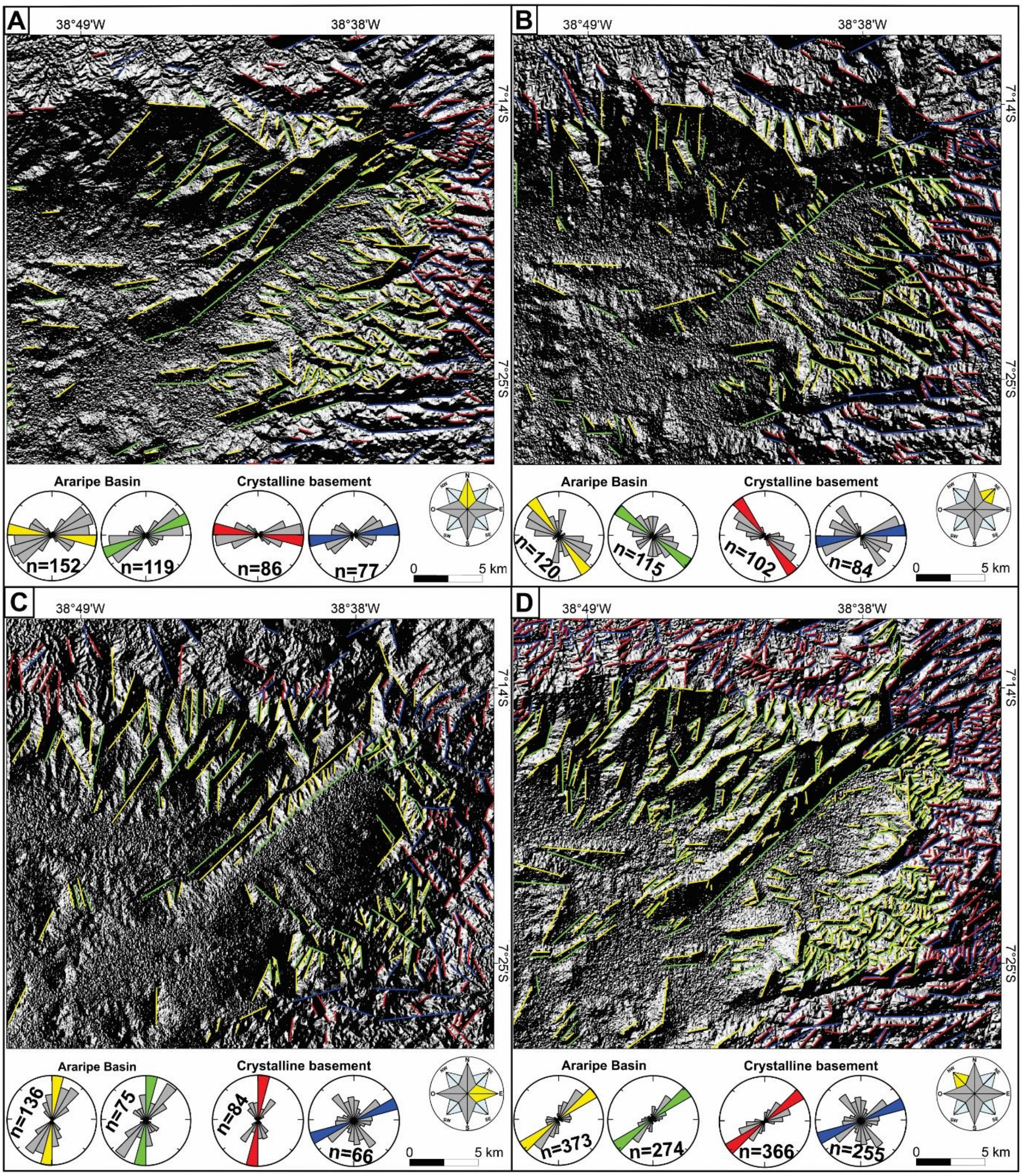

Figure 3. Digital elevation model of the eastern border of the Araripe Basin using SRTM (Shuttle Radar Topography Mission) data, with 45° altimetric insolation in four directions, with their respective rose diagrams: A) 0º lighting; B) 45º lighting; C) 90º lighting; D) 315° lighting. In the basin sector, crest lineaments are marked in yellow and valley lineaments are marked in green. In the crystalline basement sector crest, lineaments are red and valley lineaments are blue. n = number of lineaments.

4.1.2. Aeromagnetic lineaments

The study area reveals a residual magnetic anomaly (Fig. 4A) ranging between -0.37 and 0.23 nT, and residual magnetic anomalies reduced to the pole (Fig. 4B) range between -0.39 and 0.31 nT. The high magnetic anomalies are mainly elongated and show two principal orientations: a) E-W, and b) ENE-WSW, for both basement and basin sectors. Locally, in the aeromagnetic map reduced to the residual pole, we also observed NW-SE anomalies, occurring mainly in the basement sector.

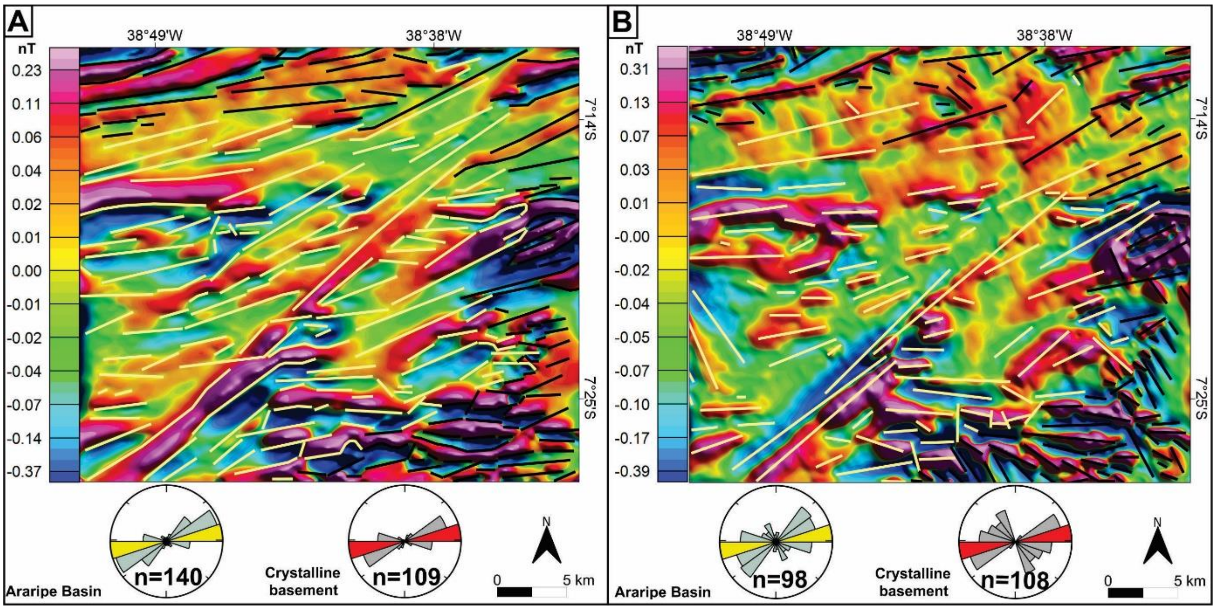

Figure 4. Residual aeromagnetic maps from the database of the Brazilian Geological Survey showing the anomaly lineaments and their corresponding rose diagrams. The yellow lines represent lineaments in the basin sector and the black lines represent lineaments in the crystalline basement sector. n = number of lineaments. A) Residual data (basin sector, n = 140 and crystalline basement, n = 109); B) Residual data reduced to the pole (basin sector, n = 98 and crystalline basement, n = 108).

4.2. Outcrop scale

We analyzed the brittle deformation in the basal interval of the Araripe Basin, the Cariri Formation. The Cambrian Cariri Formation comprises very coarse-to medium-grained highly silicified sandstones (Fig. 5A). These sandstones show a gentle bedding dip from 4° to

12° to NE and ENE (Fig. 5B, and 6A). The Cariri Formation shows a tabular cross-bedding stratification, which dips mainly between 10° and 43°, predominantly to ENE (Fig. 5B, and 6B).

The brittle deformation in the Cariri Formation is mostly characterized by deformation bands. These structures occur either as single bands or as clusters (swarms) of bands (Fig. 5C). The clusters can be observed as positive relief features in the outcrop (Fig. 5C). The deformations bands display a complex geometric relationship arranged in conjugate pairs (Fig. 5D). Two conjugate pairs of bands define the orientations of the principal trends as a) NW-SE and N-S; b) ENE-WSW and NNE-SSW (Fig. 6C-F).

These deformation bands have different kinematics, which could be verified from the displacement (cross-cutting relationship) between these structures. When possible, we verify that the ENE-WSW and NNE-SSW deformation bands show sinistral shear movement, and the N-S bands display dextral shear. The deformation bands of the Cariri Formation have thicknesses ranging from 0.33-2.15 mm (Site 1), 0.115-5 mm (Site 2), 0.14-10 mm (Site 3), and 0.265-5 mm (Site 4).

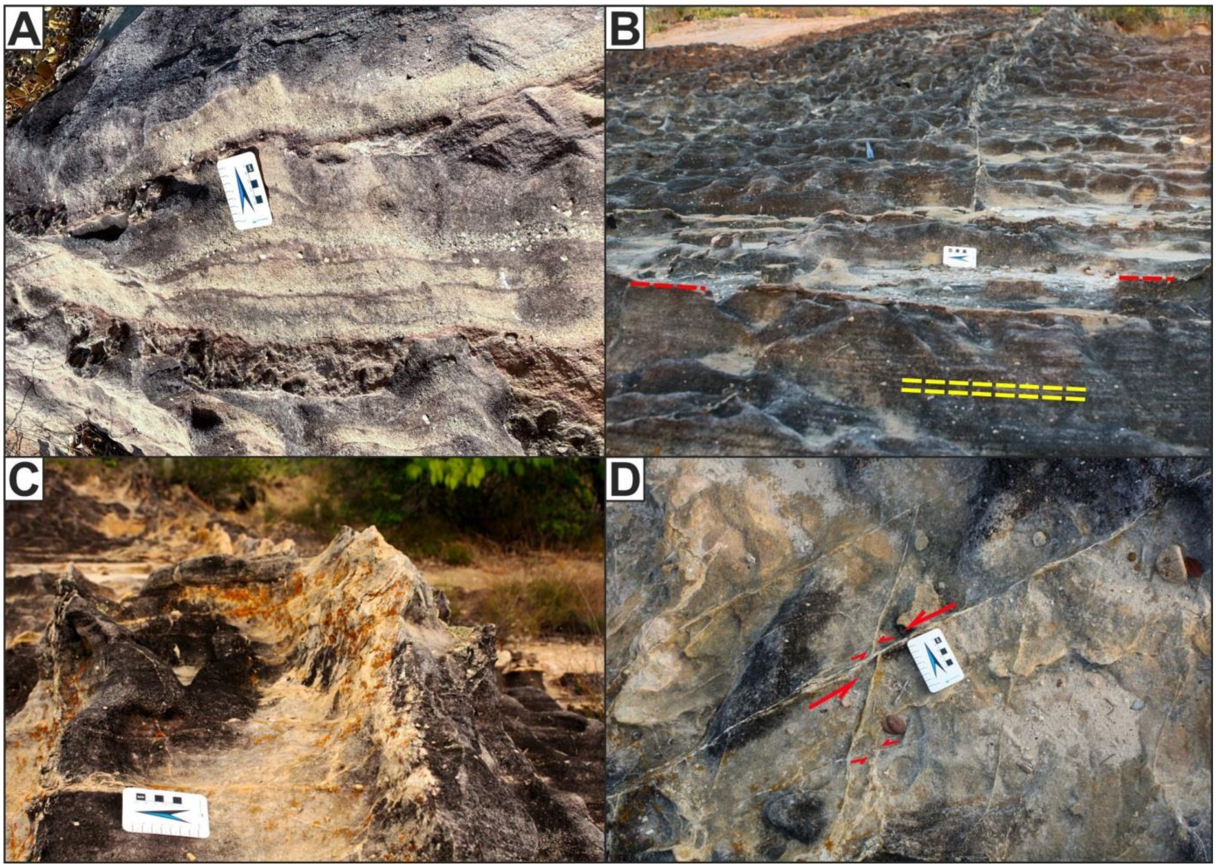

Figure 5. Field aspects of the Cariri Formation, the eastern border of the Araripe Basin. A) Sandstone with very coarse to medium grain. B) Detail of bedding that is represented by red dashed lines, and the cross-bedding indicated by yellow lines. C) Clusters of deformation bands showing positive relief. D) ENE-WSW deformation band showing sinistral kinematic movement, the red arrows represent the kinematic indicators.

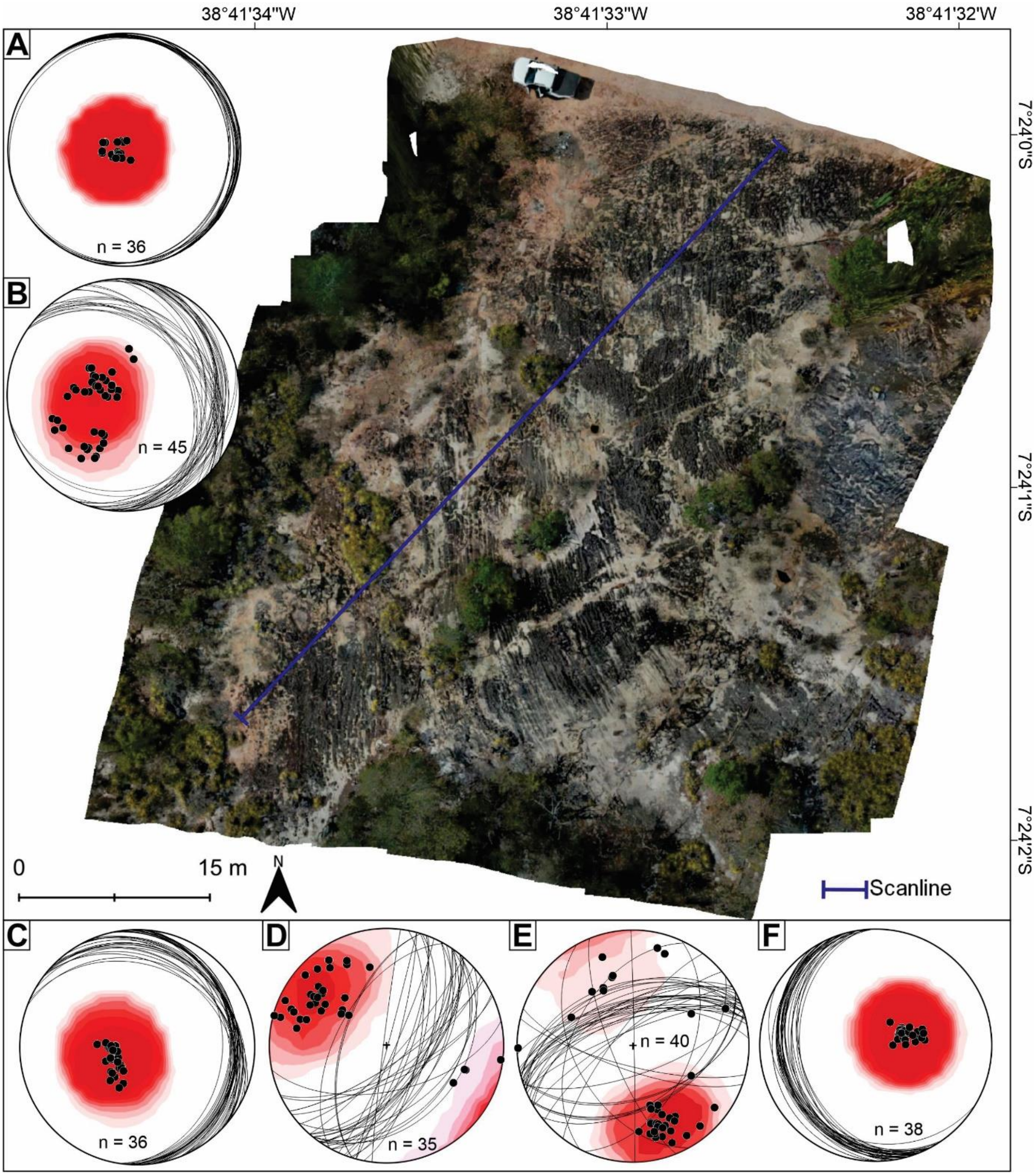

Figure 6. Orthomosaic illustrating the outcrop Site 2 (Fig. 1) of the Cariri Formation sandstone, eastern border of the Araripe Basin. The blue line represents the position of the scanline. A) Stereographic projections with pole densities contour for bedding planes (contour interval (C.i.) = 16.7%). B) Stereographic projections demonstrate the density contour of the poles referring to the cross-bedding stratifications (C.i. = 16.7%)). C - F) Stereographic

projections showing the density contour of the poles (C.i. = 18.4%), obtained for each set of deformation bands. n = number of deformation bands.

4.3. Spatial arrangement analysis

4.3.1. Coefficient of variation

The analysis of the CV showed a wide variation, suggesting the presence of regular, random, and clustered arrangements in different locations (Table 1). The scanlines acquired with the topographic data showed a CV range between 0.89 and 1.54, suggesting that most of the scanlines show an arrangement close to random (CV~1), with scanlines 2 and 3 being outliers with higher CVs, suggesting clustering. The aeromagnetic data showed a contrasting result with all scanlines having CV < 0.63, suggesting a regular arrangement in this data, reaching values as low as 0.41 in scanline 7. The outcrop data showed values of CV > 1, reaching values as high as 2.07 in site 3, suggesting a strong clustering in this site. Overall, the outcrop data showed higher CVs than the regional data, suggesting a more clustered arrangement in outcrop.

Table 1. Coefficient of variation (CV) for the scanlines acquired with topographic, aeromagnetic, and outcrop data.

	Scanline 1	**Scanline 2**	**Scanline 3**	**Scanline 4**	**Scanline 5**	**Scanline 6**	**Scanline 7**	**Site 1**	**Site 2**	**Site 3**	**Site 4**
Topography	0.98	1.47	1.54	0.98	1.03	0.89	1.06	-	-	-	-
Aeromagnetic	0.63	0.55	0.41	0.62	0.46	0.49	0.41	-	-	-	-
Outcrop	-	-	-	-	-	-	-	1.05	1.79	2.07	1.44

4.3.2. Normalized correlation count

Most of the scanlines acquired with the topographic showed random arrangements, with exception of scanline 3 (Table 2). The number of analyzed featured ranged between 46 and 113, with varying high-intensity peaks, mostly forming non-significant clusters along the scanline. In scanlines 1, 4, and 5 the high-intensity peaks are coincident with the Mauriti Fault position (Fig. 7). High-intensity positions on scanlines 2, 3, and 4 are located near the Coité Fault. While in scanlines 5 and 6, some high-intensity positions occur between the Coité and Umburanas faults. At normalized intensity, the significant topographic clusters exhibited up to 3.5 km in width, spaced between 1.7 km to 20 km. The NCC plot of the significant clusters in Scanline 3 is 7 Km wide and is spaced by 22 Km.

Table 2. Results from the Normalized intensity and normalized correlation count analysis on scanline data with topographic lineaments.

	Scanline 1	Scanline 2	Scanline 3	Scanline 4	Scanline 5	Scanline 6	Scanline 7
Nr. Features	86	113	92	106	82	71	46
High-intensity positions (km)	7.5/13/17.8	4/7/24.5/17.5	11/21/31	13.5/15.5/ 20.2/25.5/30.5	1/23/32	31	17.5
NCC Type	Random	Random	Clustered	Random	Random	Random	Random
Cluster Size/ Spacing (km)	-	-	7/22	-	-		-
Significant length scale at 95% (km)	0.065/0.225/5	0.022	0.35-3	0.055/1	-		0.225/0.775
Significant length scale at 68% (km)	0.55-1	0.6-6	-	-	0.225-1		0.325/0.475
Fault position (km)							
Mauriti	13	15	18	20	23	23	19
Coité	-	22.5	25	27	29	28.5	25.6
Umburanas	-	-	-	-	34.2	32.5	28.3

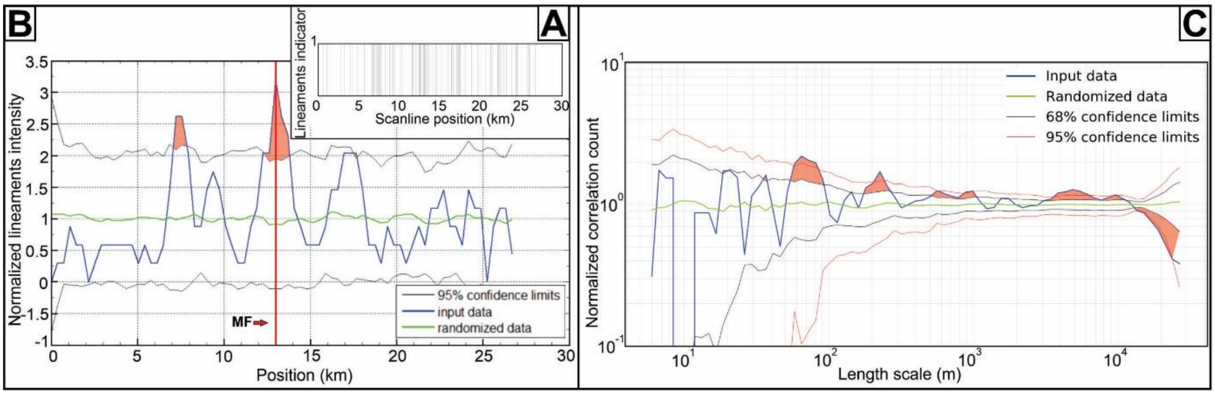

Figure 7. Results of the spatial arrangement analysis for the topographic lineaments in Scanline 1. A) Stick plot, n = 86. In the stick-plot graph, the indicator = 1 shows the occurrence of the lineament, and the indicator = 0, the absence of the lineament. B) Normalized lineaments intensity plot. C) NCC plot. MF = Mauriti Fault, CF = Coité Fault, UF = Umburanas Fault. Clusters with statistically significant values are indicated by orange

polygons. Observe the high-intensity of lineaments around the position of Mauriti Fault. See appendix A for a full description of all graphics.

Most of the scanlines based on aeromagnetic lineaments showed an anti-clustered or regular spatial arrangement (Table 3). The number of features analyzed in each scanline ranges from 19 to 31. The normalized intensity plot did not show any significant peak, suggesting that the lineament intensity is mostly similar along the scanlines (Fig. 8). Many of the NCC plots showed a significant lack of smaller length scales, suggesting an anti-clustering behavior, along with a wavy pattern, suggesting repetition of length scales at determined distances. There are no significant changes in intensity on positions where Mauriti, Coité, and Umburanas faults are intersected.

Table 3. Results from the Normalized intensity and normalized correlation count analysis on scanline data with aeromagnetic lineaments.

	Scanline 1	**Scanline 2**	**Scanline 3**	**Scanline 4**	**Scanline 5**	**Scanline 6**	**Scanline 7**
Nr. Features	24	23	31	30	30	25	19
High-intensity positions (km)	-	-	-	-	-	-	-
NCC Type	Anti-clustered	Random	Anti-clustered	Anti-clustered	Anti-clustered	Random	Anti-clustered
Cluster Size/Cluster Spacing (km)	-	-	-	-	-	-	
Significant length scale at 95% (km)	0.65/0.75	-	-	-	2.5	-	1.6
Significant length scale at 68% (km)	2/2.8/3.8	0.65/1.1/2.3	0.95/1.8/3	1.1	1.5/4/5	2.3	-
Fault position (km)							
Mauriti	13	15	18	20	23	23	19
Coité	-	22.5	25	27	29	28.5	25.6
Umburanas	-	-	-	-	34.2	32.5	28.3

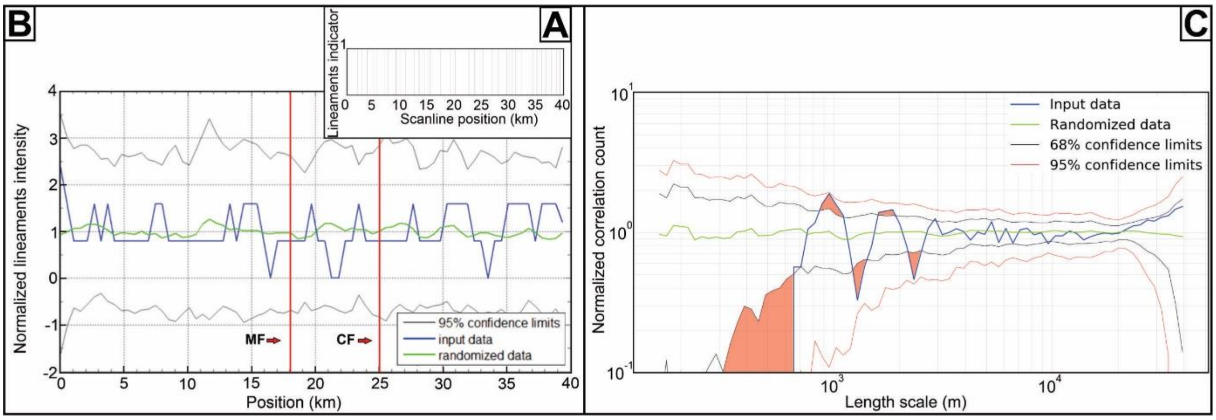

Figure 8. Results of the spatial arrangement analysis for the aeromagnetic lineaments in Scanline 3. A) In the stick plot graph, the indicator = 1 shows the occurrence of the lineament, and the indicator = 0, the absence of the lineament, n = 31. B) Normalized lineaments intensity plot. C) NCC plot. MF = Mauriti Fault, CF = Coité Fault, UF = Umburanas Fault. Clusters with statistically significant values are indicated by orange polygons. See supplementary files for a full description of all graphics.

The scanlines acquired in the outcrop showed some sort of clustered behavior in all four sites (Table 4). The number of deformation bands analyzed ranged from 13 to 110. All scanlines showed significant high-intensity peaks, suggesting a clustered spatial arrangement. The Normalized correlation count also suggests a clustered behavior for most of the scanline, except for site 1, where the spatial arrangement is random, with non-significant clustering. The scanline at site 2 showed a significant cluster plotting very high above the confidence interval and following a linear trend, suggesting a strong clustering with a fractal internal organization (Fig. 9).

Table 4. Results from the Normalized intensity and normalized correlation count analysis on deformation bands scanline data.

	Site 1	**Site 2**	**Site 3**	**Site 4**
Nr. Features	13	110	55	57
High-intensity positions (m)	1.4/1.95/2.65/3.39/3.65/3.9/4.05/4.35	1/9/11/18.5/25/37/45/55/56/58	1.5/3.13/8.4/8.7/9	0.825/3.2/3.5/4/4.39/4.9/5.05
NCC Type	Random	Clustered	Clustered	Clustered
Cluster Size/ Spacing (m)	-	1.1/-	0.7/-	0.1/-

Significant length scale at 95% (m)	-	0.004/0.175/2	0.018	0.007/0.023/0.07
Significant length scale at 68% (m)	0.24-3.1	-	-	-

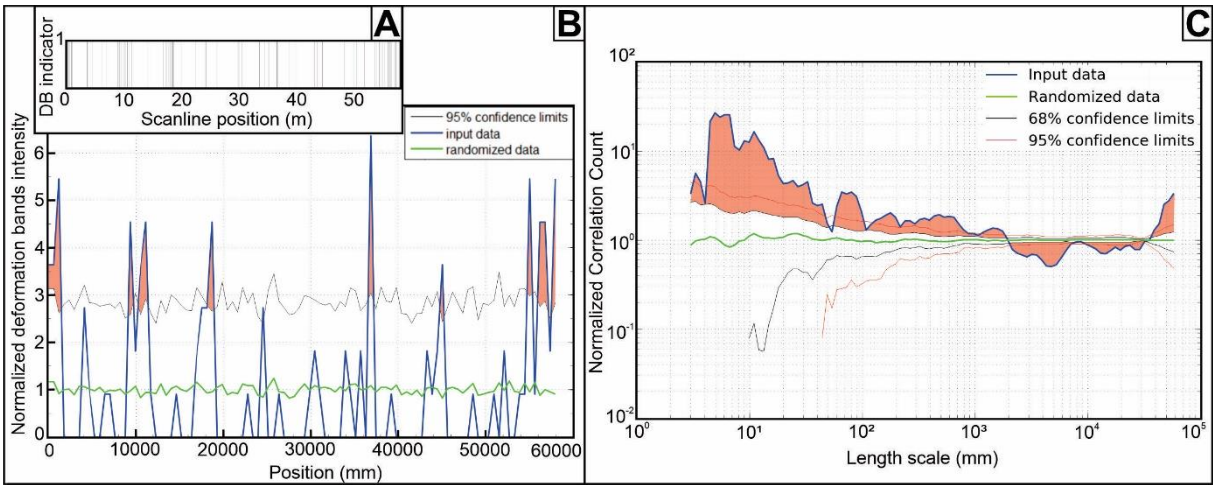

Figure 9. Results of the spatial arrangement analysis for the deformation bands in Site 2. Clusters with statistically significant values are indicated by orange polygons. A) In the stick plot graph, the indicator = 1 shows the occurrence of the deformation bands (DB), and the indicator = 0, the absence of the bands. n = 110. H) Normalized deformation bands intensity plot. I) NCC plot. See appendix A for a full description of all graphics.

5. Discussion

5.1. Correlation of regional lineaments and brittle deformation

We found that the position of the Mauriti Fault is coincident in many cases with the position of high-intensity in topographic lineaments. While the Coité and Umburanas faults, show proximity of up to 3 km for a high-intensity position for the topographic lineaments. This finding suggests that the topography in the eastern border of the Araripe basin has been imprinted by the underlying brittle deformation in the rocks. The positive (crests) and negative (valleys) reliefs can reflect the tectonic framework of a certain area which may correspond to traces of foliation (basement sector), fractures, and faults. (e.g., Wise et al., 1985; Pontes et al., 2019; Lima and Sá, 2017; Barbosa et al., 2021). For the regional structural data, information on morphotectonics can indicate and help potential sites for field study (e.g., Crepani, 1987). Barbosa et al. (2021) argue that positive reliefs may be related to proximity to fault systems, presence of deformation bands, and presence of more resistant sandstones.

We have verified clusters for scanlines 1 (peak at 13 km), 2 (valley at 17.5 km) 3 (valley at 20.2 km), 4 (peaks at 15.5 and 20.2 km), 5 (peak at 23 km), and 7 (peak at 17.5 km) that are located near the Mauriti Fault (up to 5 km of proximity). The high-intensity near scanlines 2 (peak at 24.5 km), 3 (peak at 31 km), and 4 (valley at 25.5 peaks at 30.5 km) are related to the Coité Fault. While in scanlines 5 (peak at 32 km) and 6 (peak at 31 km), the observed clusters point to the interaction between the position of the Coité and Umburanas fault zones.

Site 1 is related to the Mauriti Fault (180 m from this fault) and is located nearby the geological contact between the Cariri and Brejo Santo formations. The last formation possibly masks the brittle deformations in this sector, hidden due to lithological change, modified from sandstones of the Cariri Formation to shales (Fig. 1). In addition to being a younger formation (Neojurassic), not accommodate deformations in the same way as the Cariri Formation (Cambrian-Ordovician). Therefore, this fact could justify the absence of significant outcrops in the vicinity of the Mauriti Fault. Site 1 is positioned about 20 km along Scanline 4 (Fig. 1), regionally this site is found within the statistically significant peak obtained for scanline 4 (see the peak at 20.2 km, Fig. A.1K). About 2 km between scanlines 5 and 6 is Site 2 (Fig. 1), which is related to the Coité Fault, in the Cariri Formation. Regionally, the normalized intensity graphs of these scanlines (see peaks from 30 km, Fig. A.1N, and Q) show statistically significant peaks, which possibly refer to the Coité and Umburanas faults. It was not possible to establish this correlation with sites 3 and 4, which occur 1 km from Scanline 7 (Fig. 1), as the normalized intensity graph of regional lineaments did not show significant peaks near the Coité and Umburanas faults.

Our outcrop observation revealed a greater number of deformation bands (e.g., Fig. 6C), with ENE, NE, NNE, NW, and N orientations. In general, the deformation bands evidence reduction in grain size, and the fine-grained quartz shows strong increased resistance in comparison to the hosting rock (e.g., Pontes et al., 2019). Due to that, the presence of deformation bands can cause differential weathering, forming high reliefs where they are common (Fig. 5C). The weathering-resistant deformation bands due to silicification processes is responsible for the reduction of rock porosity and permeability in sedimentary basins (Ngwenya et al., 2000; Caine et al., 2010; Menezes et al., 2019). We assume that these common deformation bands around faults, such as the Mauriti reflect the association between fault position and suitable topographic features, where Cariri Formation outcrops. Despite this pattern observed in Eastern Araripe Basin, the occurrence of such pattern in the whole basin must be investigated further.

Integrating the analysis of regional structural lineaments, we observe that some lineament orientations are present in two groups of lineaments (topographic and aeromagnetic), such as the NE-SW, E-W, N-S, and NW-SE trends. We observed that these lineaments are strongly controlled by rheological domains (crystalline basement and basin) that are reflecting the reactivation of pre-existing structures in the basement. The aeromagnetic lineaments did not show any correlation between lineament intensity and fault position. We assume that the aeromagnetic lineament position was not correlated to the fault position due to the resolution of the magnetic acquisition, which hindered the observation of more nuances in the structural framework. However, the direction of the structures does correlate with the direction of the regional brittle structures. Each dataset addresses different limitations, hence the importance of gathering geological information at different scales. The results achieved through regional data, in this case, have indications of clustered regions that are coincident with the position of known faults.

Meixner et al. (2018) showed that the total length of the lineaments decreases significantly with the increase of the data resolution, while the orientations have similar trends, even if they present slightly different individual trends. The analysis of lineaments is not a complete structural geology approach due to the lack of information such as paleostress orientation or geochronology (Wise et al, 1985). Nevertheless, the combination of geophysical and topographic lineaments with documented structures in outcrop allow the production of reliable structural maps (Sanusi and Amigun, 2020). The eastern border of the Araripe Basin is an example of such correlation, mostly due to the interplay between brittle deformation and topographic features.

In the aeromagnetic map reduced to the residual pole (Fig. 4B), which positions the anomalies in the magnetic source, we note that the positive anomalies have several linear features in the NW-SE direction, which are not noticeable in the residual aeromagnetic map (Fig. 4A). These lineaments are mainly located in the north-central portion of the study area. Some of NW-SE aeromagnetic lineaments coincide with the topographic lineaments (Fig. 3B). These regions should be further investigated using detailed outcrop studies to decipher why they showed such a distinct behavior since these reduced-to-pole anomalies could reflect some important geological feature or just noise from the magnetic data.

5.2. Analysis of the spatial arrangement

We found that in our results the coefficient of variation and the normalized correlation count method showed similar interpretations mutually. Topographic lineaments, in general, have randomly arranged spatial arrangements with weak non-significant clustering. The aeromagnetic lineaments have anti-clustered or regularly arranged and the deformation bands are significantly more clustered, with some degree of fractal internal organization.

Each type of scanline (topography, aeromagnetic, deformation bands) showed overall a different type of arrangement. The reason why we found expressive variation in spatial arrangement across types of lineaments and deformation bands was not extensively investigated in this paper, but a few causes can be hypothesized such as i) observation scales; ii) resolution limitations and iii) local variability.

By analyzing the coefficient of variation of structures spacings (Table 1), it is possible to compare their spatial organization (e.g., Wang et al., 2019). Some authors studying different rocks such as carbonates (Marrett et al., 2018; Miranda et al., 2018), sandstones (Laubach et al., 2018b), and granites (Ehlen, 2000; Wang et al., 2019), obtained CV values averaging > 1, indicating that the datasets are more clustered. Our topographic data also show a CV > 1 in some scanlines (scanlines 2, 3, and 7), with more grouped lineaments, suggesting clusters. However, scanlines 1, 4, and 5, with CV values close to 1, show lineaments arranged randomly, and scanline 6, with CV < 1, show fewer lineaments grouped, representing regions of anti-clustering.

On the other hand, the scanlines performed out in the aeromagnetic data, show anti-clustered lineaments with a maximum CV of 0.63. Most of the data showed anticlustering and regular spacing, which is a distinct arrangement than observed in the other data types. Since regular spacing is commonly associated with inter-bedding jointing (Rives et al., 1992; Bao et al., 2019), it is not expected to be largely observed in regional lineaments. Due to that, we believe that this regular arrangement is associated with the resolution of the magnetometry data.

The CV obtained for the outcrop data indicates that deformation bands (ENE, NE, and NNE) have clustered arrangements, except for site 1 (ENE-WSW deformation band), which exhibits a random arrangement with non-significant clusters. The NE-SW deformation bands exhibit higher CV (Site 3, Table 1), indicating more grouped bands when compared to the other verified sites. Although random arrangement inevitably shows clusters (Priest and

Hudson, 1976), non-random arrangement can be even more strongly grouped and positively correlated (Marrett et al., 2018), implying mechanisms that promote localization.

These techniques allowed analyzing different structures (regional lineaments and deformation bands) at different scales, however, warnings about the limitations of the data used must be taken into account (e.g., Marrett et al., 2018; Li et al., 2018; Wang et al., 2019). For instance, Li et al. (2018) compared subsurface, outcrop, and core data, and found that image logs, when ideally positioned and with adequate resolution, have an advantage over cores in providing reliable and abundant spacing measurements over long distances. Regardless of the scale used, the validation of these techniques depends on the quality and quantity of input data (e.g., Laubach et al., 2018b; Li et al., 2018; Wang et al., 2019). Accuracy for a scale of hundreds of meters is controlled by the total length of the scanline, where spacings greater than half the scanline are considered artifacts (Li et al., 2018). Li et al. (2018) emphasized that, in addition to data quality, spacing of structures, and estimation of intensity can be affected by sampling bias and by changing observation scales.

We emphasize that each type of scanline data had its limitations, facilitating and complementing the analysis of the arrangement of structures at different scales. According to the analyzed feature, integration of regional and local data have shown unlike spatial arrangement, which may be caused by differences between observation scale and spatial data resolution.

5.3. Tectonic implications

Pre-existing shear zones can provide mechanical and rheological control that directly influence the geometry of rift-type intraplate basins such as the Araripe Basin (e.g., Vasconcelos et al., 2019; Celestino et al., 2020; Osagiede et al., 2020). The orientation of regional lineaments and deformation bands have significant tectonic implications for the structural model of the eastern border of the Araripe Basin. Therefore, we consider that the main aeromagnetic and topographic lineament direction (E-W) of the basement sector represents the structural inheritance of the PASZ, whereas the NE-SW trends are related to secondary shear zones related to the PASZ splay (e.g., Celestino et al., 2020). Additionally, some directions of the regional structural lineaments of the basin sector (Fig. 4 and 5) represent the same orientation as the deformation bands of the Cariri Formation (Fig. 6C-F). These deformation bands are mainly oriented to ENE, NE, and NNE which dips 17° to the sub-vertical, while the deformation bands with NW-SE and N-S orientation have smooth dips close to 30°. These deformation bands may agree with the bedding and cross-bedding stratifications orientation seen in this sandstone (Fig. 6A-D).

In this work, we suggest that the orientations a) NW-SE and N-S; b) ENE-WSW and NNE-SSW of structural lineaments and deformation bands represent conjugate pairs, which can be interpreted as the R and R' faults of the Riedel system (e.g., McClay, 1987) (Fig. 10A and B). The NW-SE and N-S conjugate pair possibly represent the deformation of dextral strike-slip regime of the PASZ, with maximum extension ($\sigma 3$) in the NE-SW direction. This conjugate pair should be related to the Paleozoic deformational phase that also acted at the northern border of the Araripe and Jatobá basins (Celestino et al., 2020; Miranda et al., 2020). The second conjugate pair (ENE-WSW and NNE-SSW) is interpreted to have occurred during the rifting of the South Atlantic Ocean in the Early Cretaceous (Matos et al., 2020; Celestino et al., 2020). At this deformational phase, the PASZ was reactivated with sinistral kinematics (Françolin et al., 1994; Nogueira et al., 2015; Araujo et al., 2018; Celestino et al., 2020) (Fig. 10).

The main deformation phase of the study area is represented by the Early Cretaceous Mauriti, Coité, and Umburanas faults (Fig. 1). These main faults were identified in our results as topographical and aeromagnetic lineaments (Fig. 3 and 4), continuum (Mauriti Fault), or discontinuous, exhibiting NE-SW and ENE-WSW orientation. In addition, the deformation bands that are parallel to these faults have grouped arrangements and irregular spacing.

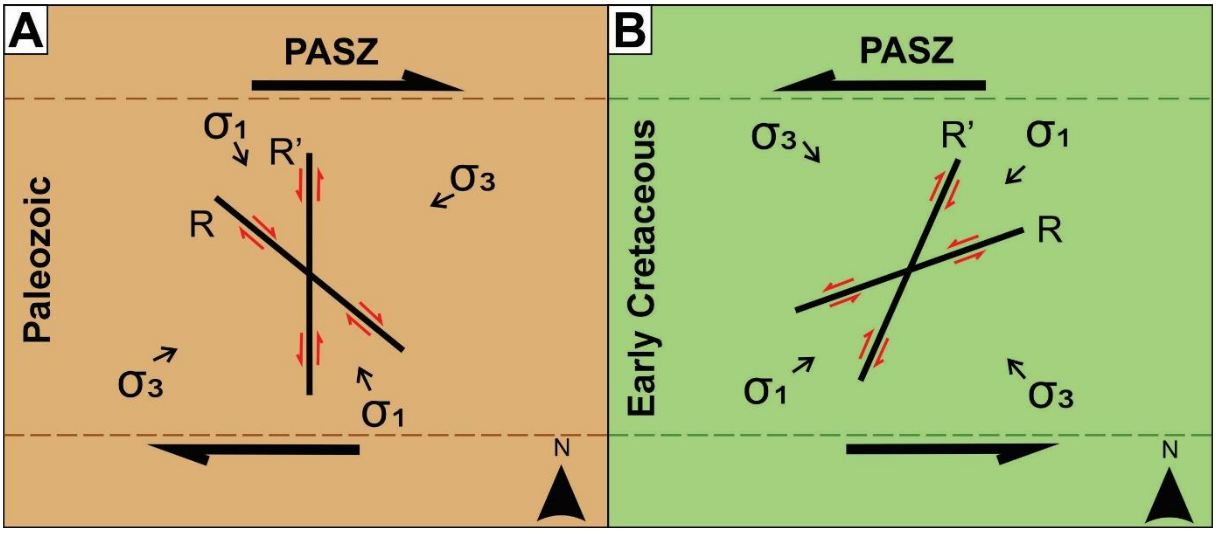

Figure 10. Schematic model of the tectonic evolution of the eastern border of the Araripe Basin. Representation of the Riedel System for structural lineaments and deformation bands A) with NW-SE (R) and N-S (R') orientation, related to dextral deformation, and B) with ENE-WSW (R) and NNE-SSW (R') orientation related to sinistral reactivation of the PASZ.

6. Conclusions

This study analyzes the spatial arrangement of the topographic and aeromagnetic lineaments and deformation bands of the eastern border of the Araripe Basin. This multi-scale approach proved to be accessible and can be used for detailed structural quantification of brittle fault zones. We present below the most important findings:

- The Mauriti, Coité, and Umburanas faults are positioned close to the high-intensity topographic lineaments. This suggests that the topography on the eastern border of the Araripe basin is imprinted by brittle deformation possibly due to the weather-resistant deformation bands located around these fault zones.

- The intensity of aeromagnetic lineaments did not correlate to the Mauriti fault position, but the orientation was similar. A possible cause for the lack of intensity variation in the aeromagnetic data is the spatial resolution.
- We found that the spatial arrangement of topographic, aeromagnetic lineaments and deformation bands are different. However, each type showed a consistent behavior separately. The different results suggest that observation scale and resolution are parameters that can affect the analysis of spatial arrangement. This study was not able to determine the cause of this difference.
- Structural lineaments and deformation bands are interpreted to be caused by the reactivation of PASZ during the Paleozoic and Early Cretaceous ages, forming conjugate shear pairs in directions expected by the Riedel diagram. The regional lineaments, in the basin sector, and the deformation bands exhibit orientations in two sets of conjugated pairs: a) dextral strike-slip deformation with NW-SE (R) and N-S (R’) orientations, while the ENE-WSW (R) and NNE-SSW (R’) pair would be reflecting the sinistral reactivation of the PASZ.

Acknowledgments

This paper was carried out with financial support from CNPq (Conselho Nacional de Desenvolvimento Científico e Tecnológico) and by the Research Project Fault Zones funded by Petrobras in cooperation with the Federal University of Pernambuco. We are grateful to Fracture Research and Application Consortium, the University of Texas at Austin for providing the CorrCount as an open-access software. We acknowledge the Brazilian Geological Survey (CPRM) for providing the aeromagnetic data. This work is part of a MSc of Vivian Passos under the postgraduate program in Geosciences of the Federal University of Pernambuco (PPGEOC - UFPE) and represents the contribution N. 04 of the Laboratório de Modelagem de Bacias (ModLad-UFPE).

Appendix A

Results of the spatial arrangement of topographic (Fig. A.1) and aeromagnetic (Fig. A.2) lineaments and deformation bands (Fig. A.3) obtain for the eastern border of the Araripe Basin, eastern Brazil.

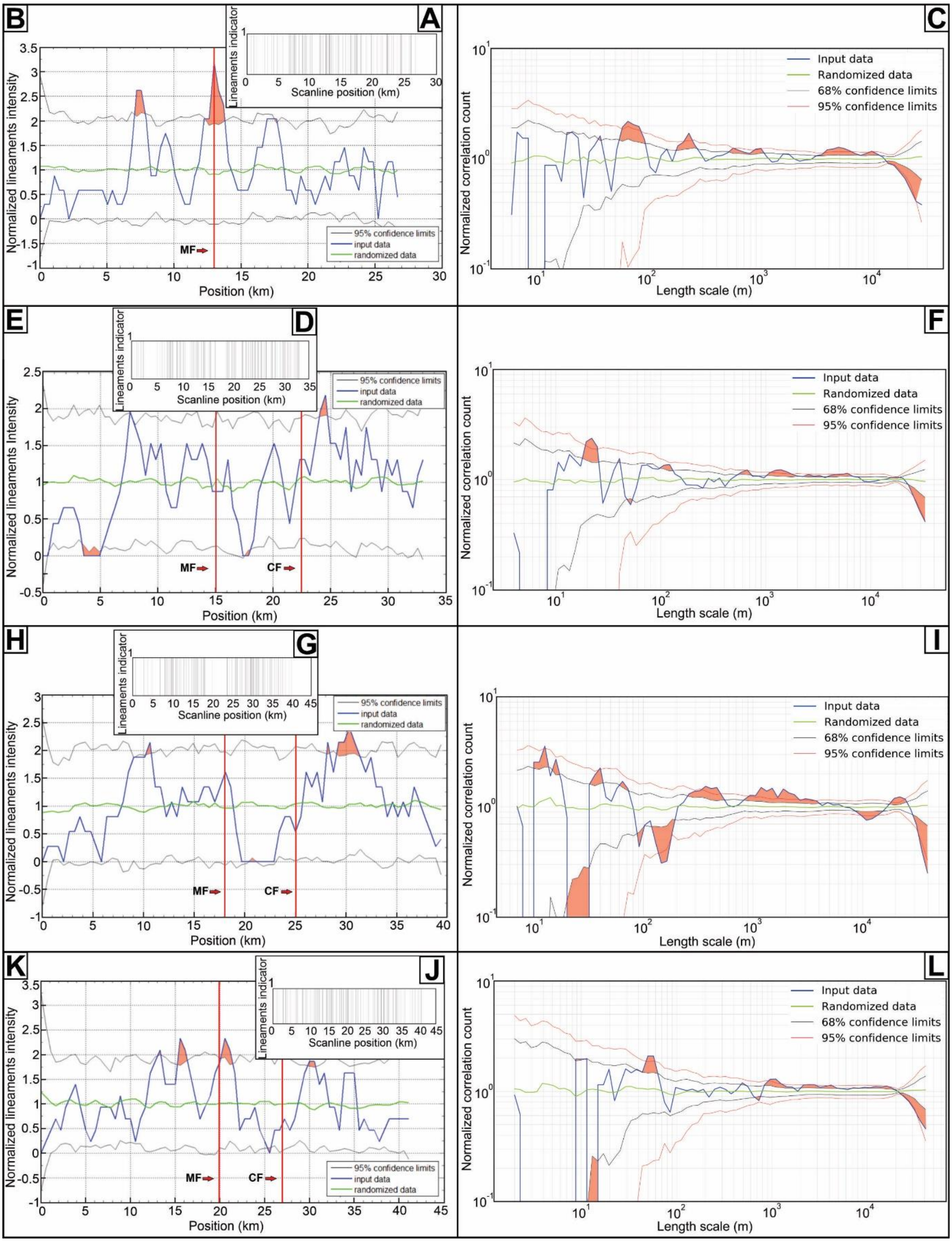

Figure A.1. Results of the spatial arrangement analysis for the topographic lineaments. In the analysis of the normalized correction count (NCC) we used the confidence intervals of 95% (red lines) and 68% (black lines). The normalized intensity graph has a 95% confidence interval (black lines). In the stick-plot graph, the indicator = 1 shows the occurrence of the lineament, and the indicator = 0, the absence of the lineament. MF = Mauriti Fault, CF = Coité Fault, UF = Umburanas Fault. n = number of lineaments. Clusters with statistically significant values are indicated by orange polygons. A) Stick plot along the scanline of scanline 1, n = 86. B) Normalized intensity for scanline 1. C) NCC for scanline 1. D) Stick plot for scanline 2, n = 113. E) Normalized intensity for scanline 2. F) NCC for scanline 2. G) Stick plot for scanline 3, n = 92. H) Normalized intensity for scanline 3. I) NCC for scanline 3. J) Stick plot for scanline 4, n = 106. K) Normalized intensity for scanline 4. L) NCC for scanline 4.

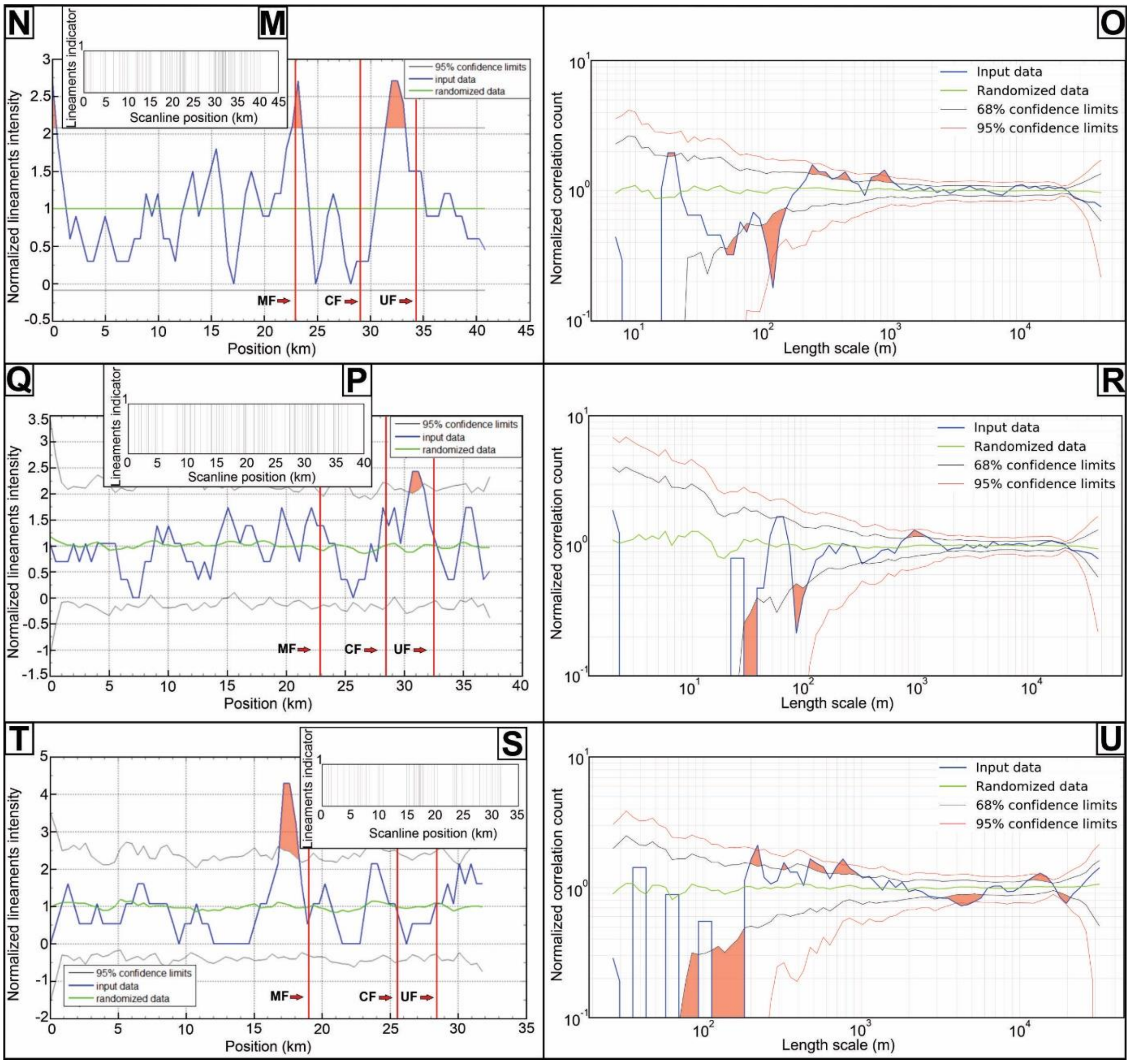

Figure A.1. (cont.). M) Stick plot for scanline 5, n = 82. N) Normalized intensity for scanline 5. O) NCC for scanline 5. P) Stick plot for scanline 6, n = 71. Q) Normalized intensity for scanline 6. R) NCC for scanline 6. S) Stick plot for scanline 7, n = 46. T) Normalized intensity for scanline 7. U) NCC for scanline 7.

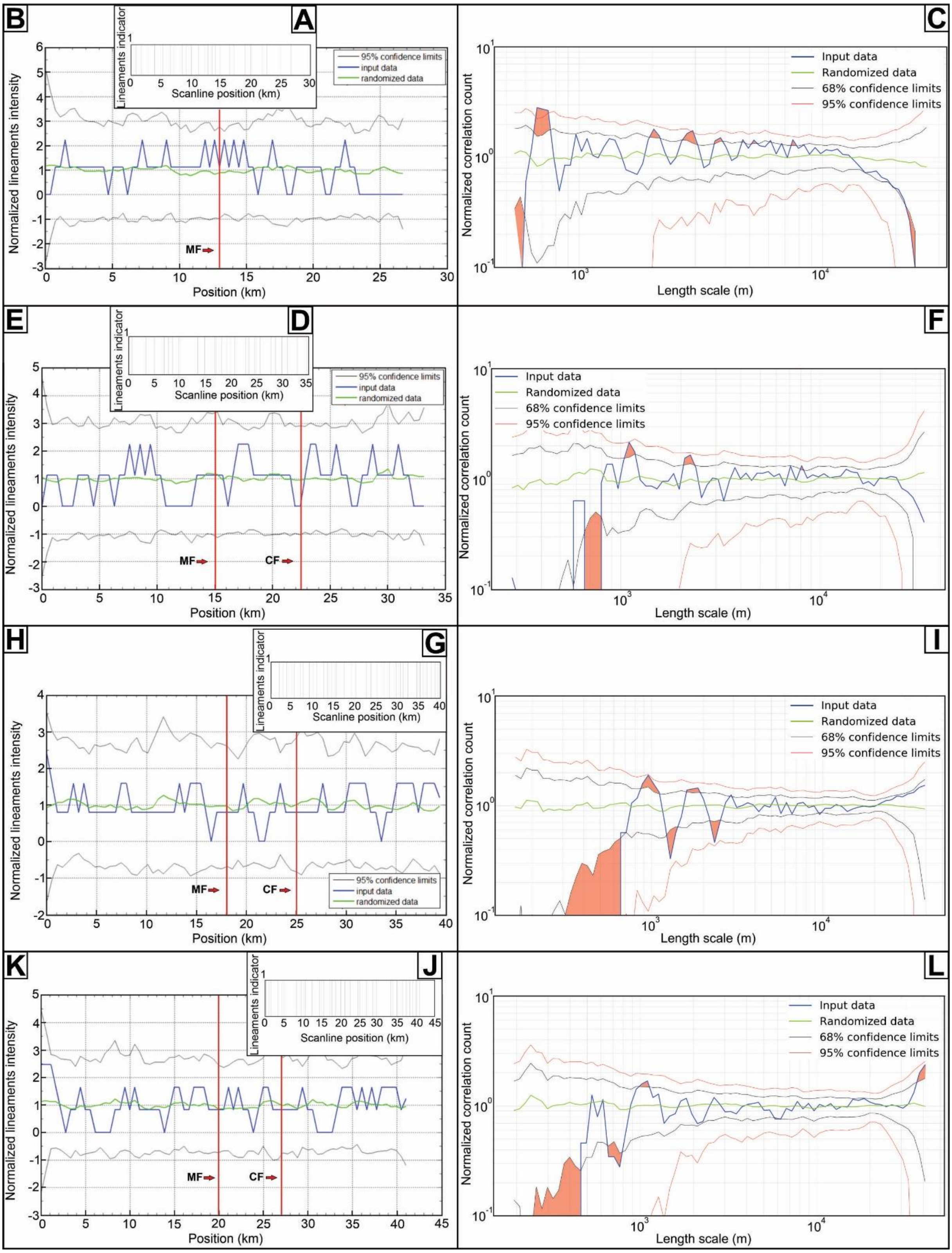

Figure A.2. Results of the spatial arrangement analysis for the aeromagnetic lineaments. In the analysis of the normalized correction count (NCC) we used the confidence intervals of 95% (red lines) and 68% (black lines). The normalized intensity graph has a 95% confidence interval (black lines). In the stick plot graph, the indicator = 1 shows the occurrence of the lineament, and the indicator = 0, the absence of the lineament. MF = Mauriti Fault, CF = Coité Fault, UF = Umburanas Fault. n = number of lineaments. Clusters with statistically significant values are indicated by orange polygons. A) Stick plot of scanline 1, n = 24. B) Normalized intensity for scanline 1. C) NCC for scanline 1. D) Stick plot for scanline 2, n = 23. E) Normalized intensity for scanline 2. F) NCC for scanline 2. G) Stick plot for scanline 3, n = 31. H) Normalized intensity for scanline 3. I) NCC for scanline 3. J) Stick plot for scanline 4, n = 30. K) Normalized intensity for scanline 4. L) NCC for scanline 4.

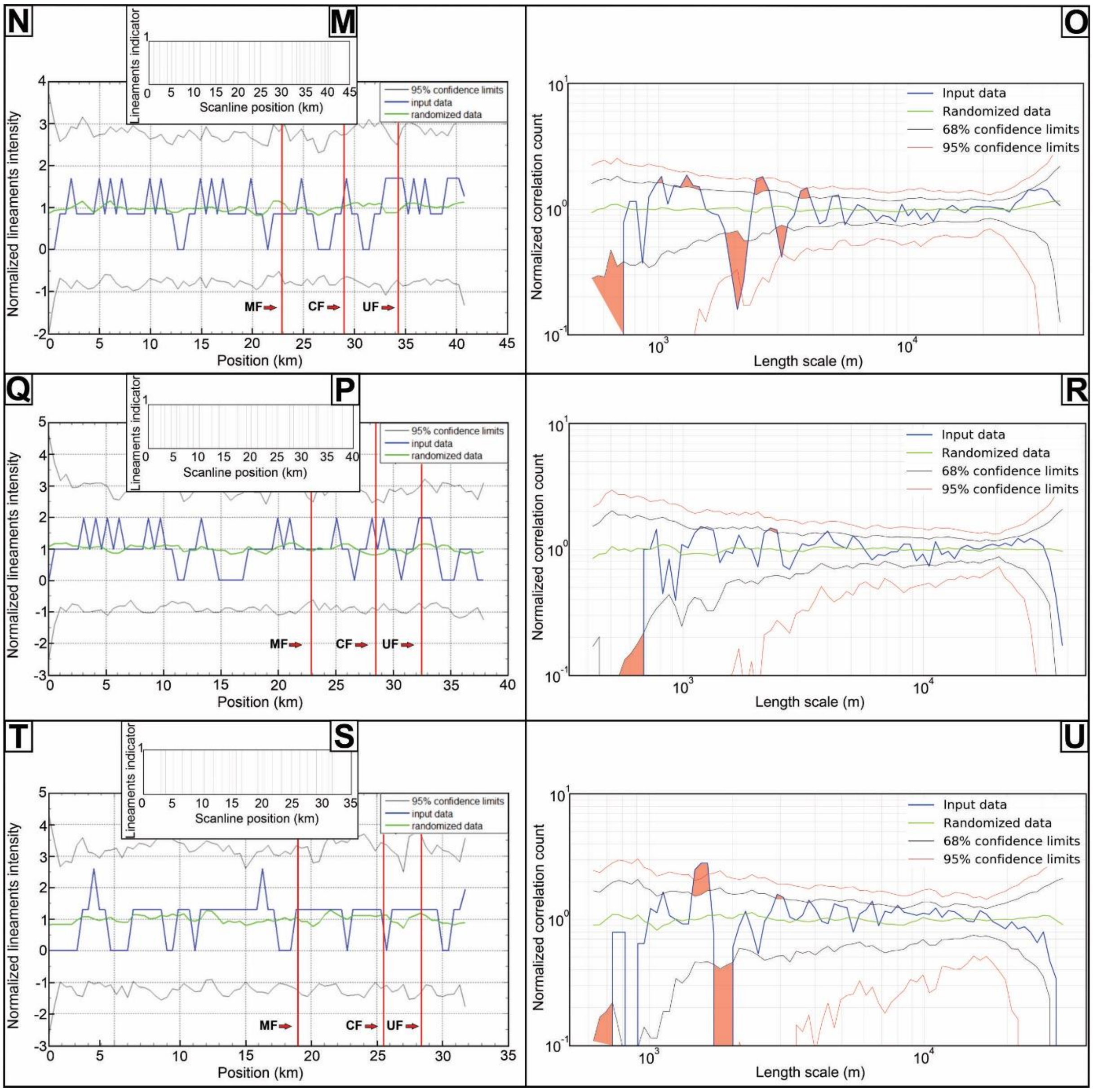

Figure A.2. (cont.). M) Stick plot for scanline 5, n = 30. N) Normalized intensity for scanline 5. O) NCC for scanline 5. P) Stick plot for scanline 6, n = 25. Q) Normalized intensity for scanline 6. R) NCC for scanline 6. S) Stick plot for scanline 7, n = 19. T) Normalized intensity for scanline 7. U) NCC for scanline 7.

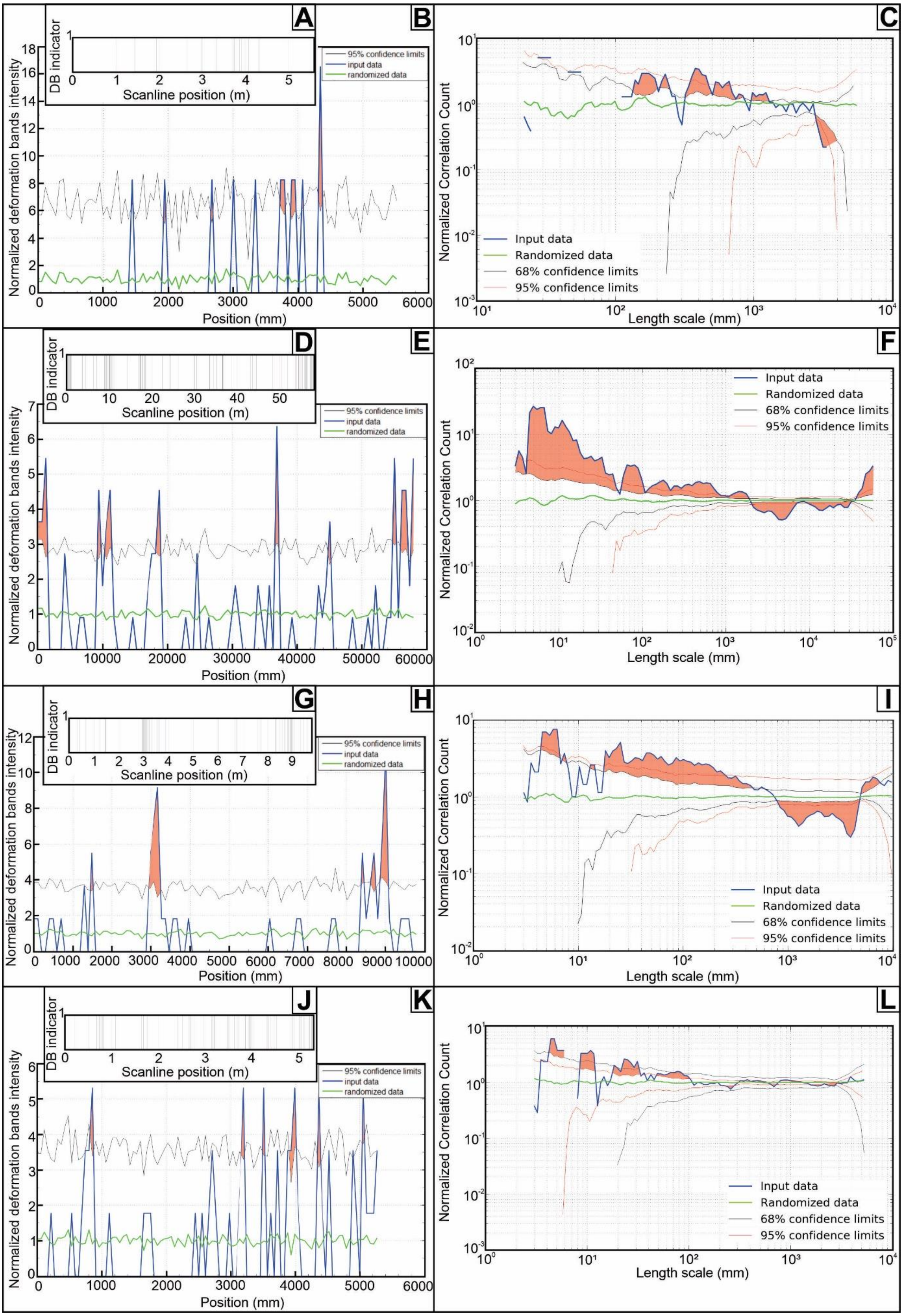

A
B
C
D
E
F
G
H
I
J
K
L
DB indicator
Scanline position (m)
Normalized deformation bands intensity
Position (mm)
95% confidence limits
input data
randomized data
Normalized Correlation Count
Length scale (mm)
Input data
Randomized data
68% confidence limits
95% confidence limits

Figure A.3. Results of the spatial arrangement analysis for the deformation bands. In the analysis of the normalized correction count (NCC) we used the confidence intervals of 95% (red lines) and 68% (black lines). The normalized intensity graph has a 95% confidence interval (black lines). In the stick plot graph, the indicator = 1 shows the occurrence of the deformation bands (DB), and the indicator = 0, the absence of the deformation bands. n = number of deformation bands. A) Stick plot of the scanline (with 5.7 m lengths, oriented WNW-ESE) performed at Site 1, n = 13. B) Normalized intensity for Site 1. C) NCC for Site 1. D) Stick plot for scanline (oriented WNW-ESE, 58 m lengths) from Site 2, n = 110. E) Normalized intensity for scanline 2. F) NCC for scanline 2. G) Stick plot for scanline (E-W orientation, and 10 m extension) from Site 3, n = 55. H) Normalized intensity for Site 3. I) NCC for Site 3. J) Stick plot for scanline (with 5.9 m extension, and oriented ENE-WSW) obtained for Site 4, n = 57. K) Normalized strain band intensity at Site 4. L) NCC for Site 4.

References

Abdelkareem, M., Akrby, A., Fakhry, M., Mostafa, M., 2018. Using of Remote Sensing and Aeromagnetic Data for Predicting Potential Areas of Hydrothermal Mineral Deposits in the Central Eastern Desert of Egypt. Remote Sensing. 7 (1), 1-13. https://doi.org/10.18282/rs.v7i1.112.

Airo, M., Wennerström, M., 2010. Application of regional aeromagnetic data in targeting detailed fracture zones. Journal of Applied Geophysics. 71, 62-70. https://doi.org/10.1016/j.jappgeo.2010.03.003.

Araujo, R.E.B., Bezerra, F.H.R., Nogueira, F.C.C., Balsamo, F., Carvalho, B.R.B.M., Souza, J.A.B., Sanglard, J.C.D., de Castro, D.L., Melo, A.C.C., 2018. Basement control on fault formation and deformation band damage zone evolution in the Rio do Peixe Basin, Brazil. Tectonophysics 745, 117–131. https://doi.org/10.1016/j.tecto.2018.08.011.

Araújo Neto, J.F., Santos, G.L., Souza, I.M.B.A., Barreto, S.B., Santos, L.C.M.L., Bezerra, J.P.S., Carrino, T.A., 2018. Integration of remote sensing, airborne geophysics, and structural analysis to geological mapping: a case study of the Vieirópolis region, Borborema Province, NE Brazil. Geol. USP. 18(3), 8-103. http://dx.doi.org/10.11606/issn.2316-9095.v18-140834.

Assine, M.L., 1992. Análise estratigráfica da Bacia do Araripe, Nordeste do Brasil. Revista Brasileira de Geociências. 22 (3), 289-300.

Assine, M.L., 2007. Bacia do Araripe. Boletim de Geociências da Petrobras. 15 (2), 371-389.

Assine, M.L., Perinotto, J.A.J., Custódio, M.A., Neumann, V.H., Varejão, F.G., Mescolotti, P.C., 2014. Sequências deposicionais do Andar Alagoas da Bacia do Araripe, Nordeste do Brasil. B. Geoci. Petrobras. 22 (1), 3-28.

Balsamo, F., Clemenzi, L., Storti, F., Solum, J., Taberner, C., 2019. Tectonic control on vein attributes and deformation intensity in fault damage zones affecting Natih platform carbonates, Jabal Qusaybah, North Oman. J. Struct. Geol. 122, 38-57. https://doi.org/10.1016/j.jsg.2019.02.009.

Bao, H., Zhai, Y., Lan, H., Zhang, K., Qi, Q., Yan, C., 2019. Distribution characteristics and controlling factors of vertical joint spacing in sand-mud interbedded strata. Journal of Structural Geology. 128, 103886.

Barbosa, A.B.S., Maia, R.P., Pontes, C.C.C, Nogueira, F.C.C., Bezerra, F.H.R., 2021. Condicionamento do relevo ao longo de zonas de falha com bandas de deformação na Bacia Sedimentar Rio do Peixe, Brasil. Revista Brasileira de Geomorfologia. 22 (2), 385-406. http://dx.doi.org/10.20502/rbg.v22i2.1948.

Baranov, V., 1957. A new method for interpretation of aeromagnetic maps: Pseudo-gravimetric anomalies. Geophysics. 22, 359-383.

Boyce, J.I., Morris, W.A., 2002. Basement-controlled faulting of Paleozoic strata in southern Ontario, Canada: new evidence from geophysical lineament mapping. Tectonophysics. 353, 151- 171.

Caine, J.S., Bruhn, R.L., Forster, C.B., 2010. Internal structure, fault rocks, and inferences regarding deformation, fluid flow, and mineralization in the seismogenic Stillwater normal fault, Dixie Valley, Nevada. J. Struct. Geol. 32, 1576–1589. https://doi.org/10.1016/j.jsg.2010.03.004.

Cardoso, F.M.C., 2010. O graben de Palestina: contribuição à estratigrafia e estrutura do estágio rift na Bacia do Araripe, Nordeste do Brasil. Natal. Master's dissertation, Post-graduate Program in Geodynamics and Geophysics, Federal University of Rio Grande do Norte. 107p.

Castro, D.L., Fuck R.A., Phillips, J.D., Vidotti, R.M., Bezerra, F.H., Dantas, E.L., 2014. Crustal structure beneath the Paleozoic Parnaíba Basin revealed by airborne gravity and magnetic data, Brazil. Tectonophysics. 614, 128-45. https://doi.org/10.1016/j.tecto.2013.12.009.

Celestino, M.A.L., Miranda, T.S., Correia Filho, O.J., Barbosa, J.A., 2018. Aspectos tectônicos da borda Ne da bacia de fátima, província Borborema - NE do Brasil. Estudos Geológicos. 27 (2), 3-19. https://doi.org/10.18190/1980-8208/estudosgeologicos.

Celestino, M.A.L., Miranda, T.S., Mariano, G., Alencar, M.L., Carvalho, B.R.B.M., Falcão, T.C., Topan, J.G., Barbosa, J.A., Gomes, I.F., 2020. Fault damage zones width: Implications for the tectonic evolution of the northern border of the Araripe Basin, Brazil, NE Brazil. J. Struct. Geol. 138, 1-16. https://doi.org/10.1016/j.jsg.2020.104116.

Cerri, R.I., Warren, L.V., Spencer, C.J., Varejão, F.G., Promenzio, P., Luvizotto, G.L., Assine, M.L. 2022. Using detrital zircon and rutile to constrain sedimentary provenance of Early Paleozoic fluvial systems of the Araripe Basin, Western Gondwana. Journal of South American Earth Sciences. 116. https://doi.org/10.1016/j.jsames.2022.103821.

Cianfarra, P., Salvini, F., 2015. Lineament domain of regional strike-slip corridor: Insight from the Neogene transtensional De Geer transform fault in NW Spitsbergen. Pure and Applied Geophysics. 172 (5), 1185-201.

Choi, J.H., Edwards, P., Ko, K., Kim, Y.S., 2016. Definition and classification of fault damage zones: a review and a new methodological approach. Earth Sci. Rev. 152, 70-87. https://doi.org/10.1016/j.earscirev.2015.11.006.

Crepani, E., 1987. Análise de fraturas através de imagens fotográficas de baixa resolução espacial: uma contribuição ao estudo da evolução tectônica da região da Chapada do Araripe-NE do Brasil. Tese de Doutorado. Universidade de São Paulo.

Drury, S.A., 2001. Image Interpretation in Geology. 3rd ed. Cheltenham: Nelson Thornes.

Ehlen, J., 2000. Fractal analysis of joint patterns in granite. International Journal of Rock Mechanics and Mining Sciences, 37, 909-922, https://doi.org/10.1016/S1365-1609(00)00027-7

Fletcher, J.M., Teran, O.J., Rockwell, T.K., Oskin, M.E., Hudnut, K.W., Spelz, R.M., Lacan, P., Dorsey, M.T., Ostermeijer, G., Mitchell, T.M., Akciz, S.O., Hernandez-Flores, A. P., Hinojosa-Corona, A., Peña-Villa, I., Lynch, D.K., 2020. An analysis of the factors that control fault zone architecture and the importance of fault orientation relative to regional stress. Geological Society of America Bulletin. 132 (9-10): 2084-2104. https://doi.org/10.1130/B35308.1.

Françolin, J.B.L., Cobbold, P.R., Szatmari, P., 1994. Faulting in the early cretaceous Rio do Peixe Basin (NE Brazil) and its significance for the opening of the Atlantic. J. Struct. Geol. 16, 647-661.

Gale, J.F.W., Reed, R.M., Holder, J., 2007. Natural fractures in the Barnett Shale and their importance for hydraulic fracture treatments. Am. Assoc. Petrol. Geol. Bull. 91,603-622. https://doi.org/10.1306/11010606061.

Garcia, X., Julià, J., Nemocón, A.M., Neukirch, M., 2019. Lithospheric thinning under the Araripe Basin (NE Brazil) from a long-period magnetotelluric survey: constraints for tectonic inversion. Gondwana Research. 68, 174-184. https://doi.org/10.1016/j.gr.2018.11.013.

Gillespie, P. A., Johnston, J. D., Loriga, M. A., McCaffrey, K. J. W., Walsh, J. J., Watterson, J., 1999. Influence of layering on vein systematics in line samples. Geological Society, London, Special Publications. 155(1), 35-56.

Gomez, L.A., Laubach, S.E., 2006. Rapid digital quantification of microfracture populations. J. Struct. Geol. 28, 408-420. https://doi.org/10.1016/j.jsg.2005.12.006.

Guerriero, V., Iannace, A., Mazzoli, S., Parente, M., Vitale, S., Giorgioni, M., 2010. Quantifying uncertainties in multi-scale studies of fractured reservoir analogues: implemented statistical analysis of scanline data from carbonate rocks. J. Struct. Geol. 32, 1271-1278. https://doi.org/10.1016/j.jsg.2009.04.016.

Grohmann, C.H., Smith, M.J., Riccomini, C., 2011a. Multi-scale Analysis of Topographic Surface Roughness in the Midland Valley, Scotland. IEEE Transactions on Geoscience and Remote Sensing. 49, 1200-1213. https://doi.org/10.1109/TGRS.2010.2053546.

Grohmann, C.H., Riccomini, C., Chamani, M.A.C., 2011b. Regional scale analysis of landform configuration with base-level (isobase) maps. Hydrol. Earth Syst. Sci. 15, 1493-1504. https://doi.org/10.5194/hess-15-1493-2011.

Hansberry, R.L., King, R.C., Holford, S.P., Hand, M., Debenham, N., 2021. How wide is a fault damage zone? Using network topology to examine how fault-damage zones overprint regional fracture networks. J. Struct. Geol. 146, 104-327.

Harris, S.D., McAllister, E., Knipe, R.J., Odling, N.E., 2003. Predicting the three-dimensional population characteristics of fault zones: a study using stochastic models. J. Struct. Geol. 25, 1281-1299.

Hooker, J.N., Laubach, S.E., and Marrett, R., 2018. Microfracture spacing distributions and the evolution of fracture patterns in sandstones. Journal of Structural Geology. 108, 66-79. https://doi.org/10.1016/j.jsg.2017.04.001.

Jacques, P.D., Machado, R., Oliveira, R.G., Ferreira, F.J.F, Castro, L.G., Nummer, A.R., 2014. Correlation of lineaments (magnetic and topographic) and Phanerozoic brittle structures with Precambrian shear zones from the basement of the Paraná Basin, Santa Catarina State, Brazil. Brazilian Journal of Geology. 44 (1), 39-54. https://doi.org/10.5327/Z2317-4889201400010005.

Kinabo, B.D., Hogan, J.P., Atekwana, E.A., Abdelsalam, M.G., Modisi, M.P., 2008. Fault growth and propagation during incipient continental rifting: Insights from a combined aeromagnetic and Shuttle Radar Topography Mission digital elevation model investigation of the Okavango Rift Zone, northwest Botswana. Tectonics. 27, 1-16. https://doi.org/10.1029/2007TC002154.

Laubach, S.E., Lamarche, J., Gauthier, B.D.M., Dunne, W.M., Sanderson, D.J., 2018a. Spatial arrangement of faults and opening-mode fractures. J. Struct. Geol. 108, 2-15. https://doi.org/10.1016/j.jsg.2017.08.008.

Laubach, S.E., Hundley, T.H., Hooker, J.N., Marrett, R.A., 2018b. Spatial arrangement and size distribution of normal faults, Buckskin detachment upper plate, Western Arizona. J. Struct. Geol. 108, 230-242. https://doi.org/10.1016/j.jsg.2017.10.001.

Li, J.Z., Laubach, S.E., Gale, J.F.W., Marrett, R.A., 2018. Quantifying opening-mode fracture spatial organization in horizontal wellbore image logs, core and outcrop: Application to Upper Cretaceous Frontier Formation tight gas sandstones, USA. J. Struct. Geol. 108, 137-156. http://dx.doi.org/10.1016/j.jsg.2017.07.005.

Li, Y., Oldenburg, D.W., 1998. Separation of regional and residual magnetic field data. Geophysics. 63 (2), 431-439.

Lin, A., Yamashita, K., 2013. Spatial variations in damage zone width along strike-slip faults: an example from active faults in southwest Japan. J. Struct. Geol. 57, 1-15. https://doi.org/10.1016/j.jsg.2013.10.006.

Lima, F.G.F., and Sá, E.F.J., 2017. Controle estrutural da borda sudeste da Bacia do Parnaíba, Nordeste do Brasil: relação com eventos geodinâmicos no Gondwana. Geol. USP, Sér. Cient. 17(3), 3-21. https://doi.org/10.11606/issn.2316-9095.v17-125909.

Lu, Y.C., Tien, Y.M., Juang, C.H., 2017. Uncertainty of 1-D fracture intensity measurements. J. Geophys. Res. Solid Earth. 122, 9344-9358. https://doi.org/10.1002/2016JB013620.

Marques, F.O., Nogueira, F.C.C., Bezerra, F.H.R., Castro, D.L., 2014. The Araripe Basin in NE Brazil: An intracontinental graben inverted to a high-standing horst. Tectonophysics. 630, 251-264. http://dx.doi.org/10.1016/j.tecto.2014.05.029.

Marrett, R., 1996. Aggregate properties of fracture populations. J. Struct. Geol. 18, 169-178. https://doi.org/10.1016/S0191-8141(96)80042-3.

Marrett, R., Ortega, O.J., Kelsey, C.M., 1999. Extent of power-law scaling for natural fractures in rock. Geology. 27, 799-802. https://doi.org/10.1130/0091-7613(1999)027<0799:EOPLSF>2.3.CO;2.

Marrett, R., Gale, J.F.W., Gomez, L., Laubach, S.E., 2018. Correlation analysis of fracture arrangement in space. J. Struct. Geol. 108, 16-33. https://doi.org/10.1016/j.jsg.2017.06.012.

Martinelli, M., Bistacchi, A., Mittempergher, S., Bonneau, F., Balsamo, F., Caumon, G., Meda, M., 2020. Damage zone characterization combining scan-line and scan-area analysis on a km-scale Digital Outcrop Model: The Qala Fault (Gozo). J. Struct. Geol. 140. https://doi.org/10.1016/j.jsg.2020.104144.

Matos, R.M.D., 1992. The Northeast Brazilian Rift System. Tectonics. 11 (4), 766-791.

Matos, R.M.D., 1999. History of the northeast Brazilian rift system: kinematics implications for the break-up between Brazil and West Africa. In: Cameron, N.R.; Bate, R.H.; Clure, V.S. (eds.) The Oil and Gas Habitats of the South Atlantic Geological Society, London, Special Publications.155, 55-73.

Matos R.M.D., 2000. Tectonic evolution of the Equatorial South Atlantic. In: Mohriak W, Taiwani M (eds) Atlantic rifts and continental margins. Geophysical Monograph Series 115, 331.354. Doi.org/10.1029/GM115p0331.

Matos, R.M.D., 2019. Norton, I., Casey, K., Krueger, A. An Orthogonal Zone between the Equatorial and South Atlantic Margins: Relevance and Control in the Evolution of the Afro-Brazilian Basins - 16th International Congress of the Brazilian Geophysical Society. SBGf - Sociedade Brasileira de Geofísica- Rio de Janeiro. Expanded Abstract.

Matos, R.M.D., Krueger, A., Norton, I., Casey, K., 2021. The fundamental role of the Borborema and Benin–Nigeria provinces of NE Brazil and NW Africa during the development of the South Atlantic Cretaceous Rift system. Marine and Petroleum Geology. 127. https://doi.org/10.1016/j.marpetgeo.2020.104872.

McClay, K.R., 1987. The Mapping of Geological Structures. Geological Society of London handbook, p. 161p.

Meixner, J., Grimmer, J.C., Becker, A., Schill, E., Kohl, T., 2018. Comparison of different digital elevation models and satellite imagery for lineament analysis: Implications for identification and spatial arrangement of fault zones in crystalline basement rocks of the southern Black Forest (Germany). J. Struct. Geol. 108, 256-268. https://doi.org/10.1016/j.jsg.2017.11.006.

Menezes, C.P., Bezerra, F.H.R., Balsamo, F., Mozafari, M., Vieira, M.M., Srivastava, N.K., Castro, D.L., 2019. Hydrothermal silicification along faults affecting carbonate-sandstone units and its impact on reservoir quality, Potiguar Basin, Brazil. Marine and Petroleum Geology. 110, 198-217. https://doi.org/10.1016/j.marpetgeo.2019.07.018.

Miranda, T.S., Magalhães, J.R., Barbosa, J.A., 2012. Bacia do Araripe: Possível Sistema Pull-Apart? In: 46° Congresso Brasileiro de Geologia, Anais: Sociedade Brasileira de Geologia. Santos.

Miranda, T.S., Magalhaes, J.R., Barbosa, J.A., Correia Filho, O., Alencar, M.L., 2014. Araripe Basin, NE Brazil: a rift basin implanted over a previous pull-apart system? In: 4th Atlantic Conjugate Margins Conference, vol 3.

Miranda, T.S., Santos, R.F., Barbosa, J.A., Gomes, I.F., Alencar, M.L., Correia, O.J., Falcão, T.C., Gale, J.F.W., Neumann, V.H., 2018. Quantifying aperture, spacing and fracture intensity in a carbonate reservoir analogue: Crato Formation, NE Brazil. Mar. Petrol. Geol. 97, 556-567. https://doi.org/10.1016/j.marpetgeo.2018.07.019.

Miranda, T.M., Neves, S.P., Celestino, M.A.L., Roberts, N.M.W., 2020. Structural evolution of the Cruzeiro do Nordeste shear zone (NE Brazil): Brasiliano-Pan-African- ductile-to-brittle transition and Cretaceous brittle reactivation. J. Struct. Geol. 141. https://doi.org/10.1016%20/%20j.jsg.2020.104203.

Neumann, V.H.M.L., 1999. Estratigrafia, Sedimentologia, Geoquímica y Diagénesis de los Sistemas Lacustres Aptienses-Albienses de lá Cuenca de Araripe (Nororeste do Brasil). Barcelona. Doctoral thesis, Facultat de Geologia, Universitat de Barcelona. 293p.

Neves, S.P., Alcantara, V.C., 2010. Geochemistry of orthogneisses and metasedimentary rocks across a proposed terrane boundary in the Central Domain of Borborema Province, NE Brazil: geodynamic implications. Journal of South American Earth Sciences. 29, 498-511. https://doi.org/10.1016/j.jsames.2009.08.002.

Ngwenya, B.T., Elphick, S.C., Main, I.G., Shimmield, G.B., 2000. Experimental constraints on the diagenetic self-sealing capacity of faults in high porosity rocks. Earth Planet. Sci. Lett. 183, 187-199. https://doi.org/10.1016/S0012-821X(00)00261-2.

Nicolas, M.P.B., Clayton, B.W., 2015. Lineament mapping of the Hudson Bay Lowland using remote-sensing methods, northeastern Manitoba (parts of NTS 53N, O, 54). In: Report of Activities 2015, Manitoba Mineral Resources, Manitoba Geological Survey, p. 89-96.

Nogueira, F.C.C., Marques, F.O., Bezerra, F.H.R., de Castro, D.L., Fuck, R.A., 2015. Cretaceous intracontinental rifting and post-rift inversion in NE Brazil: insights from the Rio do Peixe Basin. Tectonophysics 644, 92–107. https://doi.org/10.1016/j.tecto.2014.12.016.

O'Hara, A.P., Jacobi, R.D., Sheets, H.D., 2017. Predicting the width and average fracture frequency of damage zones using a partial least squares statistical analysis: Implications for fault zone development. J. Struct. Geol. 98, 38-52. https://doi.org/10.1016/j.jsg.2017.03.008.

Oliveira, R.G., 2008. Arcabouço geofísico, isostasia e causas do magmatismo cenozoico da província Borborema e de sua margem continental (Nordeste do Brasil). Natal.

Doctoral thesis. Post-graduate Program in Geodynamics and Geophysics, Federal University of Rio Grande do Norte. 415p.

Ortega, O.J., Marrett, R.A., Laubach, S.E., 2006. A scale-independent approach to fracture intensity and average spacing measurement. Am. Assoc. Petrol. Geol. Bull. 90, 193-208. https://doi.org/10.1306/08250505059.

Osagiede, E.E., Rotevatn, A., Gawthorpe, R., Kristensen, T.B., Jackson, C. A., Marsh, N., 2020. Pre-existing intra-basement shear zones influence growth and geometry of non-colinear normal faults, western Utsira High-Heimdal Terrace, North Sea. Journal of Structural Geology 130, 103908. https://doi.org/10.1016/j.jsg.2019.103908.

Peulvast, J.P., Betard, F., 2015. A history of basin inversion, scarp retreat and shallow denudation: the Araripe basin as a keystone for understanding long-term landscape evolution in NE Brazil. Geomorphology. 233, 20-40. https://doi.org/10.1016/j.geomorph.2014.10.009.

Pilkington, M., Roest, W.R., 1997. Suppressing varying directional trends in aeromagnetic data, application of regional and Geophysical and Geochemistry.

Pontes, C.C.C., Nogueira, F.C.C., Bezerra, F.H.R., Balzamo, F., Miranda, T.S., Nicchio, M.A., Souza, J.A.B., Carvalho, B.R.B.M., 2019. Petrophysical properties of deformation bands in high porous sandstones across fault zones in the Rio do Peixe Basin, Brazil. International Journal of Rock Mechanics and Mining Sciences.114, 153-163. https://doi.org/10.1016/j.ijrmms.2018.12.009.

Priest, S.D., 1993. Discontinuity Analysis for Rock Engineering. Chapman and Hall, London 473p.

Priest, S.D., Hudson, J.A., 1976. Discontinuity spacings in rock. Int. J. Rock Mech. 13, 135-148.

Reeves C., 2005. Aeromagnetic Surveys. Principles, Practice and Interpretation. Earthworks, Geosoft. 155p.

Riley, P.R., Goodwin, L.B., Lewis, C.J., 2010. Controls on fault damage zone width, structure, and symmetry in the Bandelier Tuff, New Mexico. J. Struct. Geol. 32, 766-780.

Rives, T., Razack, M., Petit, J. P., Rawnsley, K. D., 1992. Joint spacing: analogue and numerical simulations. Journal of Structural Geology. 14(8-9), 925-937.

Salamuni, E., Ebert, H.D., Hasui, Y., 2004. Morfotectônica da bacia sedimentar de curitiba. Rev. Bras. Geociências 34, 469-478. https://doi.org/10.25249/0375-7536.2004344469478.

Santos, E.J., Van Schmus, R.W., Brito Neves, B.B., Oliveira, R.G., Medeiros, V.C., 1999. Terranes and their boundaries in the Proterozoic Borborema Province, Northeast Brazil. In: Estended Abstracts 7 Simpósio Nacional de Estudos Tectônicos. 121-124.

Santos, R.F.V.C., Miranda, T.S., Barbosa, J.A., Gomes, I.F., Matos, G.C., Gale, J., Neumann, V.H., Guimarães, L.J., 2015a. Characterization of natural fracture systems: analysis of uncertainty effects in linear scanline results. AAPG (Am. Assoc. Pet. Geol.) Bull. 99 (12), 2203-2219. https://doi.org/10.1306/05211514104.

Santos, R. F. V., Miranda, T. S., Barbosa, A., Gomes, I. F., Matos, G. C., Neumann, V. H. M. L., Guimarães, L. N., Gale, J., 2015b. Analysis of potential uncertainties in opening-mode fractures characterization through the scanline technique of aptian carbonates, Araripe Basin, Northeast of Brasil. In: AAPG Annual Convention and Exhibition, Denver, CO.

Sanusi, S.O., Amigun, J.O., 2020. Structural and hydrothermal alteration mapping related to orogenic gold mineralization in part of Kushaka schist belt, North-central Nigeria, using airborne magnetic and gamma-ray spectrometry data. SN Applied Sciences. 2 (9), 1-26.

Scherer, C.M.S., Jardim de Sá, E.F., Córdoba, V.C., Sousa, D.C., Aquino, M.M., Cardoso, F.M.C., 2014. Tectono-stratigraphic evolution of the Upper Jurassic-Neocomian rift succession, Araripe Basin, Northeast Brazil. Journal of South American Earth Sciences. 49, 106-122. https://doi.org/10.1016/j.jsames.2013.10.007.

Silvestre, D.C., Fambrini, G.L., Santos, A.A.f., 2017. Caracterização faciológica das formações Cariri e Brejo Santo em afloramentos a NE do município Missão Velha (Ceará - Brasil). Estudos Geológicos, 27(1). https://doi.org/10.18190/1980-8208/estudosgeologicos.v27n1p19-33.

Soliman, A., Han, L., 2019. Effects of vertical accuracy of digital elevation model (DEM) data on automatic lineaments extraction from shaded DEM. Advances in Space Research. 64, 603-622. https://doi.org/10.1016/j.asr.2019.05.009.

Torabi, A., Ellingsen, T.S.S., Johannessen, M.U, Alaei, B., Rotevatn, A., Chiarella, D., 2020. Fault zone architecture and its scaling laws: where does the damage zone start and stop? Geological Society of London. 496 (1), 99-124. https://doi.org/10.1144/SP496-2018-151.

Van Schmus, W.R., Kozuch, M., Brito Neves, B.B., 2011. Precambrian history of the Zona Transversal of the Borborema Province, NE Brazil: Insights from Sm-Nd and U-Pb geochronology. Journal of South American Earth Sciences. 3, 227-252. https://doi.org/10.1016/j.jsames.2011.02.010.

Vasconcelos, D.L., Bezerra, F.H.R., Medeiros, W.E., de Castro, D.L., Clausen, O.R., Vital, H., Oliveira, R.G., 2019. Basement fabric controls rift nucleation and postrift basin inversion in the continental margin of NE Brazil. Tectonophysics. 751, 23-968 40. https://doi.org/10.1016/j.tecto.2018.12.019.

Wang, Q., Laubach, S.E., Gale, J.F.W., Ramos, M.J., 2019. Quantified fracture (joint) clustering in Archean basement, Wyoming: application of the normalized correlation count method. Petroleum Geoscience. 25 (4). http://dx.doi.org/10.1144/petgeo2018-146.

Wise, D.U., Funiciello, R., Parotto, M., Salvini, F., 1985. Topographic lineament swarms: Clues to their origin from domain analysis of Italy. Geological Society of America Bulletin. 96, 952-967.

Zhang, Y., Langhi, L., Schaubs, P.M., Delle Piane, C., Dewhurst, D.N., Stalker, L., Michael, K., 2015. Geomechanical stability of CO_2 containment at the South West Hub Western Australia: A coupled geomechanical-fluid flow modelling approach. International Journal of Greenhouse Gas Control. 37, 12-23. https://doi.org/10.1016/j.ijggc.2015.03.003.

4.2 THE CHARACTERIZATION OF FAULT GEOMETRIES USING EULER DECONVOLUTION: INSIGHTS FROM THE EASTERN BORDER OF THE ARARIPE BASIN, NE BRAZIL

The characterization of fault geometries using Euler deconvolution: Insights from the eastern border of the Araripe Basin, NE Brazil

Vivian Silvani de Arruda Passos[1], Jefferson Tavares Cruz Oliveira[2], Tiago Siqueira de Miranda[2], Maria Alcione Lima Celestino[1]

[1]Geosciences Graduate Program, Federal University of Pernambuco, Recife, PE, 50740-530, Brazil (vivian.silvani@gmail.com; alcionelimma22@gmail.com)

[2]Department of Geology, Federal University of Pernambuco, Recife, PE, 50740-530, Brazil (jefferson.tavares@ufpe.br, tiago.smiranda@ufpe.br)

Abstract

In this study, Euler deconvolution was used to analyze the geometry of the main fault zones on the eastern border of the Araripe Basin, northeastern Brazil. The structural context provided by Euler deconvolution can be an important tool in areas where seismic data are scarce or not available, as is the case in the Araripe Basin. In this study, Euler deconvolution was applied to anomalous and reduced-to-pole aeromagnetic data using different structural indices. Our results show that the main fault zones (the Mauriti, Coité, and Umburanas faults) have magnetic source depths between 200 and 800 m that vary along the length of the fault, with the solutions indicating shallower depths closer to the border of the basin. These fault zones are represented in the field as faults and deformation bands that are consistent with the tectonic fabrics inherited from basement structures (Precambrian fabric). These structures are also highlighted by regional aeromagnetic lineaments. Our results confirm that the

displacement of the fault zones of the eastern border of the Araripe basin is responsible for the delineation of grabens and horsts that are present in the eastern sector of the basin.

Keywords: aeromagnetic; fault depth estimates; brittle deformation; fault zones.

1. Introduction

Fault zones are complex, lithologically heterogeneous, anisotropic, and discontinuous structures (Caine et al., 1996; Harris et al., 2003; Faulkner et al., 2010; Fletcher et al., 2020; Fossen et al., 2020). Understanding the geometry of fault zones allows geologists to estimate and constrain their dimensions through the use of information about their length (the dimension of the fault parallel to its strike), height (the dimension of the fault parallel to its dip), and displacement (Barnett et al., 1987; Walsh and Watterson, 1988; Torabi and Berg, 2011). The structural context of the subsurface can be determined using Euler Deconvolution (ED) (Ferraccioli et al., 2009; Castro et al., 2014; Abdelkareem, et al., 2018), making it possible to predict the depths of magnetic anomaly sources in fault zones.

ED is a spatial mapping technique used to estimate the horizontal position and depths of magnetic or gravimetric sources (Reid et al., 1990; Durrheim et al., 1998; Barbosa and Silva, 2005). It is an important tool for conducting in-depth analyses of structural behavior as well as enabling studies that cover large areas. Estimates of the depth and position of magnetic sources are based on solutions to the Euler homogeneity equation (Thompson, 1982). The solutions to the homogeneity equation are strongly dependent on the structural index, which is representative of the nature of the source (Thompson, 1982; Reid et al., 1990). Different structural indices can be used to identify and characterize a wide variety of geological structures, such as contacts, foliations, faults, dikes, sills, and pipes (Thompson, 1982; Reid et al., 1990). ED also has applications in a wide range of fields, such as studies on impact structures (Werner et al., 2010) as well as fault locations (Rodrigues et al., 2014), and the connections between their hypocenters particularly in the case of seismogenic structures (Minelli et al., 2016). Furthermore, this technique can be used to map structures in

Precambrian basements (Zhang et al., 2015; Ibraheem et al., 2018), suture zones (Bournas et al., 2003), lineaments and geological contacts (Wang et al., 2017; Weiherman et al., 2018), and determine the tectono-magmatic relationship of sedimentary basins (Magalhães, 2019). However, ED has several limitations that are highlighted as follows: 1) the empirical criterion for determining the structural index (Barbosa and Silva, 2005); 2) the inadequacy of terrestrial magnetic surveys with few observations (Barbosa and Silva, 2005); 3) its ineffectiveness at determining the three-dimensional shape of anomalous sources (Uieda et al., 2014); 4) the difficulties involved with delineating the shape of the source (Mota et al., 2020); and 5) its dependency on the moving-window used (Uieda et al., 2014). Despite these limitations, ED allows us to extract important geological information from the analysis of geophysical data; in conjunction with field data, this allows us to gain insights into the geology of the studied areas (e.g., Uieda et al., 2014; Mota, 2020).

In this study, we applied ED to aeromagnetic surveys on the eastern border of the Araripe Basin, an intracontinental rift basin located in northeastern Brazil (Fig. 1). We analyzed magnetic anomaly trends and their relationship to surface morphology obtained from outcrop data to distinguish the lithological and structural heterogeneities of the crystalline basement and its overlying sedimentary sequence, the Cariri Formation. In particular, this study aims to characterize the subsurface fault zones in the study area. The eastern border of the Araripe Basin contains several significant structural lineaments that are associated with the Patos Shear Zone (PASZ), which play an important role in the understanding of the fault zones generated by the tectonic evolution of this basin (e.g., Celestino et al., 2020; Matos et al., 2021; Fossen et al., 2022). In addition, there is a lack of 2D seismic sections in the Araripe Basin, making it difficult to conduct a traditional analysis of these subsurface structures. Hence, ED is the most appropriate technique for the investigation of these fault zones.

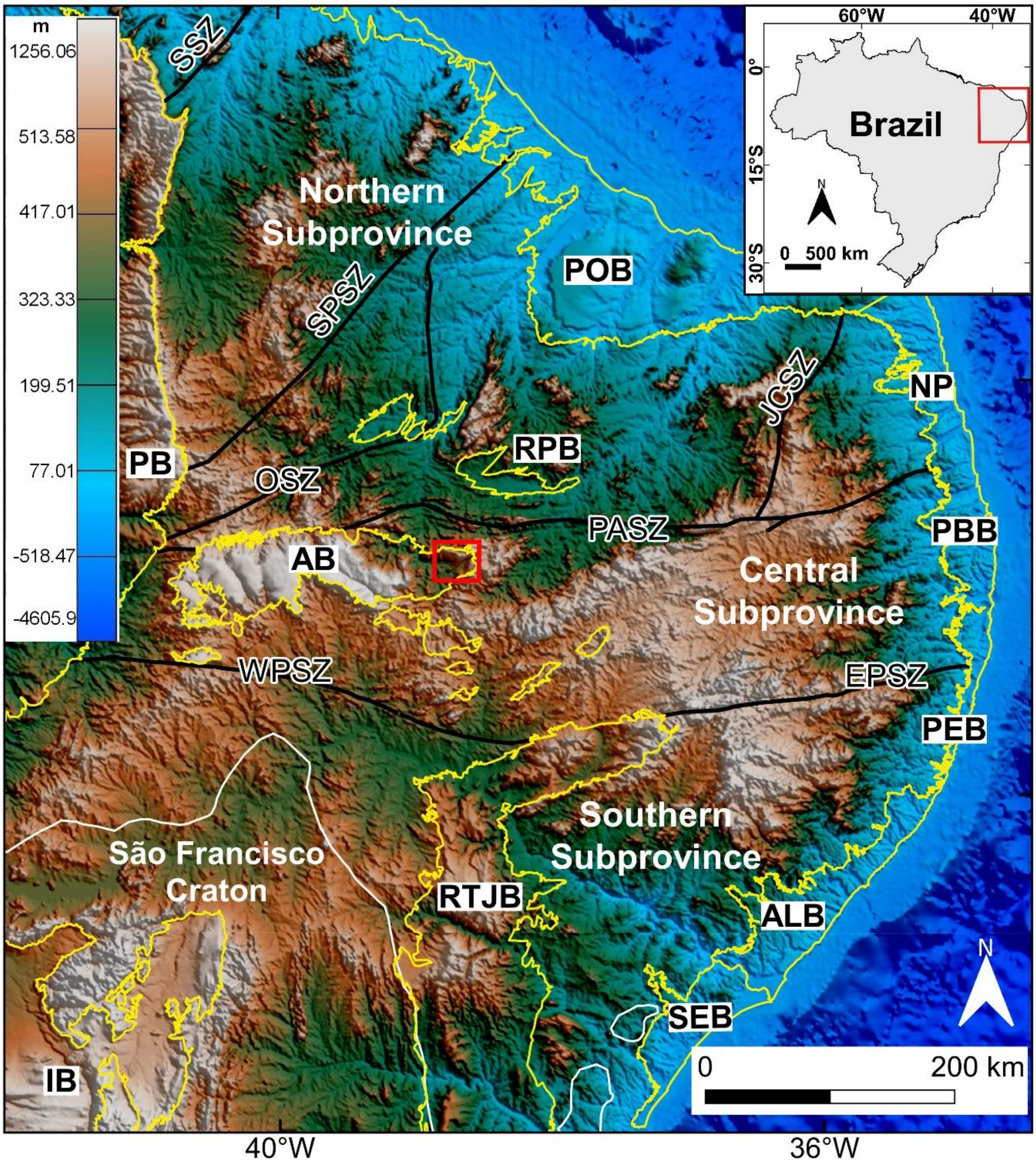

Figure 1. Topographic map of the Borborema Province and its division into northern, central, and southern subprovinces (domains) that are delimited by the Patos and Pernambuco shear zones in the east and west, respectively. The locations of the intraplate and marginal basins of NE Brazil are indicated by the yellow lines. The study area is delineated by the red square. The white line illustrates the limits of the São Francisco Craton. Abbreviated shear zones (marked with black lines) are as follows: EPSZ, East Pernambuco Shear Zone; JCSZ, Picuí-

João Câmara Shear Zone; OSZ, Orós Shear Zone; PASZ, Patos Shear Zone; SPSZ, Senador Pompeu Shear Zone; SSZ, Sobral Pedro Shear Zone; WPSZ, West Pernambuco Shear Zone. Abbreviated basins are as follows: AB, Araripe Basin; ALB, Alagoas Basin; NP, Natal Platform; PB, Parnaíba Basin; IB, PBB, Paraíba Basin; PEB, Pernambuco Basin; POB, Potiguar Basin; Irecê Basin; RPB, Rio do Peixe Basin; RTJB, Recôncavo-Tucano-Jatobá Basin; SEB, Sergipe Basin.

2. Geological setting

The Araripe Basin is an intracontinental rift basin located in the Borborema Province (Fig. 1). This province is characterized by intercalations of metaplutonic domains and metasedimentary units of different ages that are fragmented by the PASZ and the Pernambuco shear zones in the east (EPSZ) and west (WPSZ), respectively. These continental-scale structures divide the Borborema Province into the Northern, Central, and Southern structural domains (Vauchez et al., 1995; Neves and Mariano, 1999; Brito Neves et al., 2001; Van Schmus et al., 2008, 2011; Almeida et al., 2015; Neves et al., 2021). The Araripe Basin is located in the Central Subprovince or Transversal Zone Domain, which lies between the Patos (PASZ) and West Pernambuco (WPSZ) shear zones (Fig. 1). This basin is surrounded by Precambrian metaplutonic rocks (Santos et al., 1999; Oliveira, 2008; Neves and Alcantara, 2010; Van Schmus et al., 2011) that have been intruded by a Neoproterozoic granitoid, aged 590–560 Ma (Sial, 1986; Ferreira et al., 2004).

The internal structural framework of the Araripe Basin is dominated by horsts and grabens (Fig. 2). The Dom Leme Structural High has been characterized by magnetic and gravimetric data, and separates the Araripe Basin into the Feitoria and Cariri sub-basins in the west and east, respectively (Rand and Manso, 1984; Ponte and Ponte Filho, 1996). In addition, Castro and Castelo Branco (1999) confirmed the existence of these two sub-basins using 3D gravimetric modeling, which were found to reach depths of up to 1,600 m to the top of the basement. Cardoso (2010) published an interpretation of the NNW-SSE-trending 141-

RL-08 seismic line (Fig. 2), located in the south of the study area. Due to the lack of well data along the seismic section, these interpretations were made according to geological mapping data, seismic reflection patterns, as well as published well and gravimetry data from other regions of the Araripe Basin. They verified the presence of the Brejo Santo-Mauriti and Umburanas Horsts, the Palestina Graben, and the Abaiara-Jenipapeiro Half-graben in the Cariri sub-basin, and suggested that the sedimentary package had a thickness of 1,750 m in this region.

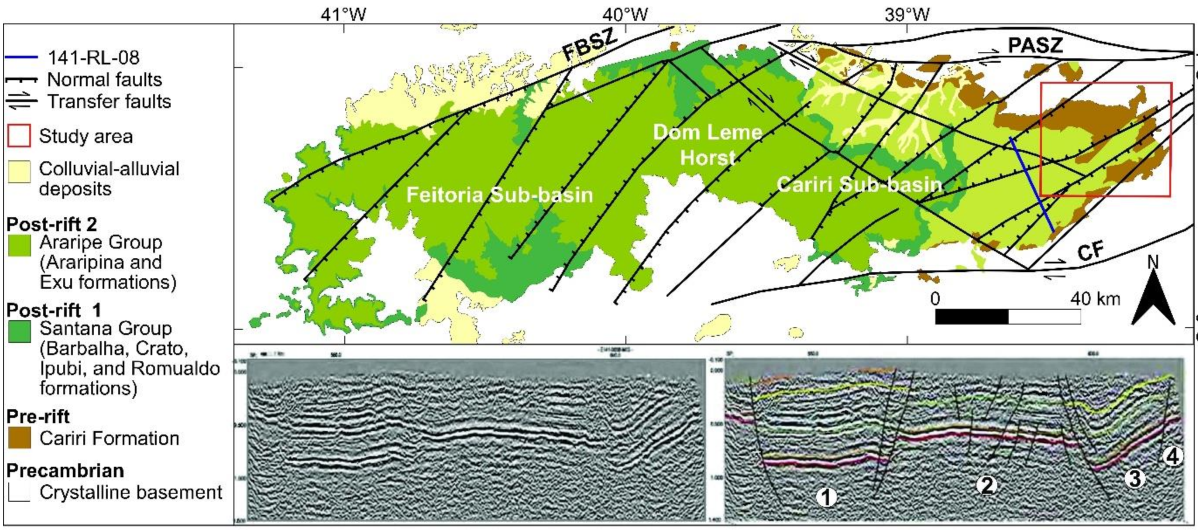

Figure 2. Geological map showing the structural compartmentalization of the Araripe Basin as well as the location of the Feitoria and Cariri sub-basins. Note the blue line, which indicates the geometry of the 141-RL-08 seismic line located in the Cariri sub-basin, as well as its interpretations as made by Cardoso (2010) — (1) Abaiara-Jenipapeiro Half-graben; (2) Brejo Santo-Mauriti Horst; (3) Palestina Graben; and (4) Umburana Horst. The study area is delineated by the red square. Shear zones: FBSZ, Farias Brito Shear Zone; PASZ, Patos Shear Zone; and CF, Falha de Conceição. Modified from Ponte and Ponte Filho (1996) and Angelim et al. (2004).

The Araripe Basin originated as an aborted rift system in which the PASZ was reactivated in a brittle manner by Cretaceous NW-SE extension (126-123 Ma), transforming the NE-SW strike-slip faults into normal faults (Matos, 1992; Matos et al., 2019, 2021). The tectonic evolution of the basin and the rearrangement of its depocenters were strongly controlled by the brittle reactivation of the ductile fabric of the Precambrian basement (Matos 1992; Françolin et al., 1994; Castro and Castelo Branco, 1999). Ponte and Ponte Filho (1996) highlighted three stages of subsidence during this extension event that was responsible for the formation of intraplate rift-type basins in northeastern Brazil. The first phase involved regional subsidence (pre-rift), while the second phase involved rapid local mechanical subsidence, resulting in the formation of graben and/or half-graben systems (rift). The final tectonic phase marked the return of regional subsidence (post-rift).

By observing the geometric and kinematic aspects of the Araripe Basin, Miranda et al. (2012, 2014) proposed a two-stage tectonic model in which phase I is characterized by a pull-apart rift that occurred during the Paleozoic, while phase II involved distension rifting during the Cretaceous. These authors emphasized that the PASZ would primarily be responsible for the formation of rhombohedral depocenters (Feitoria and Cariri sub-basins). This interpretation was supported by Matos (1992), who also discussed the possibility that the PASZ would have acted as a border fault for the Araripe Basin. Additionally, Marques et al. (2014) suggested that the accumulation of stresses during compression reactivated the shear zones on the plate, giving rise to the main inverse faults present in the Araripe Basin. Peulvast and Betard (2015) proposed that region-wide crustal elevation resulted in differential erosion in the basin, which, in turn, caused its topographical inversion. However, Garcia et al. (2019) note that the tectonic inversion developed due to the weakening of the mantle (shallow asthenosphere), which resulted in the concentration of regional compressional tensions that contributed to the local uplift of the Araripe Basin. The most recent model, proposed by Celestino et al. (2020) using topographic, gravimetric, and field data, suggests three deformational phases: the Dn phase, characterized by the ductile deformation of PAZS with dextral kinematics (Neoproterozoic); the Dn+1 phase, involving the development of structural highs in the basin related to strike-slip tectonics with dextral kinematics at shallow crustal levels (Paleozoic); and the Dn+2 phase, characterized by the fragile reactivation of PAZS with sinistral kinematics during the opening of the Atlantic Ocean (lower Cretaceous).

The lithostratigraphic units of the Araripe Basin have been traditionally divided into four pre-, syn-, and post-rift 1 and 2 sequences (Neumann, 1999; Assine, 2007; Assine et al., 2014) (Fig. 2). The pre-rift sequence is represented by the Paleozoic Cariri Formation (Cambrian–Ordovician) (Cerri et al., 2022) and by the Brejo Santo and Missão Velha Formations from the Middle to Late Jurassic. The rift sequence is defined by the Early Cretaceous Abaiara Formation. Finally, the post-rift sequence (Aptian–Cenomanian) is defined by the Barbalha, Crato, Ipubi, and Romualdo formations, which represent the post-rift 1 sequence, and the Exú Formation, which represents the post-rift 2 sequence. This study focuses on the eastern border of the Araripe Basin (Fig. 3) in which the outcrops are primarily the surface expressions of the pre- and syn-rift sequences. This sector of the basin contains important fault zones (Mauriti, Coité, and Umburanas faults) that are related to the brittle reactivations of PAZS during the Early Cretaceous (Passos et al., 2022).

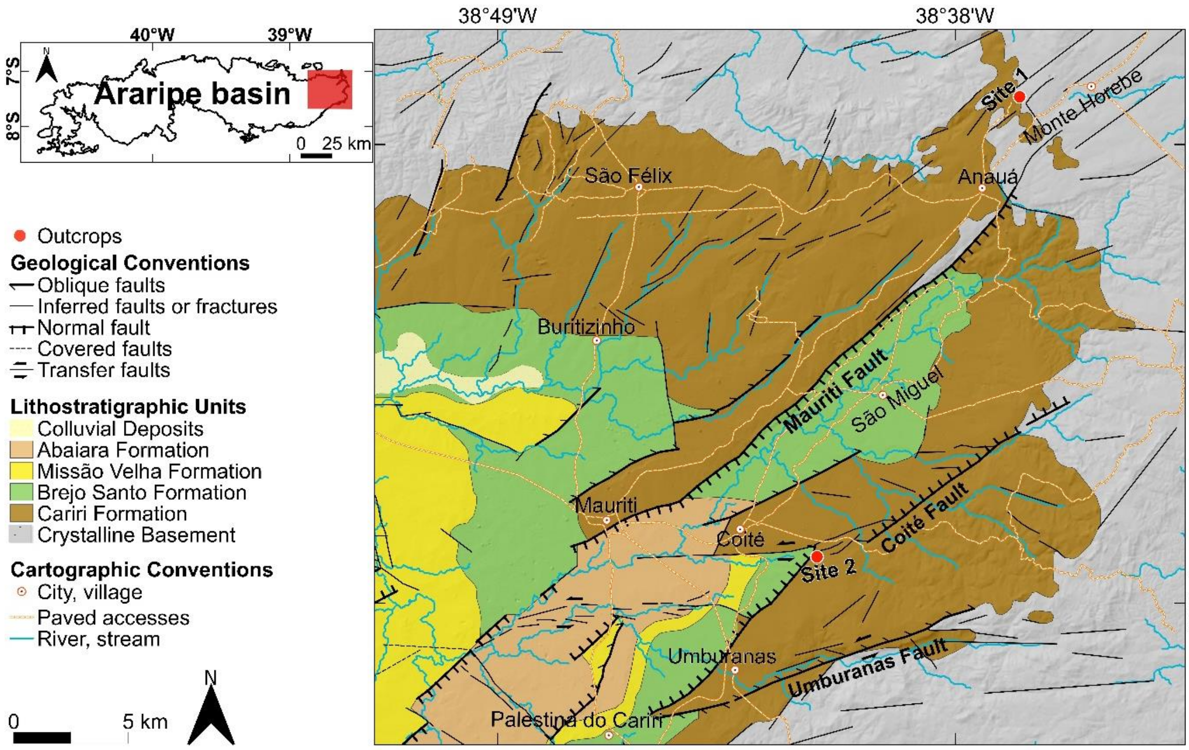

Figure 3. Geological map of the eastern border of the Araripe Basin, showing the location of key outcrops (sites 1 and 2) and fault zones (Mauriti, Coité, and Umburanas faults). The study area is delineated by the red square. Modified from Cardoso (2010).

3. Materials and methods

3.1 Aeromagnetic data

Aeromagnetic data from the eastern border of the Araripe Basin was acquired from the aerogeophysical projects Pernambuco Paraíba (1091) and Paraíba Rio Grande do Norte (1092), which can be found on the Brazilian Geological Survey’s open-access database (Brazilian Geological Survey, 2020). These magnetic surveys were acquired using N–S flight lines and E–W tie-lines with a spacing of 500 m and 10 km, respectively. These data were processed according to the workflow described in Figure 4, which was performed using the Oasis Montaj 9.1 software. Noise and background removal was performed in three stages: 1) analyzing the noise level (e.g., spike identification and removal); 2) removal of the International Geomagnetic Reference Field; and 3) use of directional cosine and Butterworth filters to remove artifacts from leveling (Pilkington and Roest, 1997). The filtered data were interpolated using the bidirectional method with a cell size of 125m (Reeves, 2005).

A reduction to the pole technique was subsequently applied to centralize the peaks of the anomalies (positive amplitude signatures) on their causative sources (Baranov, 1957). The Reduction-to-Pole transformation (RTP) was calculated using the relevant magnetic inclinations (-21°) and declinations (-22°) based on the data acquisition periods and locations. We used a pseudoinclination factor ranging from 60° to 80° to suppress the amplitude and power due to the declination direction at low magnetic latitudes (±20°). We then used a regional-residual Gaussian filter (Li and Oldenburg, 1998) on both the aeromagnetic anomalies and RTP aeromagnetic anomalies to separately interpret the shallow and deep sources. The filter was applied using a cut-off point (k_o) that was determined by an analysis of the power spectrum. The wavenumber (k_o) used was 0.1 cycles/km, which corresponded to the limit between the deepest sources basement structures at a depth between 2-3 km and the shallowest sources that are mainly associated with the brittle fabric of the basin and the basement (depth between 500 m and 2 km).

We used the borders and centers of the anomalies as the criteria for interpretation of the magnetic lineaments in the analysis of the residual aeromagnetic map and the residual RTP aeromagnetic map, respectively. Then, we calculated the orientation patterns of these magnetic lineaments on the eastern border of the Araripe Basin.

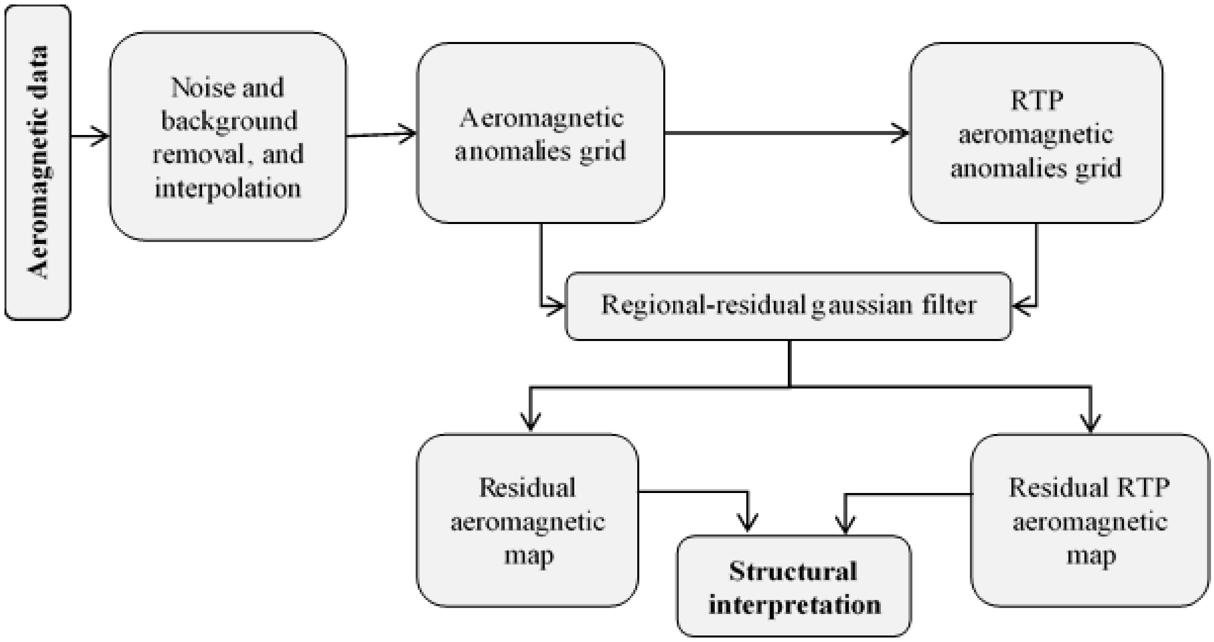

Figure 4. Flowchart summarizing the steps performed to process the aeromagnetic data using the Oasis Montaj software. Steps performed included noise and background removal, interpolation, grid filtering, and the subsequent interpretation of magnetic lineaments from shallower sources (depth between 500 m and 2 km) from the residual aeromagnetic map and the residual RTP aeromagnetic map.

3.2 Euler deconvolution (ED)

The technique used for the semiautomatic detection of magnetic sources was based on Euler's homogeneity equation (Blakely, 1996):

$$(r - r_0)\nabla T = -n\,T \quad (1)$$

where ∇T is the gradient of the magnetic anomalous field measured at the point $r = r - r_0$, and n refers to the structural index, which is a measure of the decay rate of the magnetic anomaly with increasing distance between the source and the measurement point and is an indicator of the likely geometry of the source (Thompson, 1982). Specifically, based on the nature of the magnetic source, the values for the structural index are as follows: n = 0 for contacts or steps, $n = 0.5$ for faults, $n = 1$ for sills or dikes, $n = 2$ for cylinders or pipes, and $n = 3$ for spheres or dipoles (Reid et al., 1990). The structural index (n) is Cartesian coordinate system with the positive x, y, and z axes pointing in the north, east, and down directions, respectively. Equation (1) can be written as follows (Thompson, 1982):

$$(x - x_0)\frac{dT}{dx} + (y - y_0) + \frac{dT}{dy} + (z - z_0) + \frac{dT}{dz} = -\eta\,(T - B) \qquad (2)$$

Most geological structures are represented by higher-order structural indices. However, lower indices give more accurate estimates regarding the depth to the top of the structure (Thompson, 1982). Reid et al. (1990) pointed out that real data may contain anomalies from various sources with different structural indices (ranging from 0–3). The ED technique was applied to the anomalies in the aeromagnetic grid as well as the RTP aeromagnetic anomalies (Fig. 5) to map and estimate the depth of the magnetic sources using structural indices of 0, 0.5, and 1. An index of $n = 0$ better highlights faults with large throws; $n = 0.5$ highlights faults with intermediate throws; and $n = 1$ is the most appropriate value for the characterization of dikes or faults with limited throws (Reid et al., 1990). In addition, the window size and maximum depth tolerance allowed are also important parameters in ED (Dewangan et al., 2007). In this study, we used a window size equal to ten times the grid spacing; this value was chosen based on the wavelength of the potential field signal and the target depths. We used a maximum depth tolerance of 15%; i.e., all depth solutions with an error estimate smaller than this tolerance were accepted. Smaller tolerances will result in fewer but more accurate solutions.

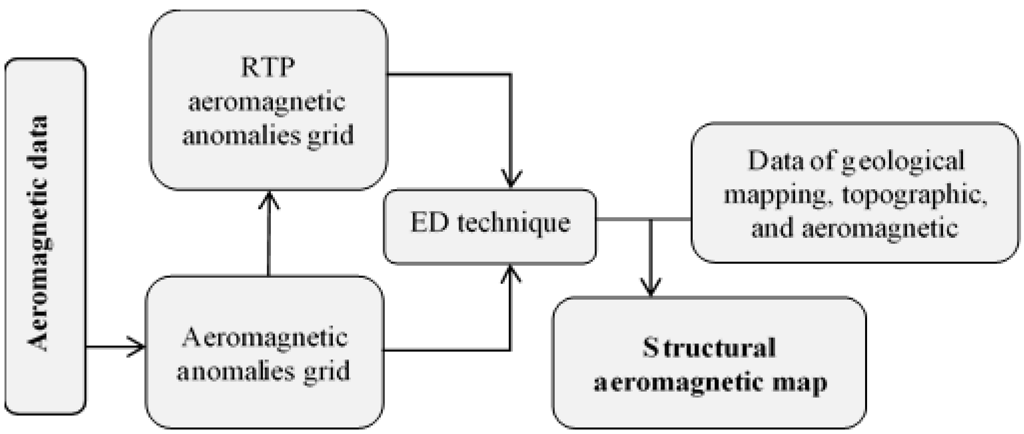

Figure 5. Flowchart illustrating the stages in the application of Euler deconvolution. The final structural aeromagnetic map generated is a combination of the results presented in this study as well as data interpreted by Passos et al. (2022) in the study area.

3.3 Structural field data

Structural field data were obtained from key outcrops on the eastern border of the Araripe Basin (Fig. 3). Site 1 represents the basin-basement limit, marked by outcrops of Neoproterozoic mylonitic granites. Site 2 comprises sandstones of the Cariri Formation, close to the Coité Fault. We collected data on the orientation of these structures using geological instruments such as Clar and Brunton compasses, as well as the Fieldmove Clino and StereoNet mobile applications. Data from other outcrops in the study area were taken from the work conducted by Passos et al. (2022).

These rocks show evidence of brittle deformation through deformational structures such as faults and deformation bands. The structural characterization described in this study allows us to characterize the differences in the distinct structural behavior of the basin and basement, increasing the reliability of the geophysical interpretations made from the combination of information from the surface outcrops and the subsurface fault zones for this sector of the basin.

4. Results

4.1 Aeromagnetic anomalies

The residual aeromagnetic anomalies ranged from -9.30 to 5.68 nT (Fig. 6A and B), while the residual RTP anomalies ranged from -8.69 to 6.24 nT (Fig. 6C and D). The residual filter allows for the investigation of shallow aeromagnetic anomalies with depths between 500 m and 2 km, which were found to be preferably oriented E–W, ENE–WSW, and NE–SW in both the basin and the basement.

The eastern border of the Araripe Basin exhibits aeromagnetic lineaments with lengths of approximately 24 km, 10 km, and 14 km that are located in areas 1, 2, and 3 (Fig. 6B and

D); these correspond to the Mauriti, Coité, and Umburanas faults, respectively. These are important fault zones in the eastern border of the Araripe Basin, comprised of a mix of normal and oblique faults trending NE–SW and ENE–WSW (Fig. 3 and 6).

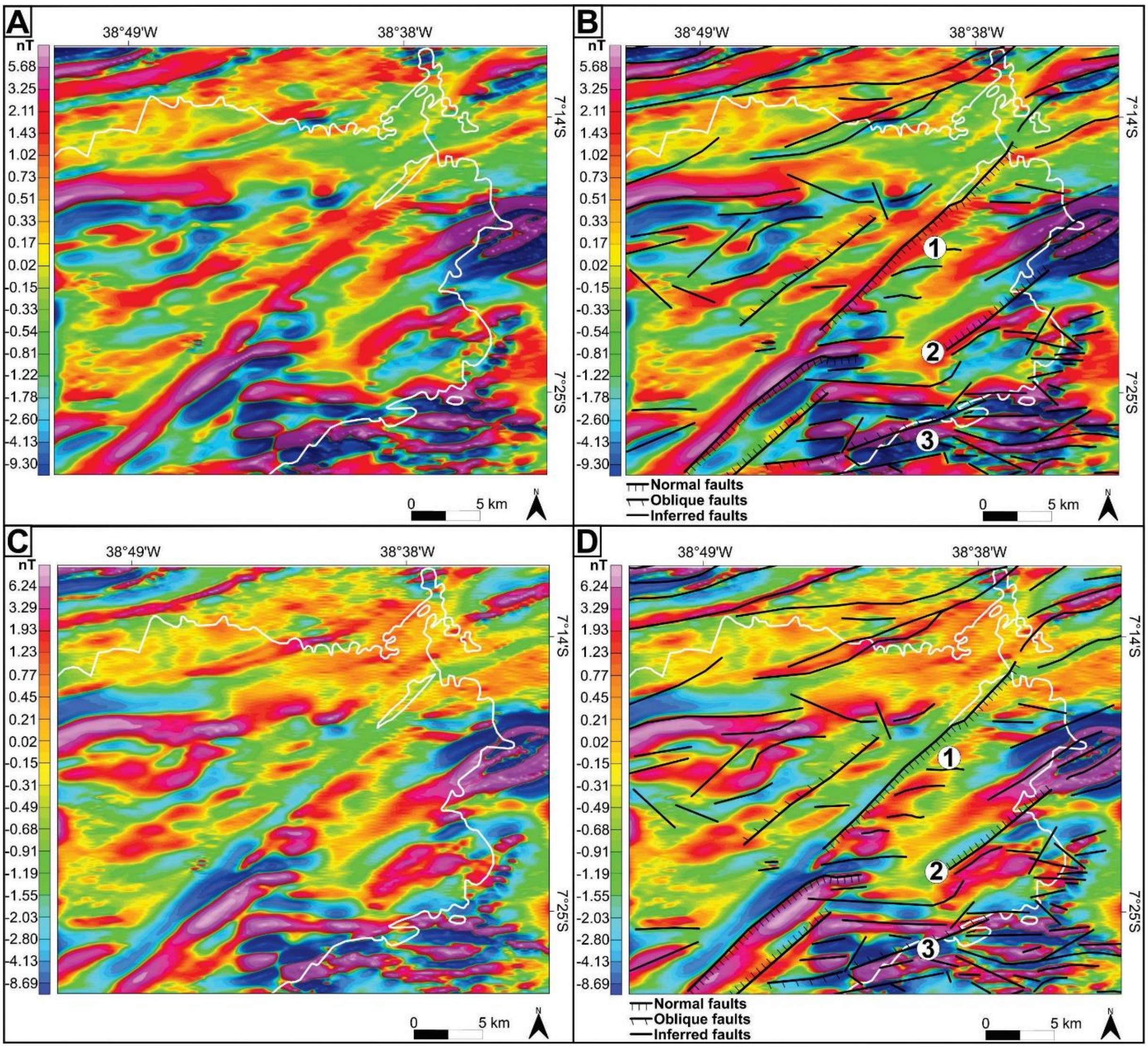

Figure 6. Lineaments of the aeromagnetic anomalies on the eastern border of the Araripe Basin as obtained from the Brazilian Geological Survey. The extent of the fault zones is indicated as follows: (1) Mauriti, (2) Coité, and (3) Umburanas. The black line illustrates the interpretations of the main aeromagnetic lineaments, while the white line indicates the limit between the basin and the basement. A, B) Residual aeromagnetic map. C, D) Residual RTP aeromagnetic map.

4.2 Euler depth solutions

In this study, we applied ED to the aeromagnetic anomalies (Fig. 7) and the RTP aeromagnetic anomalies (Fig. 8) using different structural indices to determine the depth of the sources of these anomalies. These elongated magnetic anomalies are mainly oriented E–W, ENE–WSW, and NE–SW. In this sector, the depths of the magnetic sources in the main fault zones varied along the length of the fault (Table 1). The solutions generated from the aeromagnetic anomalies map and the RTP aeromagnetic anomalies map revealed magnetic source depths of up to 600 m, in some cases reaching values greater than 800 m. A smaller number of Euler solutions were generated for the RTP aeromagnetic anomalies map, with solutions greater than 800 m being relatively rare.

In our solutions, the Mauriti Fault only had a few solutions of 800 m or greater; in most cases, the depths to the magnetic sources were found to be up to 600 m. This fault did not generate solutions in its northeast extent, with most of its solutions generated in the central-southwest portion of the fault zone (Fig. 7 and 8). Compared to the Mauriti and Umburanas faults, the Coité Fault had the most Euler solutions above 800 m. The shallowest magnetic source depths were concentrated in the NE or ENE regions of all fault zones, near the border of the basin.

Table 1. Depth values obtained from the Euler solutions for the (1) Mauriti, (2) Coité, and (3) Umburanas faults, using structural indices of 0, 0.5, and 1. A visualization of the Euler solutions for the aeromagnetic anomalies and RTP aeromagnetic anomalies maps can be found in Figures 7 and 8, respectively.

Aeromagnetic anomalies map

Structural index	**0**		**0.5**		**1**	
	Magnetic source depths (m)	**Location of solutions along the fault**	**Magnetic source depths (m)**	**Location of solutions along the fault**	**Magnetic source depths (m)**	**Location of solutions along the fault**
Mauriti Fault (1)	< 200 - 800	central-southwest	< 200 - > 800	central-southwest	< 200 - > 800	central-southwest
Coité Fault (2)	< 200 - > 800	central-	< 200 - > 800	central-	200 - > 800	central-southwest

		southwest		southwest		
Umburanas Fault (3)	< 200 - > 800	full length	< 200 - > 800	full length	< 200 - > 800	full length

RTP anomalies aeromagnetic map

Structural index	**0**		**0.5**		**1**	
	Magnetic source depths (m)	**Location of solutions along the fault**	**Magnetic source depths (m)**	**Location of solutions along the fault**	**Magnetic source depths (m)**	**Location of solutions along the fault**
Mauriti Fault (1)	< 200 - 800	southwest end	< 200 - 800	southwest end	< 200 - 800	southwest end
Coité Fault (2)	< 200 - 800	southwest end	200 - > 800	central-southwest	200 - > 800	central-southwest
Umburanas Fault (3)	< 200 - < 800	southwest end	< 200 - > 800	southwest end	< 200 - 800	central-southwest

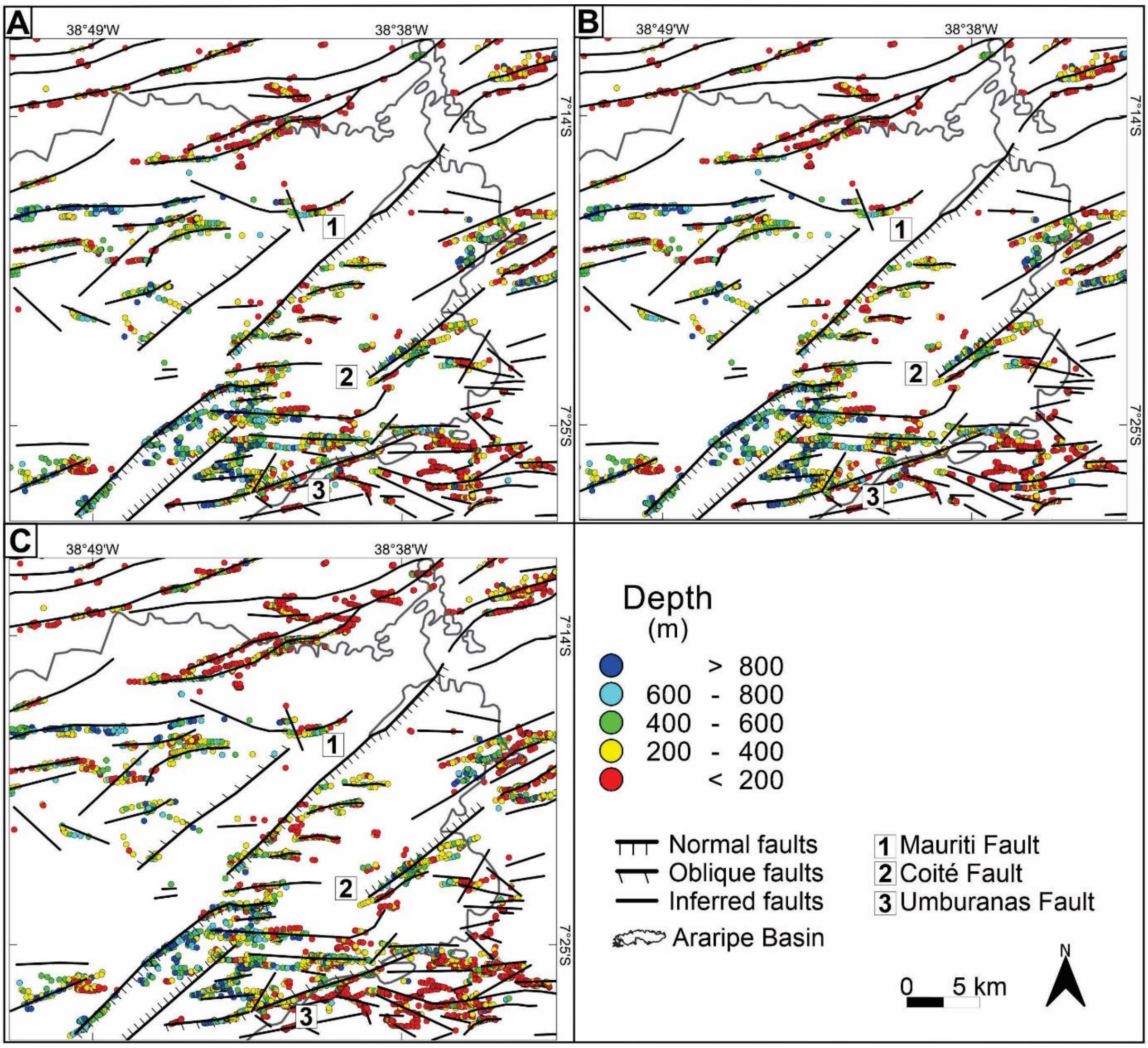

Figure 7. Aeromagnetic lineaments indicating the main structures and their Euler depth solutions as obtained from the aeromagnetic anomalies map. A) Euler deconvolution map of

structural index 0. B) Euler deconvolution map of structural index 0.5. C) Euler deconvolution map of structural index 1.

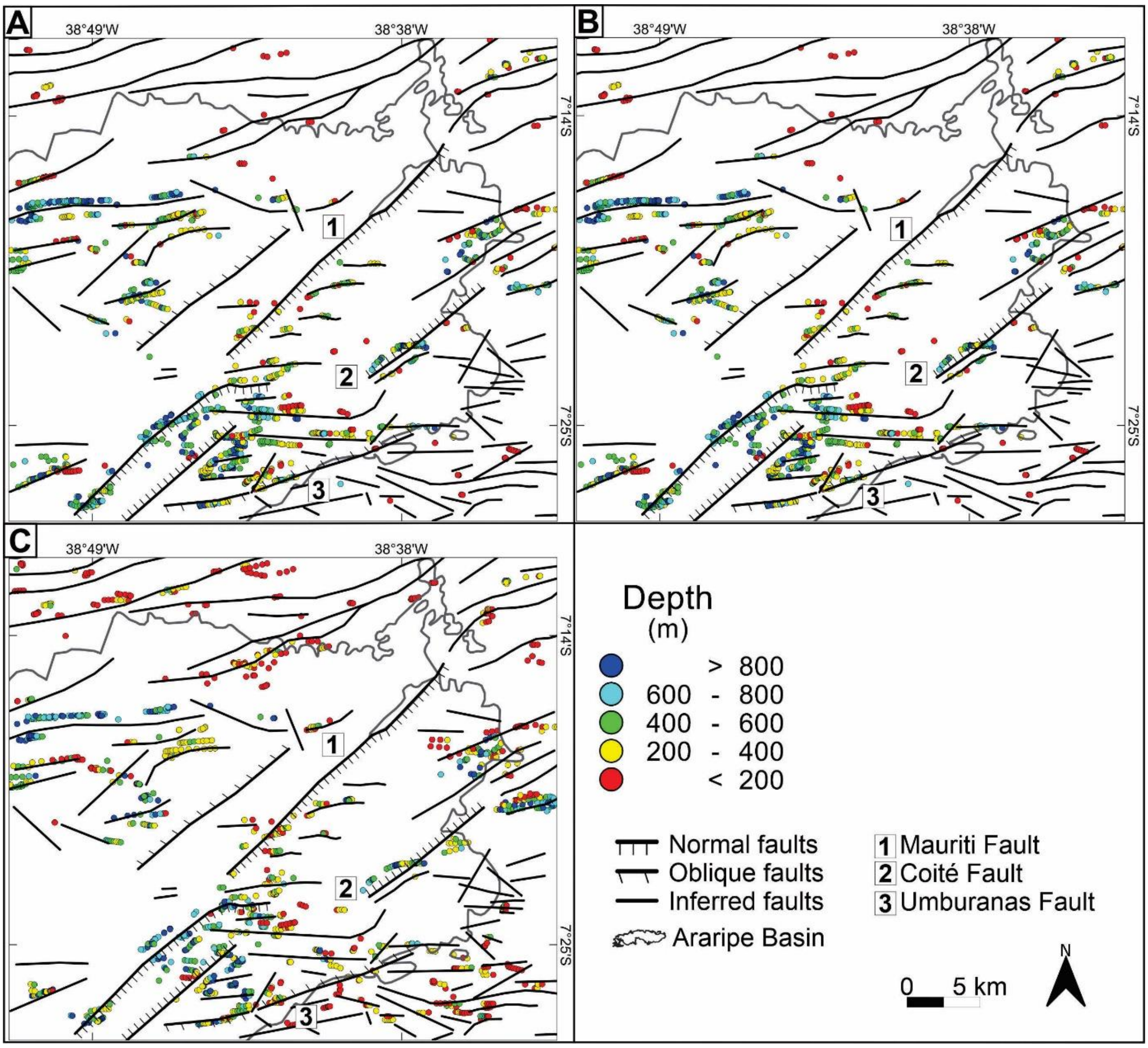

Figure 8. Aeromagnetic lineaments indicating the main structures and their Euler depth solutions as obtained from the RTP aeromagnetic anomalies map. A) Euler deconvolution map of structural index 0. B) Euler deconvolution map of structural index 0.5. C) Euler deconvolution map of structural index 1.

4.3 Structural characterization

We analyzed the brittle deformation of the crystalline Neoproterozoic granitoid basement and the basal interval of the Araripe Basin, represented by the Cariri Formation

(Cambrian–Ordovician). Locally, the crystalline basement is characterized by mylonitic granite, which is composed of porphyritic light gray to pink feldspars in a matrix composed of quartz, feldspar, biotite, and amphibole. The mylonitic foliation generally strikes ENE-WSW with a dip oscillating between 70° NNW and SSE to the vertical (Fig. 9A). The foliation planes exhibit a shallow plunging to sub-horizontal stretching lineation defined by elongated quartz crystals. The mylonitic foliation is overprinted by a system of NNE-SSW strike-slip faults (Fig. 9B). We also observed thin injections of mm- to cm-scale of pseudotachylites that are subparallel to the mylonitic foliation (Fig. 9C). Pseudotachylites have an aphanitic groundmass and dark colors, giving it glassy appearance, and are generally symmetrically emplaced about the basement foliation.

The sandstones of the Cariri Formation are highly silicified with grain sizes ranging from very coarse to medium-grained, and exhibit tabular cross-bedding stratification that dips mainly toward the ENE–WSW, between 10° and 43° (Fig. 9D). This formation contains a significant number of deformation bands that occur either as single bands or as clusters (swarms) that form positive reliefs (Fig. 9E and F). These deformation bands occasionally exhibit a complex geometric relationship, sometimes arranged in conjugate pair with NW–SE and N–S directions or as a second conjugate pair with trend NNE–SSW and ENE–WSW.

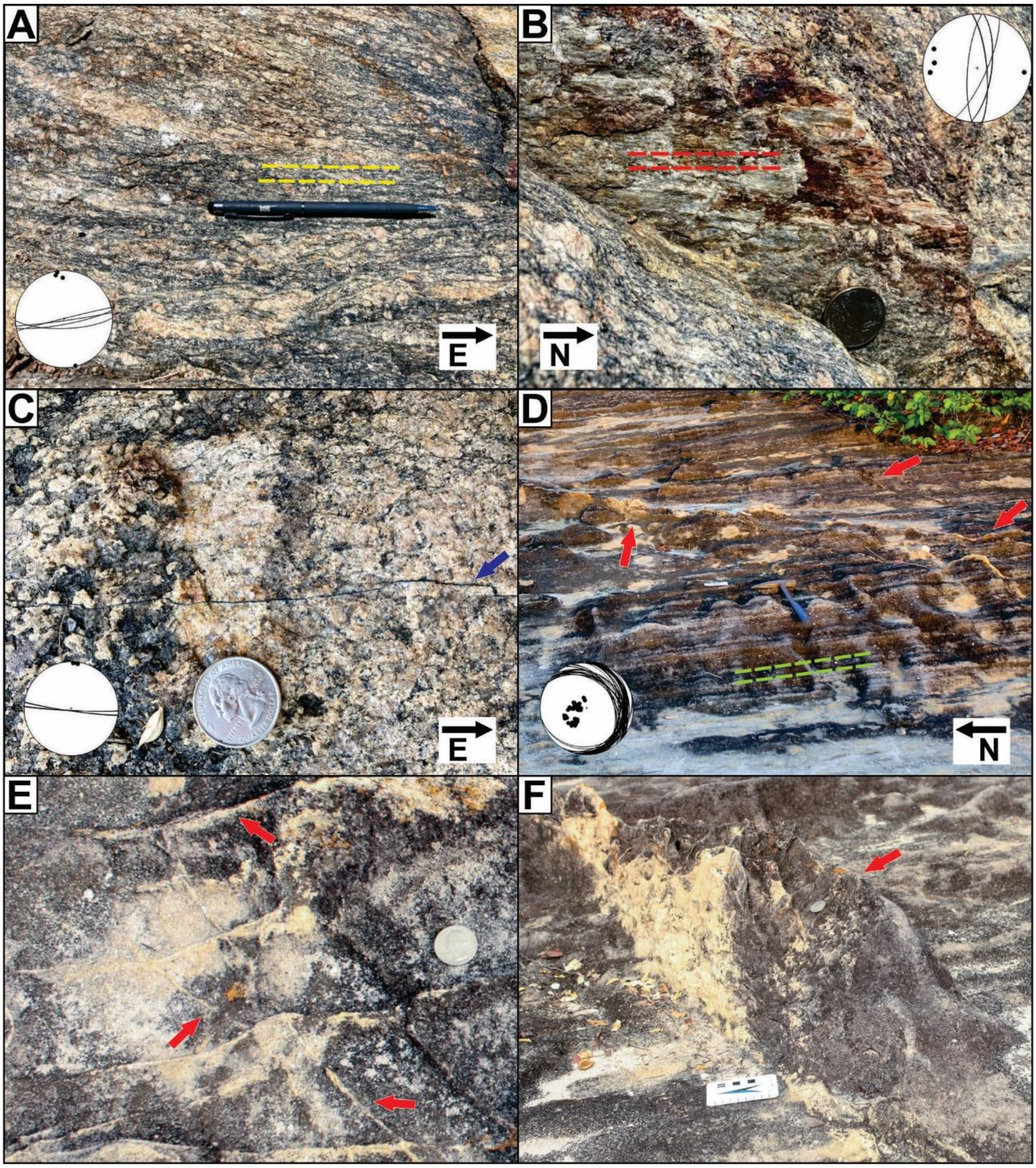

Figure 9. Field features of the mylonitic granite, with stereographic projections of the mylonitic foliation, faults, and pseudotachylites surfaces measured at Site 1 (see Fig. 3). Outcrop data from the Cariri Formation sandstone, Site 2 (see Fig. 3). A) Mylonitic granite with high-angle ENE-WSW foliation, indicated by the yellow lines, n = 4. B) Strike-slip fault-oriented NNE-SSW. The plane of the fault has been indicated with red lines, n = 6. C) Pseudotachylite (indicated by the blue arrow), subparallel to the mylonitic foliation,

exhibiting geometric aspects characterized generally by symmetrical injections (mm- to cm-scale) n = 4. D) Tabular cross-bedding stratification (indicated by green lines, stereographic projection, n = 45) cut by deformation bands (indicated by red arrows). E) Single deformation bands with different orientations (indicated by the red arrow). F) Vertical deformation bands (indicated by the red arrow) that occasionally form positive reliefs.

5 Discussion

5.1 Integration of the aeromagnetic and field data

Analyses of magnetic lineaments in aeromagnetic images allow us to gain insights into the internal structural framework of sedimentary basins (Vasconcelos et al., 2018; Celestino et al., 2020; Miranda et al., 2020). An investigation of geophysical data can be combined with different datasets (topographic, geophysical, seismic reflection, borehole, and outcrop data), depending on their availability in the area of interest, increasing the reliability and providing support for geophysical interpretations (e.g., Oliveira et al., 2018; Vasconcelos et al., 2018; Miranda et al., 2020; Passos et al., 2022). Similarly, different analyses of the same initial aeromagnetic data allow for the most amount of information to be extracted during regional structural analysis (Fossen et al., 2022). In general, aeromagnetic data allows for the generation of a greater number of Euler depth solutions compared to gravimetric data (e.g., Castro et al., 2014; Rodrigues et al., 2014; Oliveira et al., 2018), allowing for the identification of a large number of structural features in the area of interest; this is why ED was not applied to airborne and satellite-derived gravimetric data in this study. Oliveira et al. (2018) observed that the larger number of solutions generated by ED when applied to aeromagnetic data was related to the average wavelength of residual gravity anomalies and the irregular distribution of gravimetric data. In this study, the mapping of aeromagnetic anomalies using ED (Fig. 7 and 8) allowed for the identification of the lineaments based on the orientation of the magnetic anomalies, which were verified using the residual aeromagnetic and residual RTP aeromagnetic maps (Fig. 6).

The ED maps showed trends that were relatively similar to the aeromagnetic maps for each of the three structural indices (0, 0.5, and 1), which were different in terms of their clustering and depths (e.g., Reid et al., 1990). A structural index of 0.5, which corresponds to geological boundaries or faults with limited depths (Castro et al., 2014), was found to be ideal for the mapping of the magnetic lineaments due to the greater number of adequate solutions, allowing these lineament traces to be identified with a greater degree of clarity. Camacho and Sousa (2017) proposed that the Mauriti and Crato-Juazeiro magnetic domains were encompassed by the eastern border of the Araripe Basin. These lineaments are represented by elongated magnetic anomalies (trending mainly NE–SW) that can be attenuated due to the presence of sedimentary rocks; this demonstrates the structural complexity of the Cariri sub-basin.

The faults identified from geophysical data may be displaced from their actual positions due to interference effects caused by the sources (Fedi and Florio, 2001; Chen et al., 2014). To address this, we combined interpretations of the aeromagnetic lineaments and their preferential orientations, field data, and documented geological information (e.g., Cardoso, 2010) to present an aeromagnetic structural map of the eastern border of the Araripe Basin (Fig. 10). Our results showed that the basement region in the northwest sector (NE–SW) exhibits more curved aeromagnetic lineaments, possibly reflecting the presence of ductile fabrics, such as foliations and shear zones. The internal tectonic configuration of the basin includes structural highs and depocenters, such as horsts and grabens, as established from the distribution of regional lineaments, potentially reflecting Early Cretaceous rifting. For example, the Mauriti Fault is responsible for delimiting the northwest border of the Palestina Graben (NE–SW), separating it from the Brejo Santo-Mauriti Horst (NE–SW). This graben is considered to be the main depocenter in this region of the eastern border (e.g., Ponte and Ponte Filho, 1996; Cardoso, 2010). Furthermore, the Coité and Umburanas faults are embedded in the Umburanas Horst, which borders the southeast region of the Palestina Graben.

The aeromagnetic lineaments are primarily oriented E–W, ENE–WSW, and NE–SW, with a few NW–SE-trending lineaments; these are similar to the orientations obtained from other geological datasets, such as topographic and field data (Passos et al., 2022). In this study, we investigated outcrops at sites 1 and 2, which characterize the fault zones on a regional scale, allowing us to distinguish between the distinct deformation behavior in the basement and basin rocks. The outcrop data for Site 1 was characterized by mylonitic granites, strike-slip faults, and pseudotachylite venules. The structural configuration of the basement is reflected in the fault zones, which are, in turn, expressed at the outcrop-scale by ENE–WSW mylonitic foliation and NNE–SSW strike-slip faults. In contrast, the sandstones of the Cariri Formation are characterized by the abundant presence of deformation bands, which are expressed as conjugate pairs that trend NW–SE and N–S, with pairs in the NNE–SSW and ENE–WSW directions. We found that the orientations of the aeromagnetic lineaments (Fig. 6) were consistent with and showed similar trends to the structural data mapped on the outcrop-scale (Fig. 9). Despite the limitations in comparing data at different scales, it is understood that the characteristics of the fault zones are reflected in secondary structures such as the minor faults and deformation bands observed in the investigated outcrops (e.g., Caine et al., 1996; Torabi and Berg, 2011; Araújo et al., 2018; Fletcher et al., 2020).

After synthesizing the tectonic activity for this sector of the basin (e.g., Miranda et al., 2014; Matos et al., 2021; Celestino et al., 2020), we concluded that the direction of the basement structures is potentially inherited from the ductile deformation of the PASZ (E–W trends) as well as the generation of its secondary shear zones (NE–SW trends). The Paleozoic deformation basin due to the brittle reactivations of the PASZ are expressed in the form of brittle structures oriented NW–SE. In addition, the brittle reactivation of these structures during the breakup of Pangea (Early Cretaceous) generated the primarily NE–SW and ENE–WSW-trending structures. In the context of the eastern border of the Araripe Basin, brittle deformation is evidenced by fault zones (Fig. 10) characterized by secondary faults and deformation bands (Fig. 9) that are related to brittle reactivations in the PASZ.

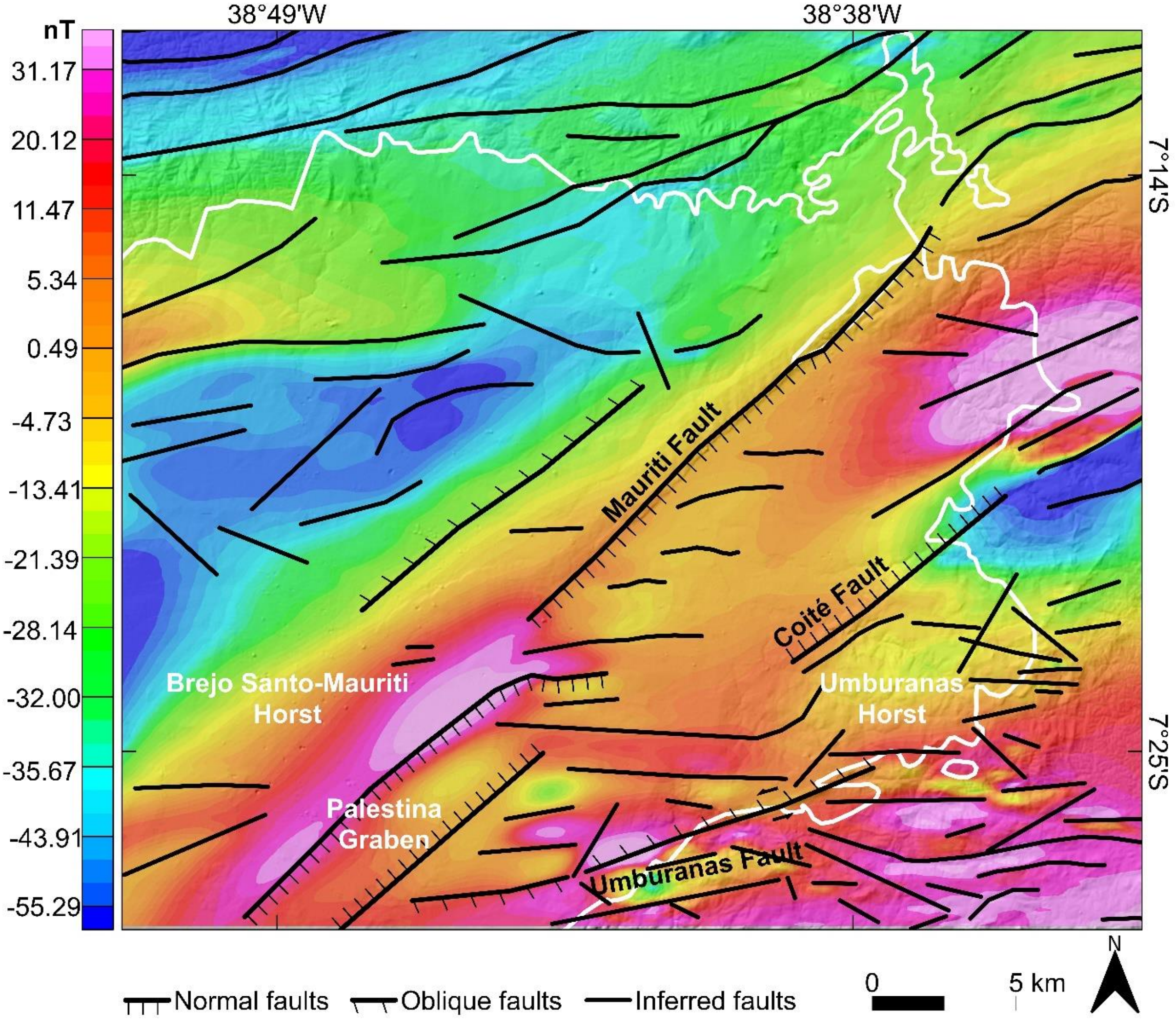

Figure 10. The aeromagnetic anomaly map from the Brazilian Geological Survey combined with a digital elevation model obtained from the Shuttle Radar Topography Mission (SRTM) showing with the main faults of the eastern border of the Araripe Basin. The white line indicates the eastern limit of the basin and the basement.

5.2 Estimates of the depth of the fault zones

Faults are complex structures that can be analyzed by the solutions to the Euler deconvolution equations (Rodrigues et al., 2014). Selecting the most appropriate structural index is the most relevant part of depth estimation, as incorrect parameters can result in overestimates (e.g., Thompson, 1982). In this study, we analyzed the Euler solutions corresponding to structural indices of 0, 0.5, and 1. The different indices provide information about the behavior of the magnetic causative sources related to faults and shear zones. In general, the Mauriti, Coité, and Umburanas faults are structures with significant vertical displacements (e.g., Reid et al., 1990), as they are detected in all structural indices (0, 0.5, and 1), with depths to the top of the basement being greater than 800 m in some areas (Fig. 6). Information on the vertical displacements can also be obtained through other techniques, such as 3D gravimetric inversion and seismic data (e.g., Castro, 2011; Castro et al., 2014; Rodrigues et al., 2014; Alaei and Torabi, 2017; Ramos et al., 2022). In this study, interpretations were indirectly correlated with information from other regions of the Araripe Basin, where well and seismic data were readily available (Cardoso, 2010; Camacho and Sousa, 2017).

Our source depth estimates of the magnetic anomalies obtained from the RTP transformations exhibited moderate values. For example, the Mauriti Fault was found to have depths that predominantly ranged from 200–600 m, while the other faults—Coité and Umburanas—exhibited 800 m depths in a few solutions. The solutions to the ED equations vary slightly with the geometry of the body and with the magnetic slope: as the magnetic slope decreases, simple models tend to overestimate the depths of the source bodies (Thompson, 1982). Thompson (1982) notes that the RTP transformation allows for more accurate estimates of depths; consequently, shallower variations of this pattern would indicate that the structures are not 2D and/or there is remaining magnetization. Reid et al. (1990) suggested that the RTP transformation was unnecessary for ED processing, assuming that the technique is correctly applied. We considered these recommendations and verified that, based on the results of ED on the magnetic anomaly data, it was possible to identify areas where there were larger variations in the depth values (Fig. 7 and 8). This allowed us to analyze the sections in which the fault was deeper, which may be related to lithological variations, source variations, or fault length asymmetry. However, we believe that the RTP transformation can also be used as a validation parameter for the ED technique when applied to aeromagnetic anomalies data, based on the observations made by Thompson (1982). This study did not verify whether the same is true for ED applied to other magnetic datasets.

The analysis of the 141-RL-08 seismic line by Cardoso (2010) (Fig. 2), despite its low quality, allowed us to estimate the depth of the sedimentary column to be approximately 1,750 m, which included the horsts, half-graben, and the main depocenter of the Cariri sub-basin (Palestina Graben). Camacho and Sousa (2017) applied the ED technique to the analytical signal anomaly map collected from this eastern sector of the basin and found that the main faults had depths that predominantly ranged between 800–999 m, reaching a maximum depth of a little less than 1,147 m. The results of this study were consistent with those obtained for the Araripe Basin, with depths increasing toward the depocenters of the basin (e.g., Ponte and Ponte Filho, 1996; Castro and Castelo Branco, 1999; Cardoso, 2010; Camacho and Sousa, 2017).

The Mauriti, Coité, and Umburanas faults bypass important geological structures, making it possible to provide estimates for the depths to the borders of certain structures, such as the aforementioned Palestina Graben and the Brejo Santo-Mauriti and Umburanas horsts (Fig. 10). The Mauriti and Coité faults, which delimit the northwest (Brejo Santo-Mauriti Horst) and southeast (Umburanas Horst) borders of the Palestina Graben, were found to reach depths of more than 800 m, which became shallower toward the northeast as they approached the border of the Araripe Basin.

5.3 Fault zone geometry

Fault geometries can vary significantly in terms of length, with most faults exhibiting a generally elliptical pattern. The displacement of the fault can also vary horizontally or vertically, though its maximum displacement is usually proportional to the length of the fault (Torabi and Berg, 2011; Jackson et al., 2017; Alaei and Torabi, 2017; Torabi et al., 2019; Fossen et al., 2020). The depths of the main fault zones (Mauriti, Coité, and Umburanas faults) in the study area vary across the zone, with magnetic source depths of up to 800 m that become shallower toward the northeast (Table 1). The lengths of the faults vary between 10–24 km, with the Mauriti Fault being the largest. The deepest Euler depth solutions are found in the central regions of the fault zones. The variations in the magnetic source depths indicate that the faults have elliptical geometries. In Fig. 11, we propose a schematic model that describes the geometry as derived from the Euler depth solutions.

The Mauriti and Coité faults were found to exhibit their maximum depths at the central-southwest portion of the faults. Although ED solutions were generated along the entirety of the Coité and Umburanas faults, the position of the deepest solutions varied between them because of the relative positions of the faults. While the central-southwest area of the Coité Fault is located closer to the basin center, the maximum depth of the Umburanas Fault was found near its central regions because the ends of this fault can be found close to the basin-basement limit.

The geometry of these faults may have been influenced by their relative location to the borders or the depocenter of the basin; this is most clearly seen in the variations in their throw (Fig. 11), which tend to be greater towards the depocenter (e.g., Castro et al., 2014; Rodrigues et al., 2014). In addition, the fault zones may interact with smaller faults that can influence the observed geometry (e.g., Fossen et al., 2020).

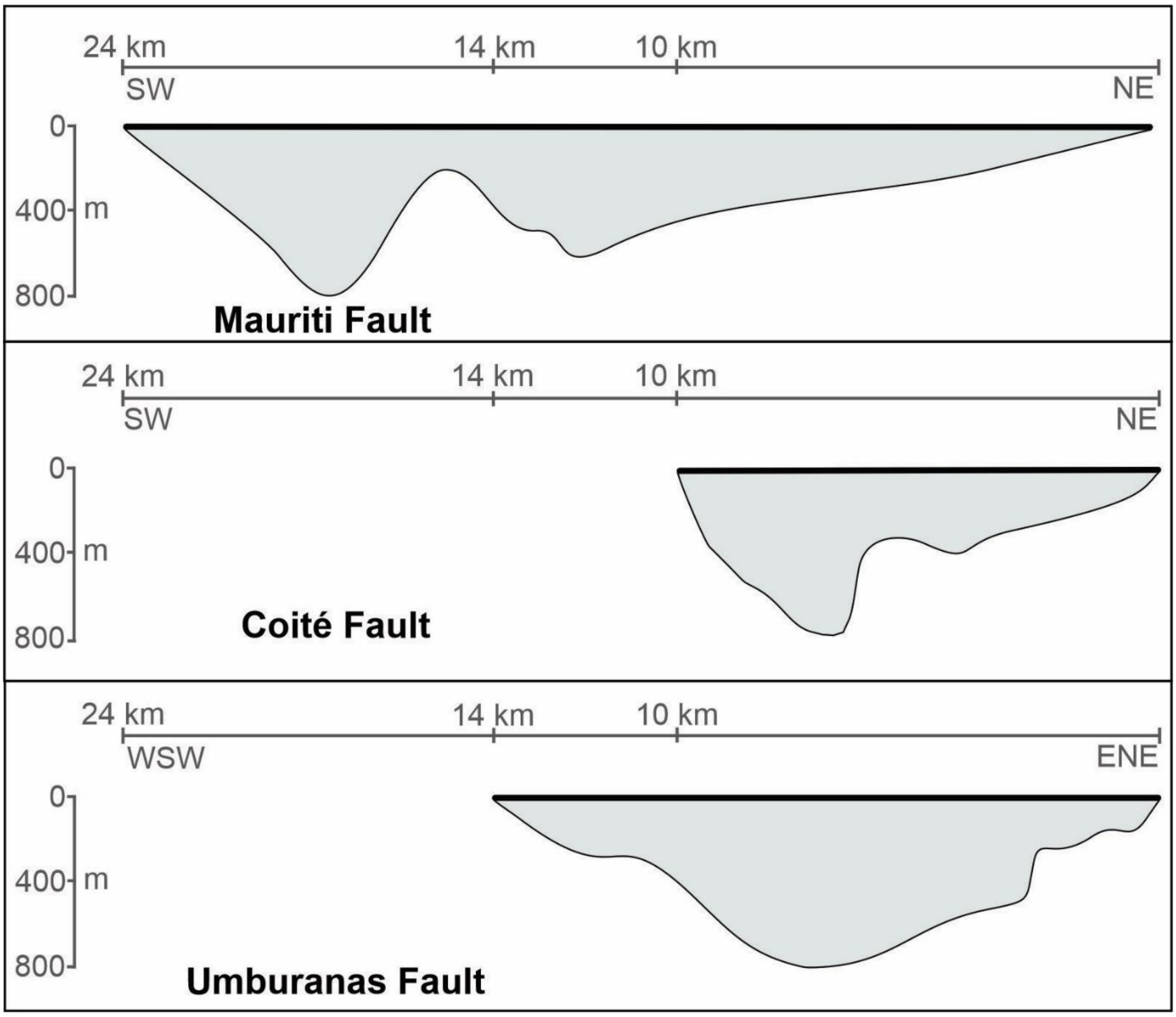

Figure 11. Schematic model illustrating the dimensions and the elliptical geometry of the Mauriti, Coité, and Umburanas faults, which exhibited displacements of up to 800 m, as obtained from the interpretations of Euler solutions.

The relationships between fault attributes, such as displacement, length, and the width and height of their damage zone have been the subject of many studies, especially concerning the ratio between the length of a fault (L) and its maximum displacement (D). Analyses have been performed for many different kinds of rocks and types of faults (e.g., Walsh and Watterson, 1988; Peacock, 1991; Peacock and Sanderson, 1991; Cowie and Scholz, 1992; Dawers et al., 1993; Cartwright et al., 1995; Schlische et al., 1996; Schultz and Fossen, 2002; Kim and Sanderson, 2005; Schultz et al., 2008; Grasemann, 2011; Gudmundsson et al., 2013;

Torabi et al., 2019). Fault analyses provide a clearer understanding of fault geometry, which allows for the validation of geological models that involve fluid flow evaluations (Torabi and Berg, 2011; Torabi et al., 2019). Here, we analyzed the displacement and the length of the Mauriti, Coité, and Umburanas fault zones from the ED solutions and the geological map, respectively. These data were compared to other data on normal faults to assess their D/L ratio (Fig. 12). It is important to note that the literature includes normal fault data from a variety of lithologies; hence, there is a certain degree of variation in the data. In addition to the lithological differences, which have a direct effect on the mechanical properties of the rock, other factors influence the D/L ratio, such as the type of fault, reactivations, linkage faults, earthquake ruptures, and slip or propagation history (Kim and Sanderson, 2005; Torabi and Berg, 2011).

Both the literature data and the data from this study show a positive correlation between fault displacement and length. The data from this study were found to cluster at D/L values of 10^{-1} (e.g., Kim and Sanderson, 2005; Schultz et al., 2008), and exhibited an approximately linear relationship.

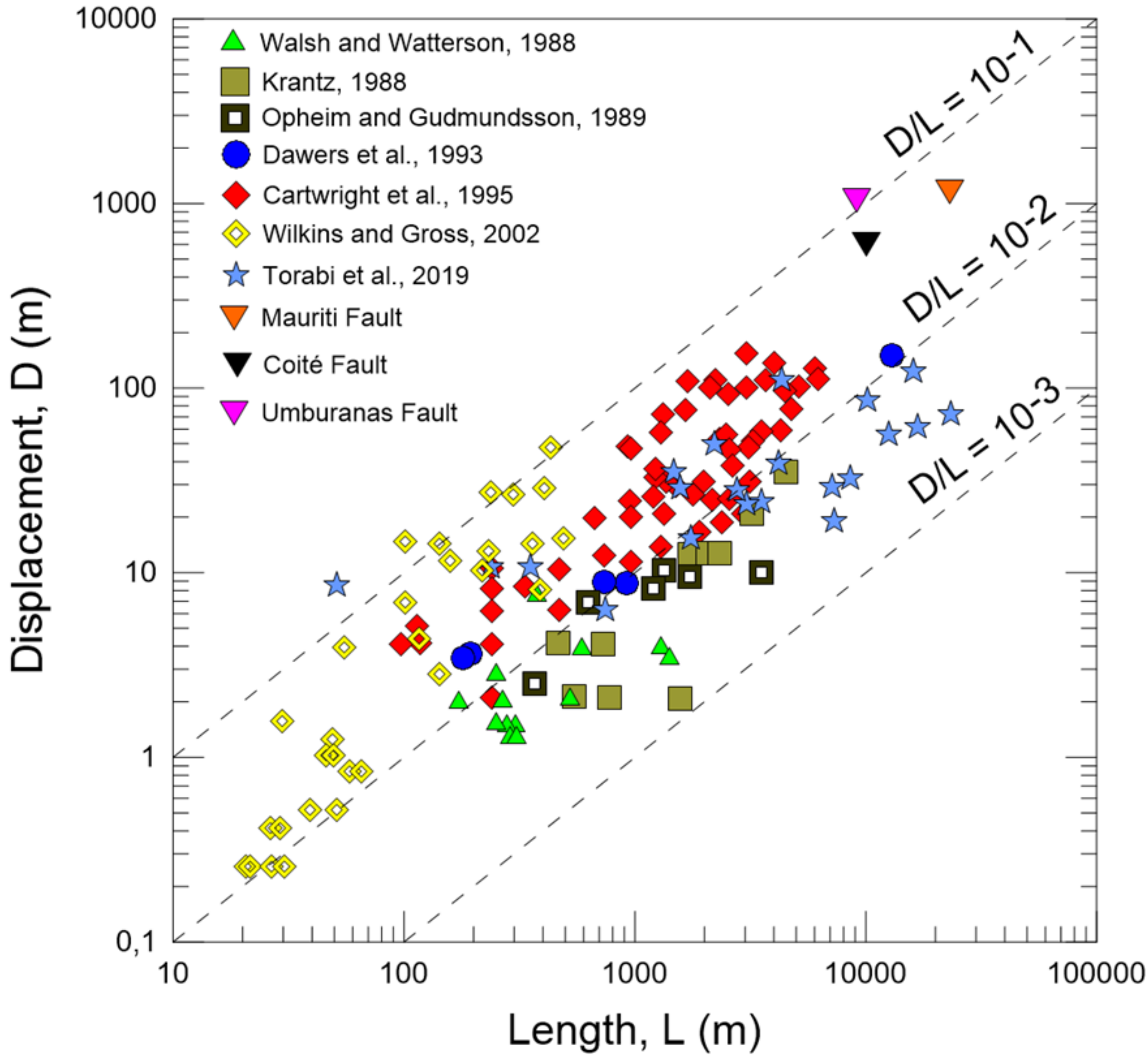

Figure 12. D/L scaling of the fault zones (Mauriti, Coité, and Umburanas faults) as well as normal fault data taken from the literature. The Mauriti, Coité, and Umburanas faults data exhibit a linear trend and are concentrated around $D/L = 10^{-1}$.

6. Conclusions

The location and depth of the magnetic anomaly sources obtained using the ED technique were used to characterize the main fault zones— the Mauriti, Coité, and Umburanas faults—on the eastern border of the Araripe Basin. The most important results of this study are listed below.

• The orientation of the faults and deformation bands were consistent with the orientations of the aeromagnetic lineaments, which included E–W, ENE–WSW, and NE–SW trends, as well as a few instances of NW–SE-trending structures. In the basement, the aeromagnetic lineaments reflect the influence of the PASZ ductile deformation, while the lineaments in the basin characterize structural highs and lows, such as horsts and grabens. Our regional- and outcrop-scale structural observations, together with other data that was available in the study area (e.g., Passos et al., 2022), suggest the tectonic evolution of this region of the basin was controlled by brittle reactivations during the Early Cretaceous.

• An analysis of the different structural indices (0, 0.5, and 1) allowed us to verify that the main fault zones (Mauriti, Coité, and Umburanas faults) have a significant throw, with variable vertical, and in some cases very large, displacements along their fault length (particularly in faults identified using a structural index of 0). A structural index of 0.5 was found to be the most suitable because the number of solutions generated allowed for a greater degree of precision with regard to the interpretation of the fault zone geometry.

• The structural geometry of the eastern border of the Araripe Basin is dominated by the Palestina Graben and the Brejo Santo-Mauriti and Umburanas horsts, which are delimited by the Mauriti, Coité, and Umburanas faults zones that trend NE–SW and ENE–WSW trends. These fault zones have magnetic source depths between 200–800 m, which shallow toward the border of the basin in the northeast.

• The Mauriti, Coité, and Umburanas faults have variable depths, reaching values that were slightly greater than 800 m. The depth distributions of the magnetic sources indicate that these fault zones had generally elliptical geometries, with maximum displacements located in the central-southwest region of the Mauriti and Coité faults, while the maximum displacement of the Umburanas Fault was found in its central regions. The location of faults relative to the depocenter of the basin controlled the observed depth variations, with shallower displacements observed near the borders of the basin.

Acknowledgments

This paper was carried out with financial support from CNPq (Conselho Nacional de Desenvolvimento Científico e Tecnológico) and by the Project Fault Zones (Petrobras-ANP-UFPE). This work is part of a MSc of Vivian Passos under the postgraduate program in Geosciences of the Federal University of Pernambuco (PPGEOC - UFPE) and represents the contribution N. 05 of the Laboratório de Modelagem de Bacias (ModLad-UFPE).

References

Abdelkareem, M., Akrby, A., Fakhry, M., Mostafa, M., 2018. Using of Remote Sensing and Aeromagnetic Data for Predicting Potential Areas of Hydrothermal Mineral Deposits in the Central Eastern Desert of Egypt. Remote Sensing. 7 (1), 1-13. https://doi.org/10.18282/rs.v7i1.112.

Angelim, L.A.A., Vasconcelos, A.M., Gomes, J.R.C., Wanderley, A.A., Forgiarini, L.L., Medeiros, M.F. 2004. Folha SB.24-Jaguaribe. In: Schobbenhaus, C., Gonçalves, J.H., Santos, J.O.S., Abram, M.B., Leão Neto, R., Matos, G.M.M., Vidotti, R.M. E Ramos, M.A.B., Jesus, J.D.A. (eds.). Geological Chart of Brazil to the Millionth, Geographic Information System - GIS, Geology of Brazil Program-CPRM, Brasília.

Alaei, B., Torabi, A. 2017.Seismic imaging of fault damaged zone and its scaling relation with displacement. Interpretation. 5 (4). http://dx.doi.org/10.1190/INT-2016-0230.1

Almeida, Y.B., Julià, J., Frassetto, A., 2015. Crustal architecture of the Borborema Province, NE Brazil, from receiver function CCP stacks: Implications for Mesozoic stretching and Cenozoic uplift. Tectonophysics. 649, 68-80. https://doi.org/10.1016/j.tecto.2015.03.001.

Araújo, R.E.B., Bezerra, F.H.R., Nogueira, F.C.C., Balsamo, F., Carvalho, B.R.B.M. Souza, J.A.B., Sanglard, J.C.D., Castro, D.L., Melo, A.C.C. 2018. Basement control on fault formation and deformation band damage zone evolution in the Rio do Peixe Basin, Brazil. Tectonophysics. 745, 117-131. https://doi.org/10.1016/j.tecto.2018.08.011.

Assine, M.L., 1992. Análise estratigráfica da Bacia do Araripe, Nordeste do Brasil. Revista Brasileira de Geociências. 22 (3), 289-300.

Assine, M.L., 2007. Bacia do Araripe. Boletim de Geociências da Petrobras. 15 (2), 371-389.

Assine, M.L., Perinotto, J.A.J., Custódio, M.A., Neumann, V.H., Varejão, F.G., Mescolotti, P.C., 2014. Sequências deposicionais do Andar Alagoas da Bacia do Araripe, Nordeste do Brasil. B. Geoci. Petrobras. 22 (1), 3-28.

Barbosa, V.C, Silva, J.B.C., 2005. Deconvolucão de Euler: passado, presente e futuro - um tutorial. Revista Brasileira de Geofísica. 23(3), 243-250.

Baranov, V., 1957. A new method for interpretation of aeromagnetic maps: Pseudo-gravimetric anomalies. Geophysics. 22, 359-383.

Barnett, J.A.M., Mortimer, J., Rippon, J.H., Walsh, J.J., Watterson, J., 1987. Displacement geometry in the volume containing a single normal fault. AAPG Bulletin, 71, 925-937.

Blakely, J.R., 1996. Potential Theory in Gravity and Magnetic Applications, 2nd ed. Cambridge University Press.

Bournas, N., Galdeano, A., Hamoudi, M., Baker, H., 2003. Interpretation of the aeromagnetic map of Eastern Hoggar (Algeria) using the Euler deconvolution, analytic signal and local wavenumber methods. Journal of African Earth Sciences. 37, 191-205.

Brazilian Geological Survey "Base de dados/http://geosgb.cprm.gov.br/”. [online] (2020). Accessed April 2020, http://geosgb.cprm.gov.br/.

Brito Neves, B.B., Van Schmus, W.R., Fetter, A.H., 2001. Noroeste da África-Nordeste do Brasil (Província Borborema) Ensaio comparativo e problemas de correlação. São Paulo. Revista do Instituto de Geociências - USP. 1, 59-78.

Caine, J.S., Evans, J.P., Forster, C.B., 1996. Fault zone architecture and permeability structure. Geology, 24, 1025-1028, https://doi.org/10.1130/0091-7613(1996)024,1025:FZAAPS.2.3.CO;2.

Camacho, C.R., Sousa, F.R.F.R.O., 2017. O arcabouço estrutural da Bacia Sedimentar do Araripe, Província Borborema, baseado em dados aeromagnetométricos. Revista do Instituto de Geociências - USP. 17 (3), 149-161. https://doi.org/10.11606/issn.2316-9095.v17-393.

Cardoso, F.M.C., 2010. O graben de Palestina: contribuição à estratigrafia e estrutura do estágio rift na Bacia do Araripe, Nordeste do Brasil. Natal. Master's dissertation. Post-graduate Program in Geodynamics and Geophysics, Federal University of Rio Grande do Norte. 107p.

Cartwright, J.A., Trudgill, B.D., Mansfield, C.S., 1995. Fault growth by segment linkage: an explanation for scatter in maximum displacement and trace length data from the Canyonlands Grabens of SE Utah. Journal of Structural Geology. 17, 1319.

Castro, D.L. Castelo Branco, R. M. G., 1999. Caracterização da arquitetura interna das bacias do Vale do Cariri (NE do Brasil) com base em modelagem gravimétrica 3-D. Brazilian Journal of Geophysics. 17, 129-144.

Castro, D.L., Fuck R.A., Phillips, J.D., Vidotti, R.M., Bezerra, F.H., Dantas, E.L., 2014. Crustal structure beneath the Paleozoic Parnaíba Basin revealed by airborne gravity and magnetic data, Brazil. Tectonophysics. 614, 128-45. https://doi.org/10.1016/j.tecto.2013.12.009.

Celestino, M.A.L., Miranda, T.S., Mariano, G., Alencar, M.L., Carvalho, B.R.B.M., Falcão, T.C., Topan, J.G., Barbosa, J.A., Gomes, I.F., 2020. Fault damage zones width: Implications for the tectonic evolution of the northern border of the Araripe Basin, Brazil, NE Brazil. J. Struct. Geol. 138, 1-16. https://doi.org/10.1016/j.jsg.2020.104116.

Cerri, R.I., Warren, L.V., Spencer, C.J., Varejão, F.G., Promenzio, P., Luvizotto, G.L., Assine, M.L. 2022. Using detrital zircon and rutile to constrain sedimentary provenance of Early Paleozoic fluvial systems of the Araripe Basin, Western Gondwana. Journal of South American Earth Sciences. 116. https://doi.org/10.1016/j.jsames.2022.103821.

Chen, Q., Dong, Y., Cheng, S., Han, L., Xu, H., Chen, H., 2014. Interpretation of fault system in the Tana Sag, Kenya, using edge recognition techniques and Euler deconvolution. Journal of Applied Geophysics. 109, 150-161. https://doi.org/10.1016/j.jappgeo.2014.07.020.

Cowie, P.A., Scholz, C.H., 1992. Displacement-length scaling relationship for faults: data synthesis and discussion. Journal of Structural Geology. 14, 1149-1156.

Dawers, N.H., Anders, M.H., Scholz, C.H., 1993. Growth of normal faults: displacement-length scaling. Geology. 21, 1107-1110.

Dewangan, P., Ramprasad, T., Ramana, M.V., Desa, M., Shailaja, B., 2007. Automatic interpretation of magnetic data using Euler deconvolution with nonlinear background. Pure Appl. Geophys. 164, 2359-2372. https://doi.org/10.1007/s00024-007-0264-x.

Durrheim, R.J, Cooper, G.R.J., 1998. Euldep: a program for the euler deconvolution of magnetic and gravity data. Computers & Geosciences. 24 (6), 545-550.

Faulkner, D.R., Jackson, C.A.L., Lunn, R.J., Schlische, R.W., Shipton, Z.K., Wibberley, C.A.J., Withjack, M.O., 2010. A review of recent developments concerning the structure, mechanics and fluid flow properties of fault zones. Journal of Structural Geology. 32, 1557-1575. https://doi .org/10.1016/ j.jsg.2010.06.009.

Fedi, M., Florio, G., 2001. Detection of potential fields source boundaries by enhanced horizontal derivative method. Geophysical prospecting. 49 (1), 40-58.

Ferraccioli, F., Armadillo, E., Jordan, T., Bozzo, E., Corr, H., 2009. Aeromagnetic exploration over the East Antarctic Ice Sheet: A new view of the Wilkes Subglacial Basin. Tectonophysics. 478, 62-77. https://doi .org/10.1016/j.tecto.2009.03.013.

Ferreira, V.P., Sial, A.N., Pimentel, M.M., Moura, C.A.V., 2004. Intermediate to acidic magmatism and crustal evolution in the Transversal Zone, Northeastern Brazil. In: Mantesso Neto, Virginio, Bartorelli, A., Carneiro, Celso Dal Ré, Brito Neves, Benjamin Bley (editors), Geologia do Continente Sul-Americano: a evolução da obra de Fernando Flávio Marques de Almeida. University of São Paulo, chapter XII, 189-201.

Fletcher, J.M., Teran, O.J., Rockwell, T.K., Oskin, M.E., Hudnut, K.W., Spelz, R.M., Lacan, P., Dorsey, M.T., Ostermeijer, G., Mitchell, T.M., Akciz, S.O., Hernandez-Flores, A. P., Hinojosa-Corona, A., Peña-Villa, I., Lynch, D.K., 2020. An analysis of the factors that control fault zone architecture and the importance of fault orientation relative to regional stress. Geological Society of America Bulletin. 132 (9-10): 2084-2104. https://doi.org/10.1130/B35308.1.

Fossen, H., Harris, L.B., Cavalcante, C., Archanjo, C.J., Ávila, C.F. 2022. The Patos-Pernambuco shear system of NE Brazil: Partitioned intracontinental transcurrent deformation revealed by enhanced aeromagnetic data. Journal of Structural Geology. 158. https://doi.org/10.1016/j.jsg.2022.104573.

Françolin, J.B.L., Cobbold, P.R., Szatmari, P., 1994. Faulting in the early cretaceous Rio do Peixe Basin (NE Brazil) and its significance for the opening of the Atlantic. J. Struct. Geol. 16, 647-661.

Garcia, X., Julià, J., Nemocón, A.M., Neukirch, M., 2019. Lithospheric thinning under the Araripe Basin (NE Brazil) from a long-period magnetotelluric survey: constraints for tectonic inversion. Gondwana Research. 68, 174-184. https://doi.org/10.1016/j.gr.2018.11.013.

Grasemann, B., Exner, U., Tschegg, C., 2011. Displacement-length scaling of brittle faults in ductile shear. Journal of Structural Geology. 33(11), 1650-1661.

Gudmundsson, A., De Guidi, G., Scudero, S., 2013. Length-displacement scaling and fault growth. Tectonophysics. 608, 1298-1309.

Harris, S.D., McAllister, E., Knipe, R.J., Odling, N.E., 2003. Predicting the threedimensional population characteristics of fault zones: a study using stochastic models. Journal of Structural Geology. 25, 1281-1299.

Kim, Y.-S., Sanderson, D.J., 2005. The relationship between displacement and length of faults: a review. Earth-Science Reviews. 68, 317-334.

Krantz, R.W. 1988. Multiplc fault sets and three-dimensional strain: theory and application. Journal of Structural Geology. 10, 225-237.

Ibraheem, I.M., Elawadi, E.A., El-Qady, G.M., 2018. Structural interpretation of aeromagnetic data for the Wadi El Natrun area, northwestern desert, Egypt: Journal of South African Earth Sciences. 139, 14-25.

Jackson, C.A.L., Bell, R.E., Rotevatn, A., Tvedt, A.B.M. 2017. Techniques to determine the kinematics of synsedimentary normal faults and implications for fault growth models. Geological Society. 439 (1). https://doi.org/10.1144/SP439.22.

Li, Y., Oldenburg, D.W., 1998. Separation of regional and residual magnetic field data. Geophysics. 63 (2), 431-439.

Magalhães, J.R.G., 2019. Estrutura crustal e relações tectono-magmáticas da Bacia de Pernambuco através do processamento e modelagem de dados magnéticos, gravimétricos e sísmicos. Doctoral thesis. Post-graduate Program in Geosciences, Federal University of Pernambuco. 86p.

Marques, F.O., Nogueira, F.C.C., Bezerra, F.H.R., Castro, D.L., 2014. The Araripe Basin in NE Brazil: An intracontinental graben inverted to a high-standing horst. Tectonophysics. 630, 251-264. http://dx.doi.org/10.1016/j.tecto.2014.05.029.

Matos, R.M.D., 1992. The Northeast Brazilian Rift System. Tectonics. 11 (4), 766-791.

Matos, R.M.D., Norton, I., Casey, K., Krueger, A., 2019. An Orthogonal Zone between the Equatorial and South Atlantic Margins: Relevance and Control in the Evolution of the Afro-Brazilian Basins - 16th International Congress of the Brazilian Geophysical Society. SBGf - Sociedade Brasileira de Geofísica- Rio de Janeiro. August 2019. Expanded Abstract.

Matos, R.M.D., Krueger, A., Norton, I., Casey, K., 2021 The fundamental role of the Borborema and Benin–Nigeria provinces of NE Brazil and NW Africa during the development of the South Atlantic Cretaceous Rift system. Marine and Petroleum Geology. 127. https://doi.org/10.1016/j.marpetgeo.2020.104872.

Medeiros, V.C., 2004. Evolução geodinâmica e condicionamento estrutural dos terrenos Piancó-Alto Brígida e Alto-Pajeú, Domínio da Zona Transversal, NE do Brasil. doctoral thesis.Post-graduate Program in Geodynamics and Geophysics, Federal University of Rio Grande do Norte. 199p.

Minelli, L., Vecchio, A., Speranza, F., Nicolosi, I., Caracciolo, F.A., Chiappini, S., Carluccio, R., Chiappini, M., 2016. Aeromagnetic investigation of southern Calabria and the Messina Straits (Italy): Tracking seismogenic sources of 1783 and 1908 earthquakes: Journal of Geophysical of Research. 121, 1297-1315.

Miranda, T.S., Magalhães, J.R., Barbosa, J.A., 2012. Bacia do Araripe: Possível Sistema Pull-Apart? In: 46° Congresso Brasileiro de Geologia, Anais: Sociedade Brasileira de Geologia. Santos.

Miranda, T.S., Magalhaes, J.R., Barbosa, J.A., Correia Filho, O., Alencar, M.L., 2014. Araripe Basin, NE Brazil: a rift basin implanted over a previous pull-apart system? In: 4th Atlantic Conjugate Margins Conference, vol 3.

Miranda, T.M., Neves, S.P., Celestino, M.A.L., Roberts, N.M.W., 2020. Structural evolution of the Cruzeiro do Nordeste shear zone (NE Brazil): Brasiliano-Pan-African- ductile-to-brittle transition and Cretaceous brittle reactivation. J. Struct. Geol. 141. https://doi.org/10.1016/j.jsg.2020.104203.

Mota, E.S.A, Medeiros, W.E, Oliveira, R.G., 2020. Can Euler deconvolution outline three-dimensional magnetic sources? Geophysical Prospecting. 68 (7). 2007-2343. https://doi.org/10.1111/1365-2478.12988.

Neumann, V.H.M.L., 1999. Estratigrafia, Sedimentologia, Geoquímica y Diagénesis de los Sistemas Lacustres Aptienses-Albienses de lá Cuenca de Araripe (Nororeste do Brasil). Tese de Doutorado. Facultat de Geologia, Universitat de Barcelona, Barcelona. 293p.

Neves, S.P., Alcantara, V.C., 2010. Geochemistry of orthogneisses and metasedimentary rocks across a proposed terrane boundary in the Central Domain of Borborema Province, NE Brazil: geodynamic implications. Journal of South American Earth Sciences. 29, 498-511. https://doi.org/10.1016/j.jsames.2009.08.002.

Neves, S.P., Mariano, G. 1999. Assessing the tectonic significance of a large-scale transcurrent shear zone system: Pernambuco Lineament, Northeastern Brazil. Journal of Structural Geology. 21, 1639-1383. https://doi.org/10.1016/S0191-8141(99)00097-8.

Neves, S.P, Tommasi, A., Vauchez, A., Carrino, T.A. 2021. The Borborema Strike-Slip Shear Zone System (NE Brazil): Large-Scale Intracontinental Strain Localization in a Heterogeneous Plate. Lithosphere. Geological Society of America, Special 6, 6407232. https://doi.org/10.2113/2021/6407232.

Oliveira, R.G., 2008. Arcabouço geofísico, isostasia e causas do magmatismo cenozoico da província Borborema e de sua margem continental (Nordeste do Brasil). Natal. Doctoral thesis. Post-graduate Program in Geodynamics and Geophysics, Federal University of Rio Grande do Norte. 415p.

Oliveira, K.M.L.,Castro, D.L., Castelo Branco, R.M.G., Oliveira, D.C., Alvite, E.N.C., Jucá, C.C.A., Castelo Branco, J.L. 2018. Architectural framework of the NW border of the onshore Potiguar Basin (NE Brazil): An aeromagnetic and gravity-based approach. Journal of South American Earth Sciences. 88, 700-714. https://doi.org/10.1016/j.jsames.2018.10.002.

Opheim, J. A. and Gudmundsson, A., 1989. Formation and geometry of fractures, and related volcanism, of the Krafla fissure swarm, northeast Iceland. Bull. geol. Soc. Am. 101, 1608-1622.

Passos, V.S.A., Miranda, T.S., Oliveira, J.T.C., Celestino, M.A.L., Corrêa, R., Topan, J.G., Falcão, T.F. 2022. Quantification of the spatial arrangement of structural lineaments and deformation bands: Implications for the tectonic evolution of the eastern border of the Araripe Basin, NE Brazil. Journal of South American Earth Sciences. 118, 103934. https://doi.org/10.1016/j.jsames.2022.103934.

Peacock, D.C.P., 1991. Displacement and segment linkage in strike-slip fault zones. Journal of Structural Geology. 13, 1025-1035.

Peacock, D.C.P., Sanderson, D.J., 1991. Displacement and segment linkage and relay ramps in normal fault zones. Journal of Structural Geology. 13, 721-733.

Peulvast, J.P., Betard, F., 2015. A history of basin inversion, scarp retreat and shallow denudation: the Araripe basin as a keystone for understanding long-term landscape evolution in NE Brazil. Geomorphology. 233, 20-40. https://doi.org/10.1016/j.geomorph.2014.10.009.

Pilkington, M., Roest, W.R., 1997. Suppressing varying directional trends in aeromagnetic data, application of regional and Geophysical and Geochemistry.

Ponte F.C., Ponte Filho F.C., 1996. Estrutura geológica e evolução tectônica da Bacia do Araripe. Recife, DNPM, 68 p.

Rand, H.M., 1983. Levantamento gravimetrico e magnetometrico da Bacia Araripe. Relatório interno da PETROBRAS. 11 p.

Rand, H.M., Manso, V.A.V., 1984. Levantamento gravimétrico e magnetométrico da Bacia do Araripe. In: 33º Congresso Brasileiro de Geologia, Anais: Sociedade Brasileira de Geologia, Rio de Janeiro, Anais. 4, 2011-2016.

Ramos, G.V., Vasconcelos, D.L., Marques, F.O., Castro, D.L., Nogueira, F.C.C., Bezerra, F.H.R., Perez, Y.A.R., Souza, J.A.B., Medeiros, V.C. 2022. Relations between inherited basement fabric and fault nucleation in a continental setting: The Rio do Peixe Basin, NE Brazil. Marine and Petroleum Geology. 139, 105635. https://doi.org/10.1016/j.marpetgeo.2022.105635.

Reeves C., 2005. Aeromagnetic Surveys. Principles, Practice and Interpretation. Earthworks, Geosoft. 155p.

Reid, A.B., Allsop, J.M. Granser; H., Millett, A.J., Somerton, I.W., 1990. Magnetic interpretation in three dimensions using Euler deconvolution. Geophysics. 55, 80-91. https://doi.org/10.1190/1.1442774.

Rodrigues, R.S., Castro, D.L., Reis Júnior, J.A., 2014. Characterization of the Potiguar rift structure based on Euler deconvolution. Revista Brasileira de Geofísica. 32(1), 109-121. http://dx.doi.org/10.22564/rbgf.v32i1.400.

Santos, E.J., Van Schmus, R.W., Brito Neves, B.B., Oliveira, R.G., Medeiros, V.C., 1999. Terranes and their boundaries in the Proterozoic Borborema Province, Northeast Brazil. In: Estended Abstracts 7 Simpósio Nacional de Estudos Tectônicos.121-124.

Schlische, R.W., Young, S.S., Ackermann, R.V., Gupta, A., 1996. Geometry and scaling relations of a population of very small rift-related normal faults. Geology. 24, 683-686.

Schultz, R.A., Fossen, H., 2002. Displacement-length scaling in three dimensions: the importance of aspect ratio and application to deformation bands. Journal of Structural Geology. 24, 1389-1411.

Schultz, R.A., Soliva, R., Fossen, H., Okubo, C.H., Reeves, D.M., 2008. Dependence of Displacement-length scaling relations for fractures and deformation bands on the volumetric changes across them. Journal of Structural Geology. 30, 1405-1411.

Scherer, C.M.S., Jardim de Sá, E.F., Córdoba, V.C., Sousa, D.C., Aquino, M.M., Cardoso, F.M.C., 2014. Tectono-stratigraphic evolution of the Upper Jurassic-Neocomian rift succession, Araripe Basin, Northeast Brazil. Journal of South American Earth Sciences. 49, 106-122. https://doi.org/10.1016/j.jsames.2013.10.007.

Sial, A.N., 1986. Granite-types of Northeast Brazil: current knowledge. Revista Brasileira de Geociências 16, 54-72.

Torabi, A., Berg, S.S., 2011. Scaling of fault attributes: A review. Marine and Petroleum Geology. 28, 1444-1460. https://doi.org/10.1016/j.marpetgeo.2011.04.003.

Torabi, A., Alaei, B., Libak, A. 2019. Normal fault 3D geometry and displacement revisited: Insights from faults in the Norwegian Barents Sea. Marine and Petroleum Geology. 99, 135-155. https://doi.org/10.1016/j.marpetgeo.2018.09.032.

Thompson, D.T., 1982. EULDPH: A new technique for making depth estimates from magnetic data. Geophysics. 47, 31-37.

Uieda, L., Oliveira, J.R., Barbosa, V.C.F., 2014. Geophysical tutorial: Euler deconvolution of potential-field data. The Leading Edge. 33, 448-450.

Van Schmus, W.R., Oliveira, E.P., Silva Filho, A.F., Toteu, F., Penaye, J., Guimarães, I.P. 2008. Proterozoic Links between the Borborema Province, NE Brazil, and the Central African Fold Belt. London. Geological Society. 66-69. https://doi.org/10.1144/SP294.5.

Van Schmus, W.R., Kozuch, M., Brito Neves, B.B., 2011. Precambrian history of the Zona Transversal of the Borborema Province, NE Brazil: Insights from Sm-Nd and U-Pb geochronology. Journal of South American Earth Sciences. 3, 227-252. https://doi.org/10.1016/j.jsames.2011.02.010.

Vasconcelos, D.L., Bezerra, F.H.R., Medeiros, W.E., Castro, D.L., Clausen, O.R., Vital, H., Oliveira, R.G. 2018. Basement fabric controls rift nucleation and postrift basin inversion in the continental margin of NE Brazil. Tectonophysics. 751, 23-40. https://doi.org/10.1016/j.tecto.2018.12.019.

Vauchez, A., Neves, S., Caby, R., Corsini, M., Silva, M.E., Arthaud, M., Amaro, V., 1995. The Borborema shear zone system, NE Brazil. Journal of South America Earth Sciences. 8, 247-266. https://doi.org/10.1016/0895-9811(95)00012-5.

Wang, J., Meng, X., Li, F., 2017. New improvements for lineaments study of gravity data with improved Euler inversion and phase congruency of the field data: Journal of Applied Geophysics. 136, 326-334.

Walsh, J.J., Watterson, J., 1988. Analysis of the relationship between the displacements and dimensions of faults. Journal of Structural Geology. 10, 239-247, https://doi.org/10.1016/0191-8141(88)90057-0.

Weihermann, J.D., Ferreira, F.J.F., Oliveira, S.P., Cury, L.F., Souza, J., 2018. Magnetic interpretation of the Paranaguá Terrane, southern Brazil by signum transform: Journal of Applied Geophysics, 154, 116-127.

Werner, S.C., Torsvik, T.H., 2010. Downsizing the Mjølnir impact structure, Barents Sea, Norway: Tectonophysics. 483, 191-202.

Wilkins, S.J., Gross, M.R., 2002. Normal fault growth in layered rocks at Split Mountain, Utah: influence of mechanical stratigraphy on dip linkage, fault restriction and fault scaling. Journal of Structural Geology 24, 1413–1429 (erratum, Journal of Structural Geology. 24, 2007).

Zhang, J., Zhao, G., Shen, W., Li, S., Sun, M., 2015. Aeromagnetic study of the Hengshan-Wutai-Fuping region: Unraveling a crustal profile of the Paleoproterozoic Trans-North China Orogen: Tectonophysics. 662, 208-218.

5 CONCLUSÕES

A partir da análise do arranjo espacial de lineamentos estruturais regionais (aeromagnéticos e topográficos) e bandas de deformações, e dos dados de posição e profundidade das anomalias aeromagnéticas provenientes da Deconvolução de Euler, foi possível concluir os seguintes pontos acerca da evolução tectônica da borda leste da Bacia do Araripe:

- A partir das interpretações dos lineamentos regionais (topográficos e aeromagnéticos) e dados de campo, verificamos que os resultados em diferentes escalas, apresentaram orientações semelhantes. Os lineamentos regionais, no setor da bacia, e as bandas de deformação da Formação Cariri, exibem orientações em pares conjugados, possivelmente relacionadas com a cinemática experimentada pelo ZCPa. Retratando assim, uma transcorrência destral, com estruturas sintéticas de orientação NW-SE (R) e antitéticas N-S (R'), enquanto o par ENE-WSW (R) e NNE-SSW (R') estaria refletindo a reativação sinistral da ZCPa.
- O arranjo espacial de lineamentos regionais exibiu resultados satisfatórios, podendo ser utilizados como ferramentas para auxiliar na quantificação estrutural de detalhe. As bandas de deformação permitiram definir o seu arranjo espacial com maior precisão quando comparadas aos dados regionais.
- A Deconvolução de Euler permitiu verificar a geometria de zonas de falha (falhas Mauriti, Coité e Umburanas). A distribuição assimétrica da profundidade da fonte magnética permitiu configurar uma geometria elíptica para essas zonas de falha. Além disso, essas falhas delineiam grabens e *horsts*, possibilitando inferir a profundidade para a borda dessas estruturas.

6 RECOMENDAÇÕES PARA TRABALHOS FUTUROS

Alguns aspectos ao longo do desenvolvimento desta pesquisa, na borda leste da Bacia do Araripe, representam pontos de interesse para abordagem mais detalhadas, como por exemplo:

- Desenvolver a classificação estrutural das bandas de deformação pertencentes a Formação Cariri, presentes nesse setor, permitindo inferir seus mecanismos de deformação;
- Investigar potenciais afloramentos indicados a partir da análise do arranjo espacial dos lineamentos regionais;
- Analisar o comportamento da deformação frágil nas rochas das demais formações que afloram na borda leste.

REFERÊNCIAS

ALMEIDA, F.F.M., HASHUI, Y., BRITO NEVES, B.B., FUCK, R.A. **Brazilian structural provinces: an introduction**. Earth Sciences Reviews, 17, ed. 1-2, 1-29. 1981.

ALMEIDA, Y.B., JULIÀ, J., FRASSETTO, A. **Crustal architecture of the Borborema Province, NE Brazil,** from receiver function CCP stacks: Implications for Mesozoic stretching and Cenozoic uplift, Tectonophysics. 2015.

ANGELIM, L.A.A., VASCONCELOS, A.M., GOMES, J.R.C., WANDERLEY, A.A., FORGIARINI, L.L., MEDEIROS, M.F. **Folha SB.24-Jaguaribe.** In: Schobbenhaus, C., Gonçalves, J.H., Santos, J.O.S., Abram, M.B., Leão Neto, R., Matos, G.M.M., Vidotti, R.M. E Ramos, M.A.B., Jesus, J.D.A. (eds.). Carta Geológica do Brasil ao Milionésimo, Sistema de Informações Geográfica - SIG, Programa Geologia do Brasil. CPRM, Brasília. 2004.

ARAÚJO NETO, J.F., SANTOS, G.L., SOUZA, I.M.B.A., BARRETO, S.B., SANTOS, L.C.M.L., BEZERRA, J.P.S., CARRINO, T.A. **Integration of remote sensing, airborne geophysics and structural analysis to geological mapping: a case study of the Vieirópolis region, Borborema Province, NE Brazil.** Geol. USP., 18(3), 8-103. 2018. http://dx.doi.org/10.11606/issn.2316-9095.v18-140834.

ASSINE, M.L. **Análise estratigráfica da Bacia do Araripe, Nordeste do Brasil.** Revista Brasileira de Geociências, 22 (3), 289-300. 1992.

ASSINE, M.L. **Bacia do Araripe.** Boletim de Geociências da Petrobras, 15 (2), 371-389. 2007.

ASSINE, M.L., PERINOTTO, J.A.J., CUSTÓDIO, M.A., NEUMANN, V.H., VAREJÃO, F.G., MESCOLOTTI, P.C. **Sequências deposicionais do Andar Alagoas da Bacia do Araripe, Nordeste do Brasil.** B. Geoci. Petrobras, 22 (1), 3-28. 2014.

BARANOV, V. **A new method for interpretation of aeromagnetic maps: Pseudo-gravimetric anomalies.** Geophysics. 22, 359-383. 1957.

BEURLEN, K. **A geologia da Chapada do Araripe.** Anais da Academia Brasileira de Ciências. 34(3), 365-370. 1962.

BLAKELY, J.R. **Potential Theory in Gravity and Magnetic Applications.** 2nd ed. Cambridge University Press, 1996.

BRITO NEVES, B.B., VAN SCHMUS, W.R., FETTER, A.H. **Noroeste da África-Nordeste do Brasil (Província Borborema) Ensaio comparativo e problemas de correlação.** São Paulo. Revista do Instituto de Geociências - USP. Sér. Cient. 1, 59-78. 2001.

CARDOSO, F.M.C. **O graben de Palestina: contribuição à estratigrafia e estrutura do estágio rift na Bacia do Araripe, Nordeste do Brasil.** Dissertação de mestrado, Programa de Pós-Graduação em Geodinâmica e Geofísica, Universidade Federal do Rio Grande do Norte. Natal. 2010. 107p.

CASTRO, D.L., CASTELO BRANCO, R.M.G**. Caracterização da arquitetura interna das bacias do Vale do Cariri (NE do Brasil) com base em modelagem gravimétrica 3-D.** Brazilian Journal of Geophysics. 17,129-144. 1999.

CELESTINO, M.A.L., MIRANDA, T.S., CORREIA FILHO, O.J., BARBOSA, J.A. **Aspectos tectônicos da borda NE da Bacia de Fátima, Província Borborema - NE do Brasil.** Estudos Geológicos. 27 (2), 3-19. 2018. https://doi.org/10.18190/1980-8208/estudosgeologicos.

CELESTINO, M.A.L., MIRANDA, T.S., MARIANO, G., ALENCAR, M.L., CARVALHO, B.R.B.M., FALCÃO, T.C., TOPAN, J.G., BARBOSA, J.A., GOMES, I.F. **Fault damage zones width: Implications for the tectonic evolution of the northern border of the Araripe Basin, Brazil, NE Brazil.** J. Struct. Geol. 138, 1-16. 2020. https://doi.org/10.1016/j.jsg.2020.104116.

CERRI, R.I., WARREN, L.V., SPENCER, C.J., VAREJÃO, F.G., PROMENZIO, P., LUVIZOTTO, G.L., ASSINE, M.L. **Using detrital zircon and rutile to constrain sedimentary provenance of Early Paleozoic fluvial systems of the Araripe Basin, Western Gondwana.** Journal of South American Earth Sciences. 116. 2022. https://doi.org/10.1016/j.jsames.2022.103821.

CIANFARRA, P., SALVINI, F. **Lineament domain of regional strike-slip corridor: Insight from the Neogene transtensional De Geer transform fault in NW Spitsbergen.** Pure and Applied Geophysics. 172 (5), 1185-201. 2015.

DELGADO, I. M., SOUZA, J. D., SILVA, L. C., SILVEIRA FILHO, N. C., SANTOS, R. A., PEREIRA, A. J., GUIMARÃES, J. T., ANGELIM, L. A. A., VASCONCELOS, A. M., GOMES, I. P., LACERDA FILHO, J. V., VALENTE, C. R., PERROTTA, M. P., HEINECK, C. A. **Geotectônica do Escudo Atlântico.** In: L. A. Bizzi, C. Schobbenhaus, R. M. Vidotti, J. H. Gonçalves (Eds.), Geologia, Tectônica e Recursos Minerais do Brasil - CPRM. 1, 227-258. 2003.

DRURY, S.A. **Image Interpretation in Geology.** 3rd ed. Cheltenham: Nelson Thornes. 2001.

DURRHEIM, R.J., COOPER, G.R.J. **EULDEP: a program for the euler deconvolution of magnetic and gravity data.** Computers & Geosciences. 24(6), 545-550, 1998.

FAMBRINI, G.L., LEMOS, D.R., TESSER JUNIOR, S., ARAÚJO, J.T., SILVA FILHO, W.F., SOUZA, B.Y.C., NEUMANN, V.H.M.L. **Estratigrafia, Arquitetura Deposicional e Faciologia da Formação Missão Velha (Neojurássico-Eocretáceo) na Área-Tipo, Bacia do Araripe, Nordeste do Brasil: Exemplo de Sedimentação de Estágio de Início de Rifte a Clímax de Rifte.** Revista do Instituto de Geociências - USP. 11(2), 55-87. 2011.

FAMBRINI, G.L., SILVA FILHO, W.F., LEMOS, D.R., SILVESTRE, D.C., ARAÚJO, J.T. MENEZES FILHO, J.A.B., TESSER JUNIOR, S., NEUMANN, V.H.M.L. **Análise tectonossedimentar das fases início de rifte e clímax de rifte da Bacia do Araripe, Nordeste do Brasil.** Revista do Instituto de Geociências - USP. 19(3), 20-236. 2019. https://doi.org/10.11606/issn.2316-9095.v19-150526.

FERREIRA, V.P., SIAL, A.N., PIMENTEL, M.M., MOURA, C.A.V. **Intermediate to acidic magmatism and crustal evolution in the Transversal Zone, Northeastern Brazil.** In: Mantesso Neto, Virginio, Bartorelli, A., Carneiro, Celso Dal Ré, Brito Neves, Benjamin Bley (editors), Geologia do Continente Sul-Americano: a evolução da obra de Fernando Flávio Marques de Almeida. Universidade de São Paulo, capitulo XII, 189-201. 2004.

FLETCHER, J.M., TERAN, O.J., ROCKWELL, T.K., OSKIN, M.E., HUDNUT, K.W., SPELZ, R.M., LACAN, P., DORSEY, M.T., OSTERMEIJER, G., MITCHELL, T.M., AKCIZ, S.O., HERNANDEZ-FLORES, A. P., HINOJOSA-CORONA, A., PEÑA-VILLA, I., LYNCH, D.K. **An analysis of the factors that control fault zone architecture and the importance of fault orientation relative to regional stress.** Geological Society of America Bulletin. 132 (9-10): 2084-2104. 2020. https://doi.org/10.1130/B35308.1.

FOSSEN, H., SOLIVA, R., BALLAS, G., TRZASKOS, B., CAVALCANTE, C., SCHULTZ, R.A. **A review of deformation bands in reservoir sandstones: geometries, mechanisms, and distribution.** Geol. Soc., Lond., Spec. Public. 459 (1), 9-33. 2017.

GARCIA, X., JULIÀ, J., NEMOCÓN, A.M., NEUKIRCH, M. **Lithospheric thinning under the Araripe Basin (NE Brazil) from a long-period magnetotelluric survey: constraints for tectonic inversion.** Gondwana Research. 68, 174-184. 2019. https://doi.org/10.1016/j.gr.2018.11.013.

GASPARY, J., ANJOS, N.F.R. **Estudo Hidrogeológico de Juazeiro do Norte - Ceará.** Recife: SUDENE, Série Hidrogeologia 3. 1964. 25 p.

GROHMANN, C.H., SMITH, M.J., RICCOMINI, C. **Multi-scale Analysis of Topographic Surface Roughness in the Midland Valley, Scotland.** IEEE Transactions on Geoscience and Remote Sensing. 49, 1200-1213. 2011. https://doi.org/10.1109/TGRS.2010.2053546.

HOOKER, J.N., LAUBACH, S.E., AND MARRETT, R. **Microfracture spacing distributions and the evolution of fracture patterns in sandstones.** Journal of Structural Geology. 108, 66-79. 2018. https://doi.org/10.1016/j.jsg.2017.04.001.

JACQUES, P.D., MACHADO, R., OLIVEIRA, R.G., FERREIRA, F.J.F, CASTRO, L.G., NUMMER, A.R. **Correlation of lineaments (magnetic and topographic) and Phanerozoic brittle structures with Precambrian shear zones from the basement of the Paraná Basin, Santa Catarina State, Brazil.** Brazilian Journal of Geology, 44 (1), 39-54. 2014. https://doi.org/10.5327/Z2317-4889201400010005.

JOHNSON A.C, SARRIS A, AMZA-PREIN.M E. **New interactive fft-based grid suturing tecnique applied to ground geophysical surveys in Greece.** Second Balkan Geophysical Congress and Exhibition. 1999.

LAUBACH, S.E., LAMARCHE, J., GAUTHIER, B.D.M., DUNNE, W.M., SANDERSON, D.J. **Spatial arrangement of faults and opening-mode fractures.** J. Struct. Geol. 108, 2-15. 2018a https://doi.org/10.1016/j.jsg.2017.08.008.

LAUBACH, S.E., HUNDLEY, T.H., HOOKER, J.N., MARRETT, R.A. **Spatial arrangement and size distribution of normal faults, Buckskin detachment upper plate,**

Western Arizona. J. Struct. Geol. 108, 230-242. 2018b. https://doi.org/10.1016/j.jsg.2017.10.001.

LI, J.Z., LAUBACH, S.E., GALE, J.F.W., MARRETT, R.A. **Quantifying opening-mode fracture spatial organization in horizontal wellbore image logs, core and outcrop: Application to Upper Cretaceous Frontier Formation tight gas sandstones, USA.** J. Struct. Geol. 108, 137-156. 2018. http://dx.doi.org/10.1016/j.jsg.2017.07.005.

LI, Y., OLDENBURG, D.W. **Separation of regional and residual magnetic field data**. Geophysics. 63 (2), 431-439. 1998.

LIMA, F.G.F., SÁ, E.F.J. **Controle estrutural da borda sudeste da Bacia do Parnaíba Nordeste do Brasil: relação com eventos geodinâmicos no Gondwana.** Geol. USP, Sér. Cient. 17(3), 3-21. 2017. https://doi.org/10.11606/issn.2316-9095.v17-125909.

MARQUES, F.O., NOGUEIRA, F.C.C., BEZERRA, F.H.R., CASTRO, D.L. **The Araripe Basin in NE Brazil: An intracontinental graben inverted to a high-standing horst.** Tectonophysics. 630, 251-264. 2014. http://dx.doi.org/10.1016/j.tecto.2014.05.029.

MARRETT, R., GALE, J.F.W., GOMEZ, L., LAUBACH, S.E. **Correlation analysis of fracture arrangement in space.** J. Struct. Geol. 108, 16-33. 2018. https://doi.org/10.1016/j.jsg.2017.06.012.

MATOS, R.M.D. **The Northeast Brazilian Rift System.** Tectonics. 11 (4), 766-791. 1992.

MATOS, R.M.D. **History of the northeast Brazilian rift system: kinematics implications for the break-up between Brazil and West Africa.** In: Cameron, N.R.; Bate, R.H.; Clure, V.S. (eds.) The Oil and Gas Habitats of the South Atlantic Geological Society, London, Special Publications.155, 55-73. 1999.

MATOS, R.M.D., NORTON, I., CASEY, K., KRUEGER, A. **An Orthogonal Zone between the Equatorial and South Atlantic Margins: Relevance and Control in the Evolution of the Afro-Brazilian Basins** - 16th International Congress of the Brazilian Geophysical Society. SBGf - Sociedade Brasileira de Geofísica- Rio de Janeiro. 2019. Expanded Abstract.

MATOS, R.M.D., KRUEGER, A., NORTON, I., CASEY, K. **The fundamental role of the Borborema and Benin–Nigeria provinces of NE Brazil and NW Africa during the development of the South Atlantic Cretaceous Rift system.** Marine and Petroleum Geology, 127. 2021. https://doi.org/10.1016/j.marpetgeo.2020.104872.

MEDEIROS, V.C. **Evolução geodinâmica e condicionamento estrutural dos terrenos Piancó-Alto Brígida e Alto-Pajeú, Domínio da Zona Transversal, NE do Brasil.** Tese de doutorado. Programa de Pós-graduação em Geodinâmica e Geofísica. Universidade Federal de Rio Grande do Norte. 2004. 199p.

MEIXNER, J., GRIMMER, J.C., BECKER, A., SCHILL, E., KOHL, T. **Comparison of different digital elevation models and satellite imagery for lineament analysis: Implications for identification and spatial arrangement of fault zones in crystalline basement rocks of the southern Black Forest (Germany).** J. Struct. Geol. 108, 256-268. 2018. https://doi.org/10.1016/j.jsg.2017.11.006.

MIRANDA, T.S., MAGALHÃES, J.R., BARBOSA, J.A. **Bacia do Araripe: Possível Sistema Pull-Apart?** In: 46° Congresso Brasileiro de Geologia, Anais: Sociedade Brasileira de Geologia. Santos, 2012.

MIRANDA, T.S., MAGALHAES, J.R., BARBOSA, J.A., CORREIA FILHO, O., ALENCAR, M.L. **Araripe Basin, NE Brazil: a rift basin implanted over a previous pull-apart system?** In: 4th Atlantic Conjugate Margins Conference, vol 3. 2014.

MIRANDA, T.S., SANTOS, R.F., BARBOSA, J.A., GOMES, I.F., ALENCAR, M.L., CORREIA, O.J., FALCÃO, T.C., GALE, J.F.W., NEUMANN, V.H**. Quantifying aperture, spacing and fracture intensity in a carbonate reservoir analogue: Crato Formation, NE Brazil.** Mar. Petrol. Geol. 97, 556-567. 2018. https://doi.org/10.1016/j.marpetgeo.2018.07.019.

MIRANDA, T.M., NEVES, S.P., CELESTINO, M.A.L., ROBERTS, N.M.W. **Structural evolution of the Cruzeiro do Nordeste shear zone (NE Brazil): Brasiliano-Pan-African-ductile-to-brittle transition and Cretaceous brittle reactivation.** J. Struct. Geol. 141. 2020. https://doi.org/10.1016%20/%20j.jsg.2020.104203.

NEUMANN, V.H.M.L. **Estratigrafia, Sedimentologia, Geoquímica y Diagénesis de los Sistemas Lacustres Aptienses-Albienses de lá Cuenca de Araripe (Noroeste do Brasil).** Tese de Doutorado. Facultat de Geologia, Universitat de Barcelona, 1999. 293p.

NEVES, S.P., MARIANO, G. **Assessing the tectonic significance of a large-scale transcurrent shear zone system: Pernambuco Lineamento, Northeastern Brazil.** Journal of Structural Geology. 21, 1639-1383. 1999.

NEVES, S.P., MARIANO, G., BELTRÃO, B.A., CORREIA, P.B. **Emplacement and deformation of the Cachoeirinha pluton inferred through petrostructural studies: constraints on regional strain fields.** Journal of South American Earth Sciences. 19, 127-141. 2005.

NEVES, S.P., ALCANTARA, V.C. **Geochemistry of orthogneisses and metasedimentary rocks across a proposed terrane boundary in the Central Domain of Borborema Province, NE Brazil: geodynamic implications.** Journal of South American Earth Sciences. 29, 498-511. 2010. https://doi.org/10.1016/j.jsames.2009.08.002.

NICOLAS, M.P.B. E CLAYTON, B.W. **Lineament mapping of the Hudson Bay Lowland using remote-sensing methods, northeastern Manitoba (parts of NTS 53N, O, 54).** In: Report of Activities Manitoba Mineral Resources, Manitoba Geological Survey. 89-96. 2015.

OLIVEIRA, R.G. **Arcabouço geofísico, isostasia e causas do magmatismo cenozoico da província Borborema e de sua margem continental (Nordeste do Brasil).** Tese de doutorado. Programa de Pós-Graduação em Geodinâmica e Geofísica, Universidade Federal do Rio Grande do Norte. Natal. 2008. 415p.

ORTEGA, O.J., MARRETT, R.A., LAUBACH, S.E. **A scale-independent approach to fracture intensity and average spacing measurement.** Am. Assoc. Petrol. Geol. Bull. 90, 193-208. 2006. https://doi.org/10.1306/08250505059.

PEULVAST, J.P., BETARD, F. **A history of basin inversion, scarp retreat and shallow denudation: the Araripe basin as a keystone for understanding long-term landscape evolution in NE Brazil.** Geomorphology. 233, 20-40. 2015. https://doi.org/10.1016/j.geomorph.2014.10.009.

PILKINGTON, M., ROEST, W.R. **Suppressing varying directional trends in aeromagnetic data**, application of regional and Geophysical and Geochemistry. 1997.

PONTE, F.C., APPI, C.J. **Proposta de revisão da coluna litoestratigráfica da Bacia do Araripe.** In: Congresso Brasileiro de Geologia, 36, Anais: SBG. Natal, p. 211-226. 1990

PONTE F.C., PONTE FILHO F.C. **Estrutura geológica e evolução tectônica da Bacia do Araripe.** Recife, DNPM. 1996. 68 p.

RAND, H.M. **Levantamento gravimetrico e magnetometrico da Bacia Araripe.** Relatório interno da PETROBRAS. 1983. 11 p.

RAND, H.M., MANSO, V.A.V. **Levantamento gravimétrico e magnetométrico da Bacia do Araripe.** In: 33º Congresso Brasileiro de Geologia, Anais: Sociedade Brasileira de Geologia, Rio de Janeiro, Anais. 4, 2011-2016. 1984.

REEVES C. **Aeromagnetic Surveys. Principles, Practice and Interpretation.** Earthworks, Geosoft. 2005. 155p.

REID, A.B., ALLSOP, J.M., GRANSER; H., MILLETT, A.J., SOMERTON, I.W. **Magnetic interpretation in three dimensions using Euler deconvolution.** Geophysics. 55, 80-91. 1990.

SANTOS, E.J., VAN SCHMUS, R.W., BRITO NEVES, B.B., OLIVEIRA, R.G., MEDEIROS, V.C. **Terranes and their boundaries in the Proterozoic Borborema Province, Northeast Brazil.** In: Estended Abstracts 7 Simpósio Nacional de Estudos Tectônicos.121-124. 1999.

SANTOS, R. F. V., MIRANDA, T. S., BARBOSA, A., GOMES, I. F., MATOS, G. C., NEUMANN, V. H. M. L., GUIMARÃES, L. N., GALE, J. **Analysis of potential uncertainties in opening-mode fractures characterization through the *scanline* technique of aptian carbonates, Araripe Basin, Northeast of Brasil.** In: AAPG Annual Convention and Exhibition, Denver, CO. 2015.

SALAMUNI, E., EBERT, H.D., HASUI, Y. **Morfotectônica da bacia sedimentar de Curitiba.** Rev. Bras. Geociências. 34, 469-478. 2004. https://doi.org/10.25249/0375-7536.2004344469478.

SCHERER, C.M.S., JARDIM DE SÁ, E.F., CÓRDOBA, V.C., SOUSA, D.C., AQUINO, M.M., CARDOSO, F.M.C. **Tectono-stratigraphic evolution of the Upper Jurassic-Neocomian rift succession, Araripe Basin, Northeast Brazil.** Journal of South American Earth Sciences. 49, 106-122. 2014. https://doi.org/10.1016/j.jsames.2013.10.007.

SIAL, A.N. Granite-types of Northeast Brazil: current knowledge. Revista Brasileira de Geociências. 16, 54-72. 1986.

SIAL, A.N., FERREIRA, V.P. **Magma associations in Ediacaran granitoids of the Cachoeirinha-Salgueiro and Alto Pajeú terranes, Northeastern Brazil: forty years of studies.** Journal of South American Earth Sciences. 68, 113-133. 2016. https://doi.org.10.1016/j.jsames.2015.10.005.

SILVESTRE, D.C., FAMBRINI, G.L., SANTOS, A.A.F. **Caracterização faciológica das formações Cariri e Brejo Santo em afloramentos a NE do município Missão Velha (Ceará - Brasil).** Estudos Geológicos, 27(1). 2017. https://doi.org/10.18190/1980-8208/estudosgeologicos.v27n1p19-33

THOMPSON, D.T. EULDPH: **A new technique for making depth estimates from magnetic data.** Geophysics, 47, 31-37. 1982.

VAN SCHMUS, W.R., OLIVEIRA, E.P., SILVA FILHO, A.F., TOTEU, F., PENAYE, J., GUIMARÃES, I.P. **Proterozoic Links between the Borborema Province, NE Brazil, and the Central African Fold Belt.** London. Geological Society. 66-69. 2008.

VAN SCHMUS, W.R., KOZUCH, M., BRITO NEVES, B.B. **Precambrian history of the Zona Transversal of the Borborema Province, NE Brazil: Insights from smend and uepb geochronology.** Journal of South American Earth Sciences. 3, 227-252. 2011.

VAUCHEZ, A., NEVES, S.; CABY, R., CORSINI, M., SILVA, M.E., ARTHAUD, M., AMARO, V. **The Borborema shear zone system, NE Brazil**. Journal of South America Earth Sciences. 8, 247-266. 1995.

WISE, D.U., FUNICIELLO, R., PAROTTO, M., SALVINI, F. **Topographic lineament swarms: Clues to their origin from domain analysis of Italy.** Geological Society of America Bulletin. 96, 952-967. 1985.